A COUPLED MODEL STUDY OF THE REMOTE INFLUENCE OF ENSO ON TROPICAL ATLANTIC SST VARIABILITY

A Dissertation

by

YUE FANG

Submitted to the Office of Graduate Studies of
Texas A&M University
in partial fulfillment of the requirements for the degree of

DOCTOR OF PHILOSOPHY

May 2005

Major Subject: Oceanography

A COUPLED MODEL STUDY OF THE REMOTE INFLUENCE OF ENSO ON TROPICAL ATLANTIC SST VARIABILITY

A Dissertation

by

YUE FANG

Submitted to Texas A&M University
in partial fulfillment of the requirements
for the degree of

DOCTOR OF PHILOSOPHY

Approved as to style and content by:

Ping Chang (Chair of Committee)	Robert O. Reid (Member)
Gerald R. North (Member)	Achim Stössel (Member)
H. Joseph Newton (Member)	Wilford D. Gardner (Head of Department)

May 2005

Major Subject: Oceanography

ABSTRACT

A Coupled Model Study of the Remote Influence of ENSO
on Tropical Atlantic SST Variability. (May 2005)
Yue Fang, B.S., Ocean University of China;
M.S., First Institute of Oceanography, State Oceanic Administration, China
Chair of Advisory Committee: Dr. Ping Chang

To investigate the tropical Atlantic response to the remote El Nino-Southern Oscillation (ENSO) forcing, a Reduced Physics – Coupled Global Circulation Model (RP-CGCM) is developed, and four experiments are carried out. The results show that the RP-CGCM is capable of capturing the major features of Tropical Atlantic Variability (TAV) and its response to ENSO forcing.

The SST response to the remote influence of ENSO may be divided into two stages. In stage one, the ENSO influences the tropical Atlantic SST primarily through the Troposphere Temperature (TT) mechanism, which predicts a uniform warming in the tropical Atlantic following the mature phase of El Nino. In the north tropical Atlantic (NTA), the Walker mechanism and the Pacific-North-American (PNA) mechanism work in concert with the TT-induced warming, giving rise to a robust SST response during the boreal spring in this region. In the south tropical Atlantic (STA), the southeasterly wind anomaly and increased stratus clouds work against the TT-induced warming, resulting in a much weaker SST response in this region. At this stage, the response can be largely explained by the ocean mixed layer response to changes in surface heat fluxes induced by ENSO.

In stage two, ocean dynamics play a more active role in determining the evolution of SST. The cross-equatorial wind anomaly in the western to central equatorial Atlantic can change the SST in the eastern equatorial Atlantic through Bjerknes feedback and the SST in the central equatorial Atlantic through Ekman feedback. These feedback result in a cooling of SST in the equatorial south Atlantic (ESA) region which

is so overwhelming that it cancels the warming effect induced by the TT mechanism and reverses the sign of the warm SST anomaly that is formed during stage one in this region.

In general, the horizontal advection of heat plays a secondary role in the SST response to the remote influence of ENSO, except in the regions where the North Equatorial Countercurrent (NECC) dominates and the SST variability is strong. Entrainment is particularly important in maintaining the correct SST structure during boreal summer.

ACKNOWLEDGMENTS

I'm truly grateful to my advisor, Dr. Ping Chang, for his patient guidance, camaraderie, and sparkling wit as we probed the boundless depths of the unknown. His scientific intellect and enthusiastic pursuit of discovery are both inspirational and legendary. The financial support provided to me by Dr. Chang gave me the opportunity to complete this research.

I would also like to thank the other committee members, Prof. Robert O. Reid, Dr. Gerald R. North, Dr. Achim Stössel, and Dr. H. Joseph Newton, for reading this dissertation and their invaluable suggestions and discussions.

Dr. Link Ji and Dr. Hank Seidel helped me a lot in various ways, especially in model programming and solving computer technical problems.

Last and foremost, I'm deeply grateful for my parents' encouragement and support that helped me conquer difficulties, and I'm deeply grateful to my wife for taking care of household duties, so that I could have more time to do research. Thanks are due also to my lovely son. With him, life is always fun.

TABLE OF CONTENTS

Page

ABSTRACT..... iii

ACKNOWLEDGMENTS..... v

TABLE OF CONTENTS..... vi

LIST OF FIGURES..... viii

LIST OF TABLES..... xii

CHAPTER

I INTRODUCTION..... 1

1. Motivation..... 1
2. Issues to Be Addressed..... 9
3. Overview..... 11

II METHODOLOGY AND APPROACH..... 12

1. Existing Approach..... 12
2. Current Modeling Approach..... 15
   2.1. Atmosphere Model..... 16
   2.2. Ocean Model..... 17
      a. Model Formulation..... 17
      b. Parameterization of Entrainment..... 19
      c. Model Configuration..... 22
3. Experiment Design..... 23

III REMOTE INFLUENCE OF ENSO..... 26

1. Model Validation..... 26
   1.1. EOF Analysis..... 27
      a. Leading Modes..... 27
      b. Seasonal Phase-locking..... 30
   1.2. Composite Analysis..... 32
      a. Winds..... 32
      b. SST..... 35
2. Extracting ENSO-forced Response Using an Ensemble of Coupled Integration..... 38
   2.1 Dominant SST “Signal”..... 39
   2.2 Heat Flux Anomaly..... 44
   2.3 Thermocline Variation..... 47
   2.4 Ekman Feedback..... 49

CHAPTER Page

3. Discussion..... 51
3.1. North Tropical Atlantic..... 51
3.2. South Tropical Atlantic..... 52
3.3. Equatorial Atlantic..... 54

IV OCEAN DYNAMICS IN REMOTE INFLUENCE OF ENSO..... 57

1. NADV Experiment..... 57
2. NENT Experiment..... 65
3. SLAB Experiment..... 69
4. Discussion..... 71

V SUMMARY AND DISCUSSION..... 78

1. Summary..... 78
2. Discussion and Future Work..... 80
2.1. Model Biases..... 80
2.2. Intrinsic TAV..... 81

REFERENCES..... 85

APPENDIX..... 91

VITA..... 93

LIST OF FIGURES

FIGURE Page

1.1 The dominant pattern of surface ocean-atmosphere variability in the tropical Atlantic region during different seasons..... 2

1.2 Correlation map of the Nino-3 index, averaged over Dec (0)-Jan (+1), with NCEP-NCAR reanalysis SLP (contours), winds (arrows), and wind divergence (shading) in Jan-Feb (+1)……..... 6

1.3 Lag correlation between the Nino-3 index and microwave sounding unit (MSU) channel-2 temperature for 1979-99……..……... 8

2.1 Schematic diagram of surface current system in the tropical Atlantic Ocean……...……..…….. 14

2.2 Schematic diagram of the vertical structure of the ocean model…….. 17

2.3 Mixed layer depth in the tropical Atlantic Ocean taken from the spatially varying observed value estimated from Levitus data (1982)……..... 23

2.4 Regional coupling strategy over the global domain……..……... 25

3.1 (a) First and (b) second leading EOFs derived from Reynolds' SST (Smith et al., 1996) over the period from 1950 to 2000 (The associated PC time series have been normalized by their standard deviations)……. 28

3.2 (a) First and (b) second leading EOFs derived from the SST "signal" of the CTRL experiment over the period from 1980 through 1999 (The associated PC time series have been normalized by their standard deviations)……..……... 29

3.3 Standard deviation of the PC time series associated with the observed (a) zonal mode and (b) meridional mode shown in Figure3.1…….……. 31

3.4 Standard deviation of the PC time series associated with the (a) zonal mode and (b) meridional mode simulated by the CTRL experiment……... 31

3.5 Evolution of wind stress anomalies from January to August constructed from NCEP/NCAR reanalysis……... 33

FIGURE Page

3.6 Evolution of wind stress anomalies from January to August constructed from the CTRL experiment……... 34

3.7 Evolution of SST anomalies from January to August constructed from Reynold's SST (Smith et al., 1996)……. 36

3.8 Evolution of SST anomalies from January to August constructed from the CTRL experiment…….. 37

3.9 (a) First leading EOFs, (b) second leading EOFs, and (c) their associated PC time series derived from the CTRL experiment……. 40

3.10 Standard deviation of the PC time series associated with the (a) first leading EOFs and (b) second leading EOFs derived from the CTRL experiment……...……. 41

3.11 First leading EOFs of (a) boreal spring and (b) boreal summer, and (c) associated PC time series derived from the CTRL experiment……. 42

3.12 Boxed areas, from north to south, are regions where the indices are defined to represent the climate variability in the NTA, equatorial Atlantic, and STA, respectively……... 44

3.13 Lag correlations between the downward surface heat flux and the SST in the (a) NTAI, (b) STAI, and (c) EAI regions computed from the CTRL experiment…….……. 45

3.14 Lag correlations between the wind stress and downward surface heat fluxes in the NTAI (upper panel), STAI (middle panel), and EAI (lower panel) regions computed from the CTRL experiment……..…... 46

3.15 (a) Correlation between the thermocline and SST at zero lag computed from the CTRL experiment; and the lag correlations between the thermocline and SST in (b) eastern equatorial Atlantic (EEA) and (c) Angola-Namibia (S1) regions…….…… 48

3.16 (a) Correlation between the entrainment velocity induced by Ekman pumping and SST at zero lag computed from the CTRL experiment; and (b) lag correlations between the entrainment velocity and SST in western equatorial Atlantic (WEA) region……..... 50

FIGURE Page

3.17 Composite map of zonally averaged SST, wind stress, and downward surface heat fluxes constructed for the CTRL experiment……. 53

3.18 Lag correlations between (a) the meridional component of wind stress and thermocline in the S1 region; (b) the thermocline in the EEA region and the S1 region; and (c) the zonal component of wind stress and SST in the S1 region…….. 55

4.1 As in Figure 3.8, but for the NADV experiment……. 58

4.2 As in Figure 3.17, but for the NADV experiment……...…… 59

4.3 Differences in SST anomalies between the NADV and CTRL experiments (NADV minus CTRL)…….. 60

4.4 As in Figure 3.6, but for the NADV experiment…….. 61

4.5 Differences in wind stress anomalies between the NADV and CTRL experiments (NADV minus CTRL)…….. 62

4.6 Composites of anomalous surface currents in May and June constructed from the CTRL experiment……... 63

4.7 SST Climatology of (a) May and (b) June derived from Reynold's SST (Smith et al., 1996) during the period of 1950 to 2000……... 64

4.8 As in Figure 3.8, but for the NENT experiment…….. 66

4.9 As in Figure 3.17, but for the NENT experiment……. 67

4.10 As in Figure 3.6, but for the NENT experiment……... 68

4.11 As in Figure 3.8, but for the SLAB experiment……...…….. 70

4.12 As in Figure 3.17, but for the SLAB experiment……..... 71

4.13 As in Figure 3.6, but for the SLAB experiment……... 72

4.14 First leading EOFs during boreal spring derived from the (a) NADV, (b) NENT, and (c) SLAB experiments……..... 73

FIGURE Page

4.15 First leading EOFs during boreal summer derived from the (a) NADV, (b) NENT, and (c) SLAB experiments…….……..... 75

5.1 (a) First and (b) second leading EOFs derived from the SST "noise" of the CTRL experiment (The associated PC time series have been normalized by their standard deviations)……..…… 83

5.2 Standard deviation of the PC time series associated with the (a) first leading EOFs and (b) second leading EOFs derived from the "noise" of the CTRL experiment……..... 84

LIST OF TABLES

TABLE Page

2.1 Description of variables used in the equations of ocean model…… 18

2.2 Description of variables used in the parameterization of entrainment……. 21

CHAPTER I

INTRODUCTION

1. Motivation

The tropical oceans are the most active regions for large-scale ocean-atmosphere interactions, and exhibit predominant climate variability at various time scales. It has long been recognized that climate variability has an important impact on human social and economic activities and can sometimes result in disastrous climate events, especially in coastal regions.

The well-known droughts in the Nordeste region of northeast Brazil, for example, have been shown to be closely related to the tropical Atlantic sea surface temperature (SST) distribution and associated anomalies in sea level pressure (SLP) and wind (Hastenrath and Heller, 1977; Moura and Shukla, 1981; Hastenrath et al., 1984; Ward and Folland, 1991; Rao et al., 1993; Nobre and Shukla, 1996). Similar climatic factors were often found to be linked to droughts in the Subsaharan Africa (Lamb 1978; Hastenrath, et al. 1984; Lough 1986; Folland et al. 1986, 1991). In fact, rainfall in the tropical Atlantic Ocean and its adjacent countries is governed by the annual migration of subtropical high pressure cells north and south of equator and strength, as well as the north-south migration and intensity of the Intertropical Convergence Zone (ITCZ), both of which are tightly linked to SST. The relationship between the rainfall patterns and the distributions of the related climate variables is clearly reflected in the Figure 1.1. Rainfall variability over the Central America - Caribean region was also found to be related to the north topical Atlantic (NTA) SST fluctuations (Hastenrath 1976, 1984; Enfield, 1996; Enfield and Elfaro, 1999; Giannini et al, 2000). In addition, the seasonal

---

This dissertation follows the style and format of *Journal of Climate*.

(a)

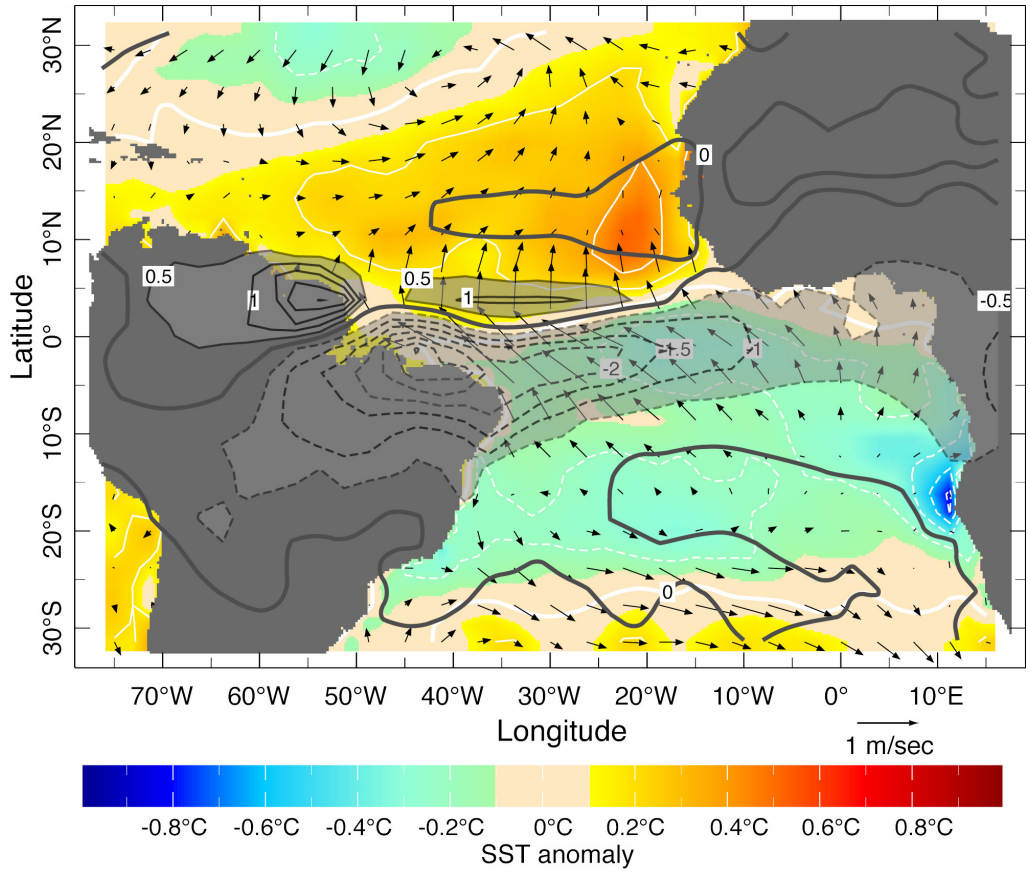

Figure 1.1. The dominant pattern of surface ocean-atmosphere variability in the tropical Atlantic region during different seasons. (a) boreal spring (March-April). The black contours depict the first EOF of the regional rainfall anomaly (from GPCP data, 1979-2001) in units of mm/day. This EOF explains 33% of the seasonal variance. The colored field is the SST anomaly regressed on the principal component time series of the rainfall EOF (units are °C, see scale below; white contours every 0.2° are added for further clarity). Arrows depict the seasonal mean surface wind vector in m/sec, regressed on the same time series. (From Kushnir et al., 2004)

(b)

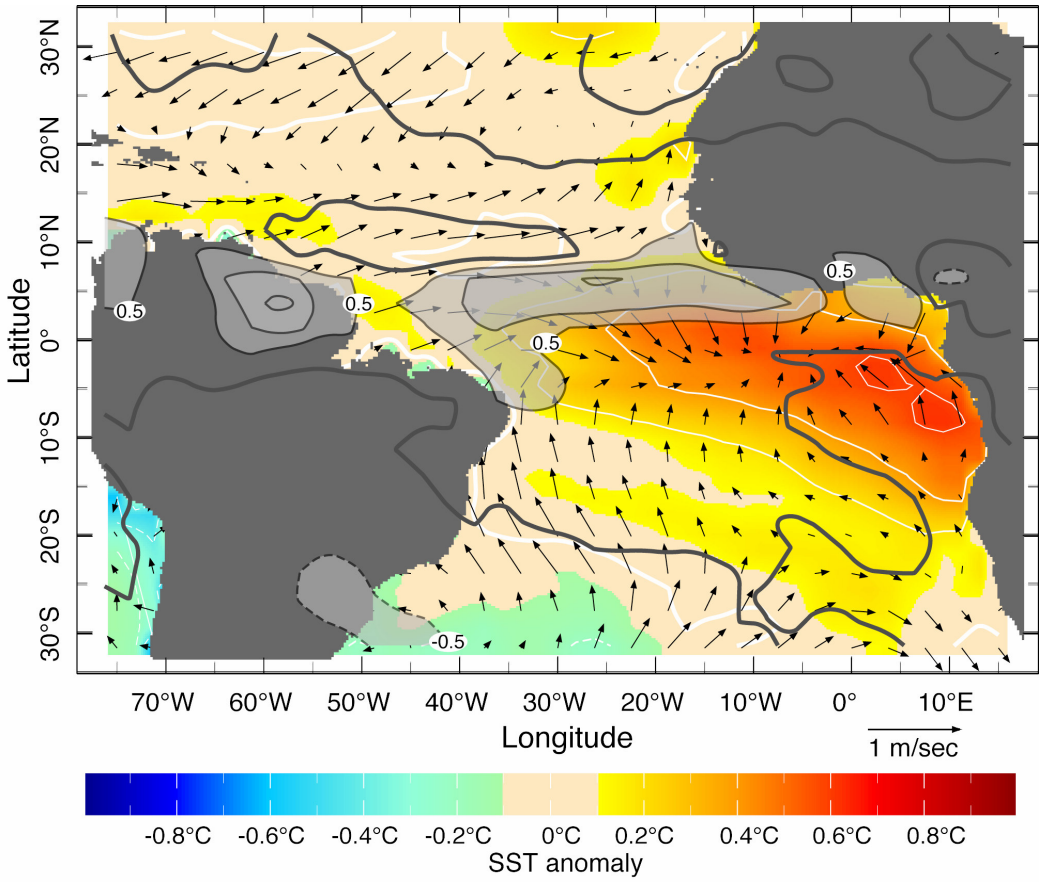

Figure 1.1. (Continued) (b) boreal summer (June-August). The black contours depict the first EOF of the regional rainfall anomaly (from GPCP data, 1979-2001) in units of mm/day. This EOF explains 23% of the seasonal variance. The colored field is the SST anomaly regressed on the principal component time series of the rainfall EOF (units are °C, see scale below; white contours every 0.2° are added for further clarity). Arrows depict the seasonal mean surface wind vector in m/sec, regressed on the same time series. (From Kushnir et al., 2004)

frequency and intensity of Atlantic hurricanes are found to be related to the SST anomaly in the subtropics (Gray, 1990; Kushnir, 1994). Therefore, understanding the mechanisms of tropical Atlantic variability (TAV) is not only of academic interests, but also of practical value.

The climate variability in the tropical Atlantic sector consists mainly of two distinctive dominant anomalous circulation patterns that manifest themselves in different seasons. During months of March-April when the warmest sea surface temperature appears in the deep tropics, a low-frequency covarying fluctuation of tropical Atlantic SST and trade winds straddling the ITCZ dominate (Figure 1.1a). Because the coupled variability in this pattern exhibits a north-south contrast, it is often called the tropical Atlantic "meridional mode" of variability. This mode is believed to involve thermodynamic air-sea feedback in the deep tropics combined with external influences from tropical Pacific and North Atlantic. During months of June-August, when the cold tongue is strongest in the equatorial eastern Atlantic, coupling between the equatorial SST anomaly in the eastern basin and the anomalous equatorial trade winds dominates the tropical Atlantic (Figure 1.1b). Because the coupled variability in this pattern shows east-west gradient along the equator, it is often referred to as the "zonal mode" or "equatorial mode", or the "Atlantic Nino" due to its resemblance to the Pacific El Nino. The similarity of this mode to Pacific El Nino hints at the important role of upper ocean dynamics in terms of changes of equatorial trade winds and thermocline variations.

The study by Zebiak (1993) showed that the air-sea feedback is insufficiently strong to make the zonal mode a self-sustained oscillation. The studies by Chang et al (1997, 2001) have reached a similar conclusion for the meridional mode. Together, these studies imply that the TAV is achieved through the synthesis of the meridional and zonal modes, and external or remotely forced perturbations. So far, at least two external sources of forcing have been identified: El Nino-Southern Oscillation (ENSO) being one and the North Atlantic Oscillation (NAO) being another one. Both of them peak in boreal winter, although one is a tropical phenomenon while the other one is an extratropical phenomenon. On the basis of the sources of forcing, TAV can be divided

into two parts: one part is induced by the local air-sea feedback and NAO, both of which are intrinsic to the Atlantic Ocean, and the other part is induced by the remote influence of ENSO, a forcing that comes from outside the Atlantic Ocean. In this study, we will only focus on the latter.

As the strongest fluctuation of the climate system at seasonal to interannual time scale, ENSO has been demonstrated by numerous observational and modeling studies to have a major influence on the boreal spring conditions in the tropical Atlantic (Covey and Hastenrath, 1978; Horel and Wallace, 1981; Hastenrath et al. 1987; Curtis and Hastenrath 1995; Norbe and Shukla, 1996; Enfield and Mayer, 1997; Saravanan and Chang, 2000; Alexander and Scott, 2002). The most significant influence of a warm ENSO in the Atlantic sector during boreal spring that was found by these studies includes: 1) a zonal seesaw in sea level pressure between the eastern equatorial Pacific and Atlantic Oceans during the onset and peak phase of ENSO, with a high sea level pressure anomaly in the northern tropical Atlantic, 2) a weakening in the meridional sea level pressure gradient between the North Atlantic subtropical high and the ITCZ accompanied by weaker than average northeasterly trades, 3) a warming of SST during boreal spring following the mature phase of ENSO, and 4) a northward shift of the ITCZ and a decrease in rainy season precipitation in northeastern Brazil (Chang et al, 2004).

Although the effects of ENSO on TAV have been well defined, the mechanism responsible for them is not entirely established. The mechanism proposed by Giannini et al. (2000) involves an anomalous Walker circulation (Kidson, 1975), which is set up by the eastward shift of the active atmospheric convection region in the Pacific and causes air to ascend over the eastern equatorial Pacific and descend over western equatorial Atlantic. This tropical atmospheric bridge effect is proposed to be the cause of the zonal seesaw in SLP (Giannini et al., 2000). The seesaw pattern (Figure 1.2) has a direct effect on convergence in the Caribbean basin and also has an indirect effect on SST by modulating wind speed and thus the latent heat flux. A recent modeling study by Saravanan and Chang (2000) provided supporting evidence for the role of Walker circulation.

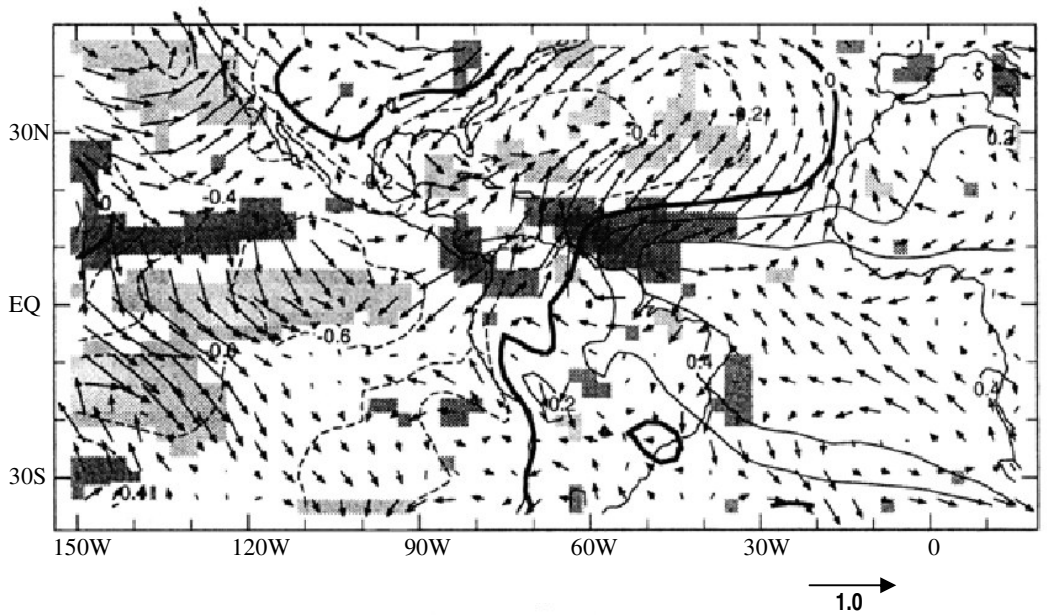

Figure 1.2. Correlation map of the Nino-3 index, averaged over Dec (0)-Jan (+1), with NCEP-NCAR reanalysis SLP (contours), winds (arrows), and wind divergence (shading) in Jan-Feb (+1). Contour interval is 0.2; negative values are dashed, positive values are solid, and the thick black line is the zero correlation line. Shading is light for negative correlation values, dark for positive ones; absolute value less than 0.3 are not shaded. (From Giannini et al., 2000)

Another mechanism, which is consistent with the Walker mechanism but posed as a different way of interpreting the Walker mechanism, is proposed by Chiang and Sobel (2002). This mechanism is referred to as Troposphere Temperature (TT) mechanism. Chiang and Sobel used observational data and a single-column atmospheric model coupled to a slab ocean mixed layer to explain how changes in tropical troposphere temperature induced by ENSO are connected to SST and precipitation in the tropical Atlantic. In this TT mechanism, the response of the coupled system, such as surface heat flux variation and precipitation, depends on the mixed layer depth. They further argued that the air-sea temperature and humidity difference is a driver of ENSO-related remote influence, particularly during the initial phase of ENSO influence. The wind-induced heat flux comes into play during the decay phase of ENSO (Figure 1.3). This mechanism is consistent with the finding by Saravanan and Chang (2000) that in the Walker circulation connection a significant portion of surface heat flux change in the tropical Atlantic is attributable to changes in air-sea surface temperature and humidity difference.

In addition to the mechanisms that are related to anomalous Walker circulation, an alternative way to explain the linkage between ENSO and TAV is the tropical-extratropical interaction, which relies on the Pacific-North-American (PNA) teleconnection pattern, originating in the tropical Pacific and propagating via the extratropics into the northwestern region of the tropical Atlantic in the form of a stationary Rossby-wave train (Wallace and Gutzler, 1981; Horel and Wallace, 1981). This pattern terminates with anomalously low SLP (during a warm ENSO) in the subtropical western Atlantic with a center of action off the coast of the southeastern United States which persists from January to April following a warm ENSO event. It is hypothesized by Giannini et al (2000) that the presence of such a SLP anomaly will act in concert with the high SLP anomaly generated by the Walker mechanism in the equatorial Atlantic to strengthen the meridional SLP gradient in the north tropical Atlantic, hence reducing the northeasterly trades and cause a warming in the SST. However, the exact role of this PNA-related ENSO remote influence mechanism has not

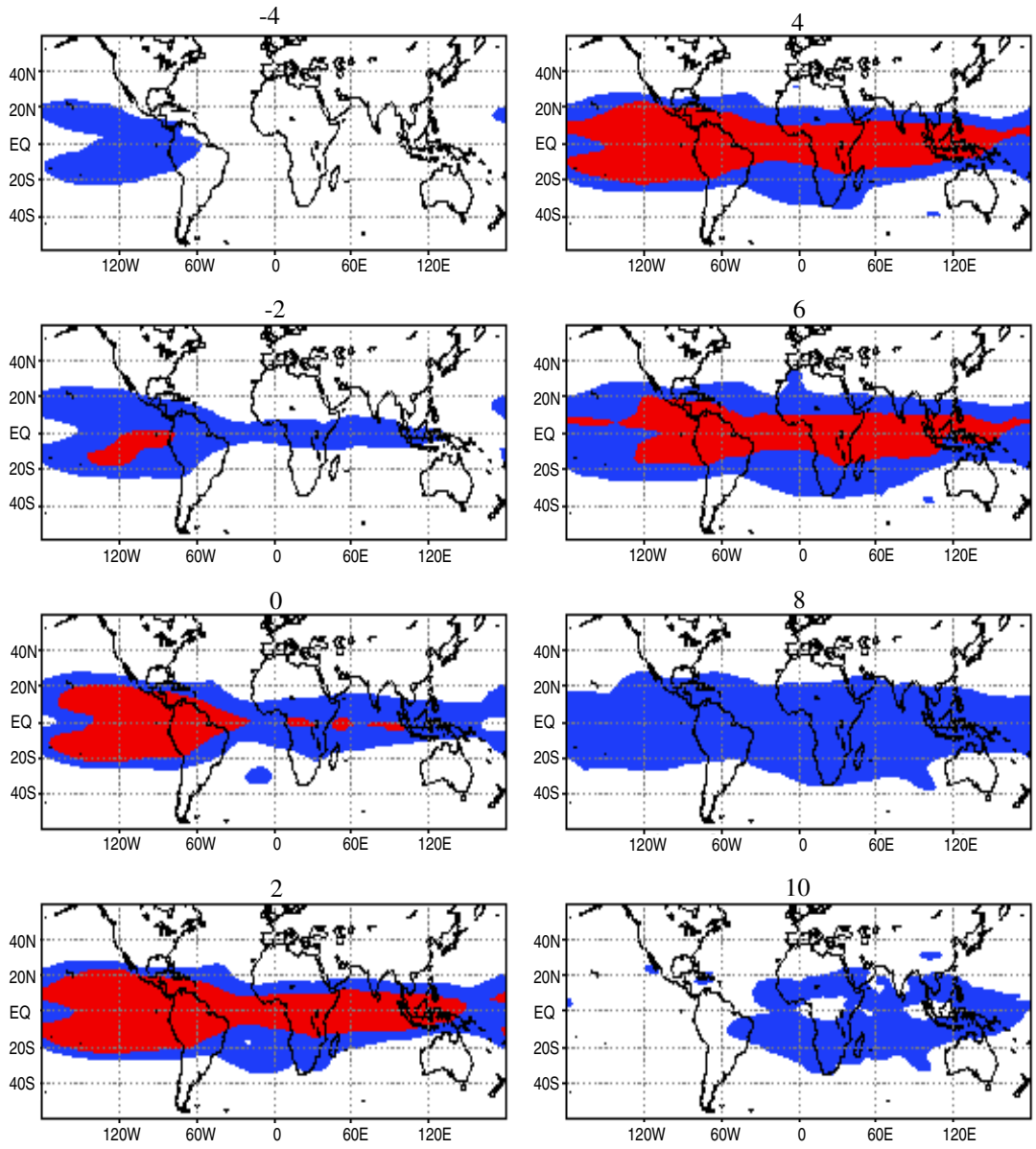

Figure 1.3. Lag correlation between the Nino-3 index and microwave sounding unit (MSU) channel-2 temperature for 1979-99. The blue shading is for 0.3<r<0.6, and the red shading is for r>0.6. The number above each panel indicates the lag or lead in months. Negative number implies MSU leads Nino-3 index; positive numbers, Nino-3 index leads MSU. (From Chiang and Sobel, 2002)

been fully explored.

All the above-mentioned mechanisms affect SST in the tropical Atlantic by changing the surface heat flux. Latif and Barnett (1995) presented a different mechanism, based on a dynamical consideration. They argued that Pacific ENSO would have an influence on the equatorial south Atlantic (ESA) SST through an adjustment of the entire tropical Walker cell. As convection moves eastward during an El Nino, the anomalous Walker circulation enhances the equatorial trades in the western Atlantic, which in turn produces a cooling in the eastern equatorial Atlantic. Therefore, with this mechanism we would expect a negative correlation between equatorial Atlantic SST and ENSO-induced SST anomalies.

2. Issues to Be Addressed

Although the remote influence of ENSO on TAV has been investigated by many studies (e.g., Covey and Hastenrath, 1978; Hastenrath et al., 1987; Curtis and Hastenrath, 1995; Enfield and Mayer, 1997; Klein et al., 1999; Giannini et al., 2000; Saravanan and Chang, 2000; Alexander and Scott, 2002; Czaja et al, 2002; Giannini et al., 2004), these studies are mainly focused on climate variabolity during boreal winter to spring, and the proposed mechanisms are only applicable to the NTA where the robust SST response to ENSO forcing is observed. Recent modeling studies indicate that much of the ENSO remote influence signal can be captured by atmospheric general circulation models (AGCMs) coupled to a slab ocean or mixed layer ocean (e.g., Alexander et al., 2002; Chang et al., 2003), suggesting that ocean dynamics are less important in this region. But a careful assessment of the importance of ocean dynamics in this region has not been made by previous studies because coupled climate models used in these studies employ a mixed layer model or the slab ocean, where ocean dynamics are absent.

The situation in the ESA is more perplexing, in this region there appears to be an inconsistency in the existing literature. On one hand, the observational analysis (e.g. Zebiak, 1993; Enfield and Mayer, 1997) finds no statistical evidence for linkage between

the SST variability in the Gulf of Guinea and Pacific ENSO, suggesting that the coupled variability in the equatorial Atlantic is largely independent of ENSO. On the other hand, there is some evidence that certain events in the equatorial Atlantic are indeed linked to strong ENSO events. For example, Delecluse et al. (1994) and Carton and Huang (1994) showed that the strong 1984 warming in the eastern equatorial Atlantic resulted from the zonal wind anomaly is related to the severe 1982-83 ENSO.

From the viewpoint of the atmospheric bridge effect, the TT mechanism would predict a warming in the ESA region simply because the El Nino-induced tropical troposphere warming is symmetric about the equator and covers the entire tropical belt between 20°S and 20°N. Indeed, the simulation of an AGCM coupled to a mixed layer ocean by Alexander et al. (2002) shows a significant positive correlation between the SST in the ESA region and ENSO. The warming, however, may be weaker south of 10°S because of the weaker vertical coupling between the boundary layer and free troposphere due to higher static stability, as suggested by Chiang and Sobel (2002). On the other hand, from the viewpoint of dynamic air-sea interaction, the mechanism proposed by Latiff and Barnett (1995) would predict a cooling in the ESA region following a warm ENSO event.

Inconsistencies among the previous findings lead us to hypothesize that ocean dynamics are very important in the equatorial Atlantic and in the STA, in particular during the late boreal spring to summer. This hypothesis is based on the following considerations: 1) Conceptually, both the thermodynamic and dynamic mechanisms are viable for establishing a link between ENSO and Atlantic Nino; 2) The cross-equatorial southeasterly wind anomaly associated with the northward cross-equatorial SST gradient in the tropical Atlantic during boreal spring (Curtis and Hastenrath, 1995; Nobre and Shukla, 1996; Enfield and Mayer, 1997) may cause changes in SST via Bjerknes feedback (Bjerknes, 1969), and Ekman feedback (Chang and Philander, 1994); 3) the thermocline depth is shallowest during the boreal summer, which favors both the Bjerknes feedback and Ekman feedback.

The overall objective of this study is to explore the importance of ocean

dynamics in contributing to SST variability, the key climate variable linking the ocean and atmosphere, in response to the remote ENSO influence. A particular focus will be placed on the oceanic processes that control SST variability in ESA region. To accomplish our objectives, a reduced physics-coupled global circulation model (RP-CGCM) is developed and four ensembles of coupled experiments are conducted with different configurations. The specific questions that will be addressed in the study include:

a) How does SST evolve in response to the remote influence of ENSO?

b) What is the difference between the forced response in boreal spring and the one in boreal summer?

c) How does the remote ENSO influence work during the boreal summer?

d) How important are the ocean dynamics in the remote influence of ENSO?

e) What are the dominant ocean dynamics in the SST response to remote ENSO forcing?

3. Overview

This study is organized as follows. Chapter II describes the numerical model and a suite of experiments to be carried out. In Chapter III, the coupled model is validated, and the model simulated tropical Atlantic response is analyzed using various statistical analysis methods. The relative importance of various oceanic processes contributing to the Atlantic SST response is further assessed in Chapter IV. Chapter V summarizes the major findings and outlines future work.

CHAPTER II

METHODOLOGY AND APPROACH

1. Existing Approach

Studies of TAV have been conducted from both the observational and modeling approaches. The observational analyses range from simple index-based correlation and regression analyses to multivariate statistical analyses, such as Empirical Orthogonal Function (EOF) and Singular Value Decomposition (SVD) analyses. Correlation and regression analyses are used to establish a first order relationship between two variables. They have been extensively used to derive the remote influence of ENSO on TAV (e.g., Enfield and Mayer, 1997; Giannini et al, 2000). EOF and SVD analyses are very helpful in identifing spatially uncorrelated dominant patterns of variables of interest (e.g., Servain and Legler, 1986; Wallace et al., 1992; Chang et al., 2001; Huang et al, 2004). Composite analysis is also widely used and effective in determining the time evolution of a variable of interest (e.g., Curtis and Hastenrath, 1995; Giannini et al., 2004). However, the results of these studies are usually less robust because the records of available observations are usually too short to make the statistical analysis conclusive. Moreover, some climate variables such as heat fluxes, thermocline depth, etc., which are crucial to the air-sea coupled climate system, are either obtained indirectly or missing from the observations. Thus the studies based entirely on observations are unable to provide a comprehensive look at the dynamical processes controlling coupled climate variability in the tropical Atlantic.

With the increase in computer speed, numerical modeling has been widely employed in TAV studies to further test and explore what has been learned from observations. Earlier numerical studies that addressed the mechanisms of TAV are based on uncoupled models, that is, the conditions of atmosphere/ocean are specified and the

ocean/atmosphere just passively responds to these forcings. Although these models can provide useful insights of TAV, we can only speculate on the feedbacks at work because the active coupling between atmosphere and ocean is missing from the models. In some circumstances, interpretation of results based on uncoupled models could be questionable. To better represent the air-sea feedbacks of the climate system, some recent numerical studies have employed coupled models, which in general fall into three categories:

1) Intermediate Coupled Model (ICM). In these models, the physics of both atmospheric and oceanic components are simplified (e.g., i.e. Zebiak 1993; Xie and Tanimoto 1998). This type of model is usually used to explore the role of a specific process in the coupled system. The advantages of these models are that they are economic while still keeping the essential physics of the atmosphere and ocean. The simplified physics of these models sometimes may cause considerable system bias and produce unrealistic results.

2) Reduced Physics-Coupled GCM models (RP-CGCM). These models couple either an atmospheric or an oceanic global circulation model (GCM) to a reduced physics model for the other component. Examples include the hybrid coupled model of Chang et al (1997, 2001) and the coupled Community Climate Model version 3 (CCM3)-ocean mixed layer model of Saravanan and Chang (1999). The sophisticated component of these coupled models allows a more detailed examination of the underlying dynamics in the coupled system. However, the simplified component in these models usually does not contain any dynamical processes. As we know, the tropical Atlantic Ocean has one of the most complex circulation systems in the world's oceans. The North Equatorial Countercurrent (NECC), North Equatorial Current (NEC), South Equatorial Current (SEC), Equatorial Undercurrent (EUC), and North Brazil Current (NBC) constitute the upper ocean circulation system in the tropical Atlantic (Figure 2.1). Since these currents are not only capable of transporting large amount of heat horizontally but are also responsible for converting cold subsurface water into warm surface water via upwelling, they can affect upper ocean thermal structures, thereby

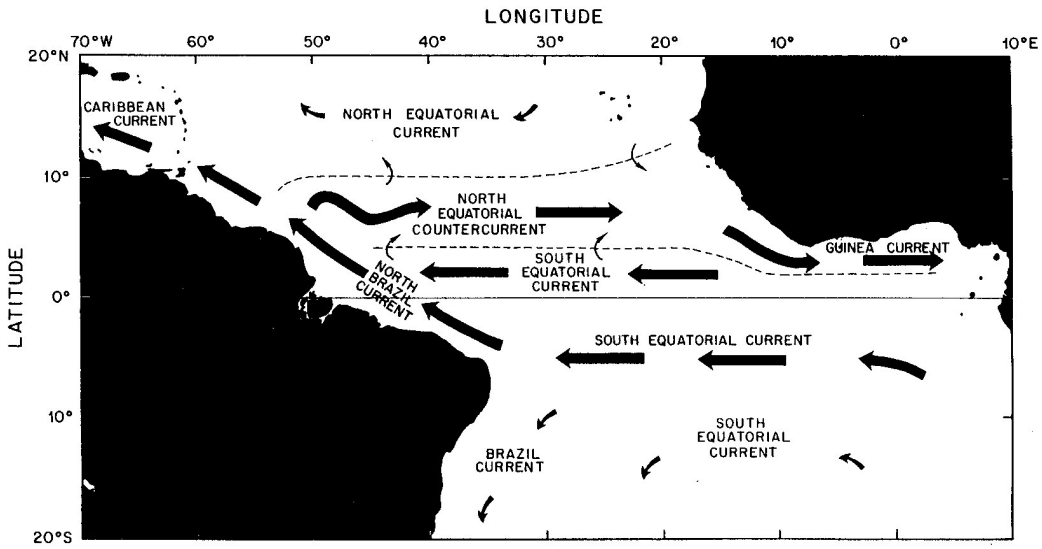

Figure 2.1. Schematic diagram of surface current system in the tropical Atlantic Ocean. (From Fratantoni et al., 2000).

having an impact on the SST variability especially in coastal and equatorial regions. Absence of these ocean dynamics in the coupled model can give rise to large system biases.

3) Coupled GCM models (CGCM). Both components in these models contain more complete physics and thus, at least theoretically, they are capable of simulating more realistic climate variability. But a common problem of these fully coupled models is that the simulated mean state of the climate usually has serious biases, which may induce unrealistic climate variability. For example, the mean SST shown by Davey et al (2000) is too cold in the tropical Atlantic warm pool and too warm in the cold tongue region. This erroneous mean SST field causes the mean position of the ITCZ move too close to the equator when compared with reality, giving rise to an unrealistic seasonal cycle in the ITCZ and distorting the coupled physics within the deep tropics. The recent

study by Huang et al (2004) also has the similar problem in their fully coupled model. An artificial "warm pool" is formed to the south of the equator extending from the Brazilian coast nearly to the eastern boundary. This unrealistic feature causes the SST fluctuations around the equator to be largely unconnected to the changes in the southeastern part of the ocean. This results in unrealistically weak SST variability at the Angola coast.

2. Current Modeling Approach

In this study, we develop a RP-CGCM, which is more sophisticated than other previous models in this class, and consists of an intermediate complexity ocean model coupled to a state of the art atmospheric GCM. To sidestep the bias in the mean state, the model is anomaly coupled only within the tropical Atlantic sector although the atmospheric GCM covers the whole globe. Outside the coupled region, observed SST is prescribed as the atmospheric model's lower boundary condition. The model's mean state is maintained by applying heat flux correction. Compared with the models employed in previous studies, this new regional-coupled model offers four major advantages: 1) the sophisticated atmospheric GCM simulates both internal and SST forced variability, thereby permitting a realistic simulation of the atmospheric bridge effect, remote forced feedback and coupled response. This overcomes the shortcoming of ICMs, where internal atmospheric variability and thermodynamic air-sea interaction are oversimplified; 2) The simple ocean model contains the essential physics of tropical oceans, which are important to local air-sea interaction but has been neglected in the previous RP-GCM studies. Moreover, its high computational efficiency permits a large number of process oriented numerical experiments; 3) The anomaly coupled approach assure that the SST anomalies will not be contaminated by an unrealistic model mean state, which has been a common problem with fully coupled models; 4) The regional coupling approach allows us to avoid the issue of systematic biases in ENSO simulation, which can distort the ENSO remote influence on TAV. This approach is justified by

previous studies (e.g. Alexander et al., 2002), which suggest that the influence of the tropical Pacific on the tropical Atlantic is predominantly one way.

Like the other coupled models, however, this coupling approach also has its limitations. The most obvious limitation is that all the processes involving deep ocean circulations, which have been demonstrated by some studies as having an impact on climate variability, cannot be simulated. Another limitation is the south and north artificial boundaries of the ocean model, which prevents the water in the tropical region from being exchanged with water at higher latitudes. But the climate variability related to deep circulation variability, which is strong at decadal or longer time scales, is very weak at interannual time scales, at which the ENSO influence is significant. Existing work has shown that the horizontal advection is less important in the off-equatorial regions. Thus, the missing deep ocean processes and the artificial boundaries are not the concern of this study. The other two major limitations of this coupling approach lie in the simple treatment of surface current and parameterization of subsurface temperature of the ocean. This may indeed cause some model errors, but these errors do not have much influence on model's ability in capturing major features of TAV.

2.1. Atmosphere Model

The atmosphere model used in this study is the Community Climate Model Version 3 (CCM3), a spectral model developed at the National Center for Atmospheric Research. CCM3 is a state-of-the-art atmospheric general circulation model (AGCM) which incorporates a comprehensive suite of physical parameterizations including non-local boundary layer parameterizations and improved radiative and convective parameterizations (Kiehl et al., 1998). Land surface processes in CCM3 are represented by a one-dimensional interactive land surface model (Bonan, 1998). The standard configuration for the CCM3 is used throughout this study, with triangular truncation at wave number 42 in the horizontal and 18 levels in the vertical, covering the whole globe.

2.2. Ocean Model

a. Model Formulation

The ocean model used in this study is an extended $1\frac{1}{2}$ layer reduced gravity model (Figure 2.2), which was first introduced by Cane (1979) to study ENSO. In this model, mass, momentum, and heat obey the conservation laws in the upper layer, and the lower layer is assumed to be infinitely deep and motionless to keep the kinetic energy finite. If the density in the upper layer is assumed to vary linearly with temperature, the momentum, continuity, and thermodynamic equations for the upper

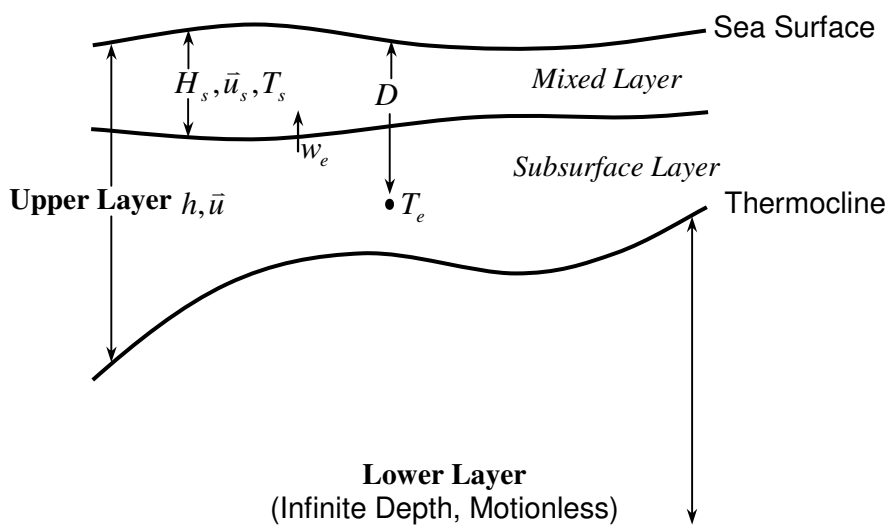

Figure 2.2. Schematic diagram of the vertical structure of the ocean model. The model consists of an active upper layer with mixed layer embedded and a motionless lower layer of infinite depth.

layer can be written as

$$\frac{\partial \vec{u}}{\partial t} + \vec{u} \cdot \nabla \vec{u} + f\vec{k} \times \vec{u} - \frac{1}{2} h \nabla b + \nabla (bh) = \frac{\vec{\tau}}{h} + \mu \nabla^2 \vec{u} - \frac{1}{h} w_e H(w_e) \vec{u} \tag{2.1}$$

$$\frac{\partial h}{\partial t} + \nabla \cdot (h\vec{u}) = w_e \tag{2.2}$$

$$\frac{\partial T}{\partial t} + \vec{u} \cdot \nabla T = \frac{Q}{\rho_0 C_p h} + \kappa \nabla^2 T - \frac{1}{h} w_e H(w_e)(T - T_r) \tag{2.3}$$

The variables in the above equations are described in Table 2.1.

Table 2.1. Description of variables used in the equations of ocean model

Variable	Description
$\vec{u}$	horizontal velocity vector
w_e	entrainment velocity at the base of mixed layer
h	thickness of upper layer
$\vec{\tau}$	wind stress vector
b	buoyancy in the upper layer
T_r	reference temperature
T	surface temperature
Q	heat flux
ρ_0	density
C_p	thermal expansion coefficient
μ	horizontal viscosity coefficient
κ	diffusivity coefficient
$H(x)$	heaviside step function $H(x) = 1$ when $x > 0$ $H(x) = 0$ when $x \leq 0$

b. Parameterization of Entrainment

To close the system equations, w_e must be parameterized in terms of internal oceanic variables and external atmospheric forcing. In this study, we adopt the parameterization that was originally proposed by Cane (1979) for the vertical entrainment process. In Cane's model, the mixed layer is treated as a slab embedded into the upper layer and therefore the dynamic equations (2.1) and (2.2) must be linearized to make the embedding of the slab possible. The buoyancy b in equation (2.1) is treated as a constant. The horizontal velocity in the mixed layer is determined by

$$\vec{u}_s = \vec{u} + \vec{u}_e (H - H_s) / H , \tag{2.4}$$

where $\vec{u}_e$ is the velocity of the Ekman flow in the mixed layer, which is given by

$$r_s \vec{u}_e - f\vec{k} \times \vec{u}_e = \frac{\vec{\tau}}{\rho H_s} , \tag{2.5}$$

where r_s is the Rayleigh friction coefficient for the surface Ekman flow. So the entrainment velocity, w_e, is determined by the divergence induced by Ekman pumping in the surface mixed layer:

$$w_e = H_s \nabla \cdot \vec{u}_s \tag{2.6}$$

Therefore, the surface temperature can be calculated from

$$\frac{\partial T_s}{\partial t} + \vec{u}_s \bullet \nabla T_s = \frac{Q}{\rho_0 C_p H_s} + \kappa \nabla^2 T_s - \frac{1}{H_s} w_e H(w_e)(T_s - T_e) \tag{2.7}$$

in which T_e is the temperature of entrained water beneath the mixed layer.

Since the model is not able to predict the variation of subsurface temperature, it is parameterized in terms of the variation of thermocline depth, i.e., upper layer depth h (Zebiak and Cane 1987; Seager et al. 1988, Battisti and Hirst 1989; Chang 1994; Wang and Li 1995). In this research, a multivariate linear relationship is used to calculate the variation of entrained subsurface temperature, T_e', using D', where $T_e' = T_e - \overline{T}_e$, and $D' = D - \overline{D}$ ($\overline{T}_e$ and $\overline{D}$ denote the climatological annual cycle of subsurface

temperature T_e and subsurface depth D, respectively. $D = \frac{H_s + h}{2}$ (Figure 2.2).

To obtain the linear relationship between T_e' and D', a regression analysis on a reduced EOF state space is employed. This procedure consists of the following steps:

1) First, the ocean model is forced with monthly averaged ensemble mean wind stress from January 1980 to December 1994 that were simulated by the CCM3 Global Ocean Global Atmosphere (GOGA) experiment, where CCM3 is forced with monthly averaged observed SSTs in the global oceans starting with different initial conditions (Chang 2000). Once the monthly averaged thermocline depths, h, are computed by the ocean model, the subsurface depths, D, and the departure from its annual cycle, D' is derived. Then D' is further expanded in terms of EOFs,

$$D' = E \bullet A, \tag{2.8}$$

where E and A are the EOFs and corresponding principal component (PC) time series, respectively.

2) Upon obtaining D in step 1, the corresponding subsurface temperature, T_e, is derived from an Ocean Data Assimilation (ODA) data product from Geophysical Fluid Dynamics Laboratory (GFDL). The departure from the climatological annual cycle, T'_e, is expanded in terms of EOFs,

$$T_e' = F \bullet B \tag{2.9}$$

where F is the EOFs of T'_e and B is the PC time series.

3) A linear relationship between D' and T'_e is derived by a multivariate regression of the PC time series of D' and T'_e, i.e.,

$$B = c \bullet A \tag{2.10}$$

where c is a regression coefficient matrix and is determined by

$$c = (BA^T)(AA^T)^{-1} \tag{2.11}$$

The above procedures establish a simple statistical relationship between subsurface temperature and subsurface depth. It enables the simple ocean model to simulate subsurface temperature on the basis of thermocline depth fluctuation, which is determined by the dynamical equations (2.1) and (2.2).

For reader's convenience, all the variables used in the parameterization of entrainment are listed in Table 2.2.

Table 2.2. Description of variables used in the parameterization of entrainment

Variable	Description
u_s	horizontal velocity in mixed layer
H_s	thickness of mixed layer
T_s	temperature of mixed layer
u_e	velocity of Ekman flow in mixed layer
r_s	Rayleigh friction coefficient
T_e	subsurface temperature
$\overline{T}_e$	annual cycle of T_e
T_e'	fluctuation of T_e
D	$(H_s + h)/2$
$\overline{D}$	annual cycle of D
D'	fluctuation of D
E	EOFs of D'
A	PC time series of D'
F	EOFs of T_e'
B	PC time series of T_e'
c	regression coefficient matrix

c. Model Configuration

The ocean model covers the tropical Atlantic Ocean from 30°S to 30°N with zonal resolution of 2° and meridional resolution of 1° throughout the entire domain. Realistic basin geometry is used. Artificial solid boundaries are used at the south and north boundaries where 5°-width sponge layers are introduced to surpress artificial coastal Kelvin waves. SST within the sponge layers is gradually relaxed to the observed climatology prescribed for the atmosphere model.

Finite difference equations are formulated on staggered "C" grid with leapfrog time stepping and a Robert filter with a coefficient of 0.005. The mean thermocline depth is taken to be 150 meters in the model. The model mixed layer depth (Figure 2.3) is taken from the spatially varying observed value estimated from Levitus data (1982). Values of parameters, ρ_0, α, C_p are set to 1.0 g cm^{-3}, 2.0 x 10^{-4} K^{-1}, and 4.2 x 10^7 J g^{-1} K^{-1}, respectively. Eddy viscosity and diffusivity coefficients μ and κ are taken to be 4.0x10^8 cm^2 s^{-1}. Reyleigh friction coefficient in the Ekman layer is chosen to be 1.667 d^{-1}. The buoyancy b is regarded as a constant and its value is set to 5.606 cm s^{-2}.

To maintain a realistic mean climatological state in the ocean model, a heat flux correction, Q_c, is added to the surface heat flux, Q, in the thermodynamic equation (2.7). This correction term is calculated by replacing Q_c with a restoring term, $-\lambda(T_{c\lim} - T_s)$, where $T_{c\lim}$ is the observed annual cycle and is a relaxation coefficient whose time scale is set to 5 days, and integrate the model for 15 years. Then the mean annual cycle of the restoring term can be computed and kept as a prescribed flux correction. This flux correction is calculated separately for each experiment described in the following section.

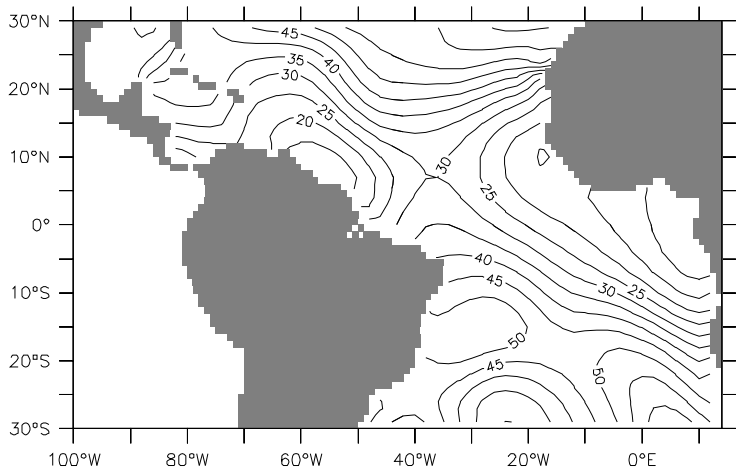

Figure 2.3. Mixed layer depth in the tropical Atlantic Ocean taken from the spatially varying observed value estimated from Levitus data (1982). Contour interval is 5 m.

3. Experiment Design

Four numerical experiments are carried out in this study. They are the Control Experiment, No-advection Experiment, No-entrainment Experiment, and Slab Ocean Experiment (referred to as CTRL, NADV, NENT, and SLAB experiments, respectively). The CTRL experiment, which includes all ocean dynamics and thermodynamics described by equations (2.1)-(2.3), is designed to single out the climate variability which is in response to the remote ENSO forcing. While in the NADV experiment, the horizontal advection term $\vec{u}_s \bullet \nabla T_s$ in the thermodynamic equation (2.7) is disabled. This experiment is designed to assess the importance of the horizontal advection process in ENSO influence. To assess the importance of entrainment from subsurface, the vertical advection term, $\frac{1}{H_s} w_e H(w_e)(T_s - T_e)$, in equation (2.7) is disabled in the NENT

experiment. The SLAB experiment contains no ocean dynamics, and is designed to investigate how much ENSO forced TAV can be retained by a slab ocean.

In all these experiments, the ocean model is anomaly coupled to the atmosphere model only within the tropic Atlantic Ocean (Figure 2.4) from 30°S and 30°N. Outside the tropical Atlantic, observed SST (Smith et al., 1996) is prescribed. So the ENSO signal from the Pacific can further influence the tropical Atlantic through the atmospheric bridge. The local feedback in the tropical Atlantic is captured by this regional coupling. The anomaly coupling procedure follows Kirtman et al (2002): the ocean affects the atmosphere only through the SST anomaly, and the atmosphere affects the ocean only through surface wind anomaly and heat flux anomaly.

Each experiment contains an ensemble of twelve runs, and each run is integrated for 20 years starting in January 1980. Initial conditions of the ocean model, which come from a spin-up run, are exactly the same in all the experiments. The atmospheric initial condition differs slightly among the same ensemble of runs to allow the atmosphere to have different realizations of chaotic internal variability. Therefore, the remote influence of ENSO can be effectively singled out by doing an ensemble mean for each experiment's ensemble. Within the same experiment, the variability induced by the remote influence of ENSO is the same because the prescribed SST in the non-coupling oceans is the same, while the variability induced by the atmospheric internal variability differs because of slightly different initial conditions. By taking the ensemble mean, this internal atmospheric variability is removed.

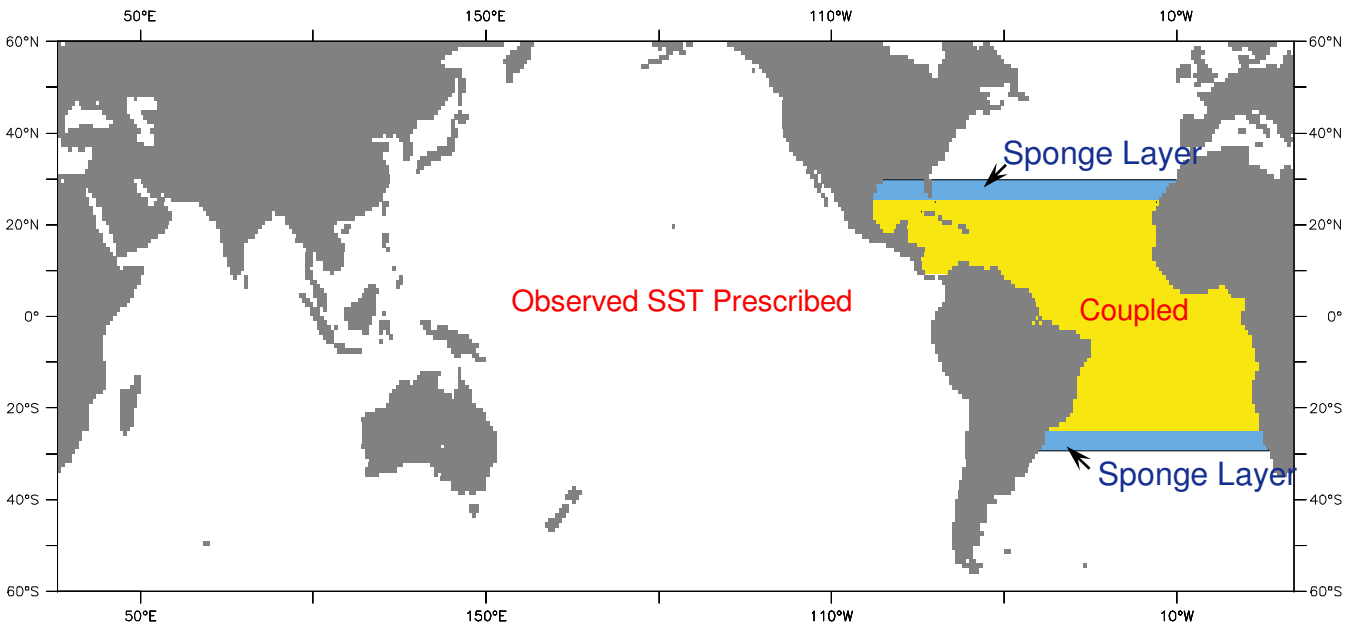

Figure 2.4. Regional coupling strategy over the global domain. The model is anomaly coupled in the yellow region. The rest of ocean regions are forced with the observed SST. Two zonal belts in blue are blending zones for SST, also serve as sponge layers of the ocean model to suppress unrealistic Kelvin waves.

CHAPTER III

REMOTE INFLUENCE OF ENSO

1. Model Validation

Before using the newly developed modeling tool to investigate the phenomena and the underlying mechanisms of the remote influence of ENSO on TAV, it is necessary to first validate that the model is capable of capturing the key features of ENSO influence that have been observed. At minimum, the model should capture the dominant modes of variability, such as the meridional mode and the zonal mode, as well as key features associated with the remote influence of ENSO. For this reason, we will first compare the first two leading modes of SST variability as well as their seasonality with the observations. This will serve as a general assessment of the model's skill in capturing the main features of climate variability in the tropical Atlantic. This comparison focuses on SST because it is the key climate variable in the coupled system and has important implications for seasonal climate prediction in this region.

Since the main objective of this study is to investigate the remote influence of ENSO, it is essential to examine the ability of the model in simulating the wind and SST responses to remote ENSO forcing. For this reason, we examine wind and SST evolution following ENSO events via a composite analysis. Theoretically, if the number of ENSO events is sufficiently large, the composite analysis should give a canonical view of ENSO's influence on TAV.

Given that we have about 50 years of observed SST (1950-1999) and an ensemble of 12 coupled model runs forced with 20 years of observed SST from 1980-1999, we use the entire data set to make our comparison. We are aware of the potential problem of using two different time periods. But the intention here is simply to make the statistical analysis as robust as possible.

1.1 EOF Analysis

a. Leading Modes

Figure 3.1 shows the first two leading EOFs (associated time series have been normalized by their standard deviations) that are derived from Reynold's SST anomalies (Smith et al., 1996) over the period from 1950-2000. The SST pattern in Figure 3.1a, which shows a strong zonal gradient in the equatorial region, is the so-called "zonal mode", while the pattern in Figure 3.1b which shows a strong cross-equatorial gradient, is the so-called "meridional mode". To compare with observations, a similar EOF analysis was performed by concatenating all 12 20-year CTRL runs together end to end. The result is shown in Figure 3.2. Note that all the time series that are associated with the EOFs shown in Figures 3.1 and 3.2 have been normalized by their standard deviations, so that the amplitude of each mode is reflected by the EOF.

By comparing Figures 3.1 and 3.2, one can see that the simulation is overall in a good agreement with the observation. Both the zonal mode and the meridional mode are well reproduced by the model. The simulated zonal mode (Figure 3.2a) bears a close resemblance to the observed one (Figure 3.1a), both in terms of spatial distribution and amplitude, except that 1) the total variance explained by this mode (28%) in the simulation is less than that (34%) in the observations; and 2) there is stronger SST variability off the coast of Africa between 15°S-10°S in the observations than in the simulation. The north-south contrast in the distribution of SST anomaly, which is a key feature of the meridional mode, is clearly shown in both the observation (Figure 3.1b) and simulation (Figure 3.2b). But the amplitude of the simulated meridional mode is weaker than the observed one. Another notable difference is that the center of the maximum amplitude in the northern hemisphere simulated by the model is closer to the center of NTA, but in the observations it is closer to the coast of Africa. In the southern hemisphere, the simulated variability is much weaker than the observed variability and

(a)

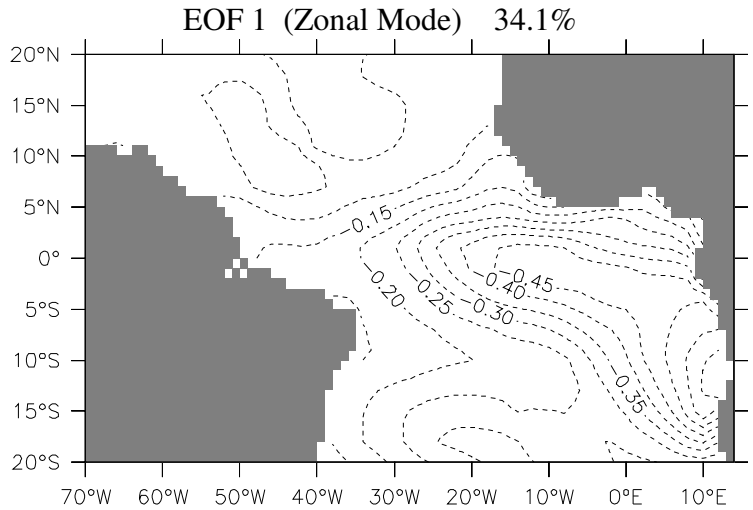

(b)

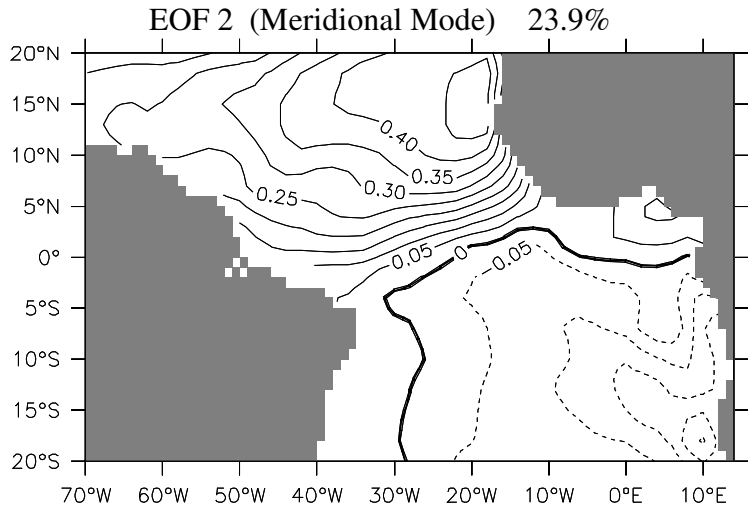

Figure 3.1. (a) First and (b) second leading EOFs derived from Reynolds' SST (Smith et al., 1996) over the period from 1950 to 2000 (The associated PC time series have been normalized by their standard deviations). Contour interval is 0.05°C.

(a)

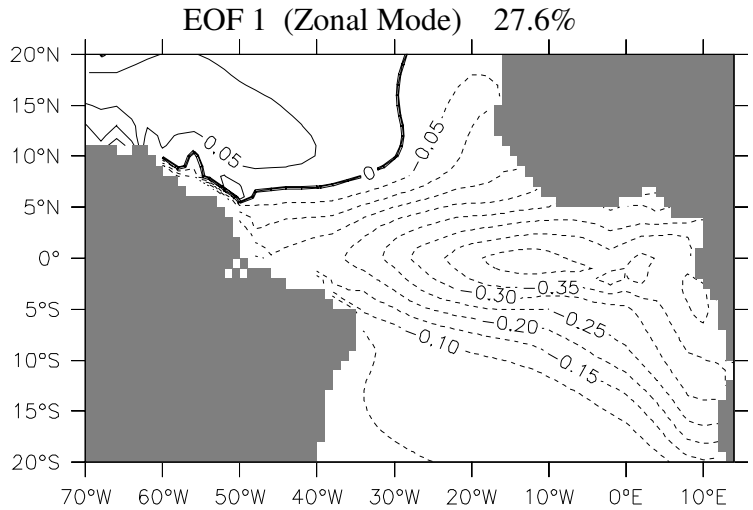

(b)

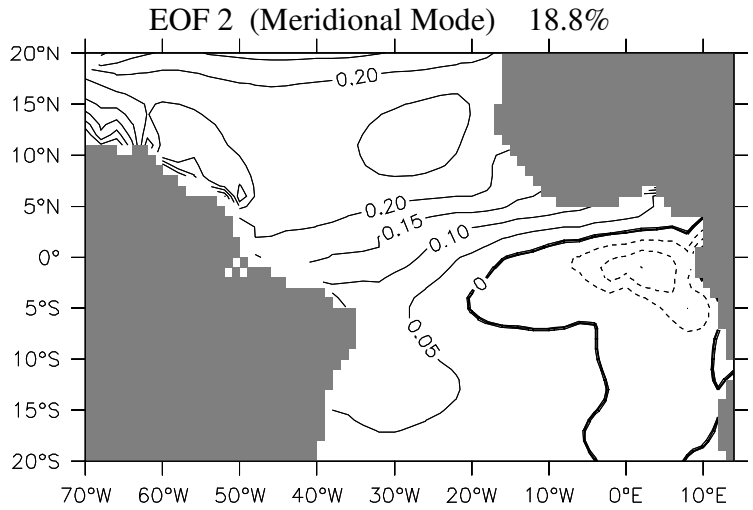

Figure 3.2. (a) First and (b) second leading EOFs derived from the SST "signal" of the CTRL experiment over the period from 1980 through 1999 (The associated PC time series have been normalized by their standard deviations). Contour interval is 0.05°C.

the center of the maximum amplitude is very close to the equator. Like the zonal mode, the variance explained by the simulated meridional mode (19%) is also less than that in the observations (24%).

b. Seasonal Phase-locking

Seasonal preference is one of the striking features of interannual climate variability in the tropical Atlantic. It has been noted that the interannual variability of the zonal mode peaks in boreal summer while that of the meridional mode peaks in boreal spring. This distinctive feature is not unexpected because the variability associated with the zonal mode is probably induced by local air-sea feedback that relies on the cold tongue dynamics in boreal summer (Sutton et al., 2000), while the variability associated with the meridional mode is likely linked to the remote forcing of NAO and ENSO, which are phase-locked to boreal winter (Czaja 2004). Figure 3.3 shows the standard deviation of the PC time series associated with the zonal mode and meridional mode as a function of the calendar month. One can see that the zonal mode shows a large amplitude during May-June-July (Figure 3.3a), while the meridional mode exhibits a large amplitude during boreal winter and spring with its strongest amplitude in March-April-May (MAM) (Figure 3.3b).

Figure 3.4 shows the seasonal dependence of the PC time series associated with the simulated zonal and meridional modes. One can see that the distinctive seasonal preferences of both modes are captured by the model. However, there are some differences between the simulation and observations. In the simulation, the peak of zonal mode in boreal summer (Figure 3.4a) is sharper than that in the observations (Figure 3.3a), and the variability during the transitional period from boreal fall to winter is overestimated by the model, although the observations also show relatively strong variability during this period. Since this study only focuses on the climate variability from boreal winter to summer, this overestimation will not affect our analysis. For the meridional mode, the simulation (Figure 3.4b) shows strong variability during boreal

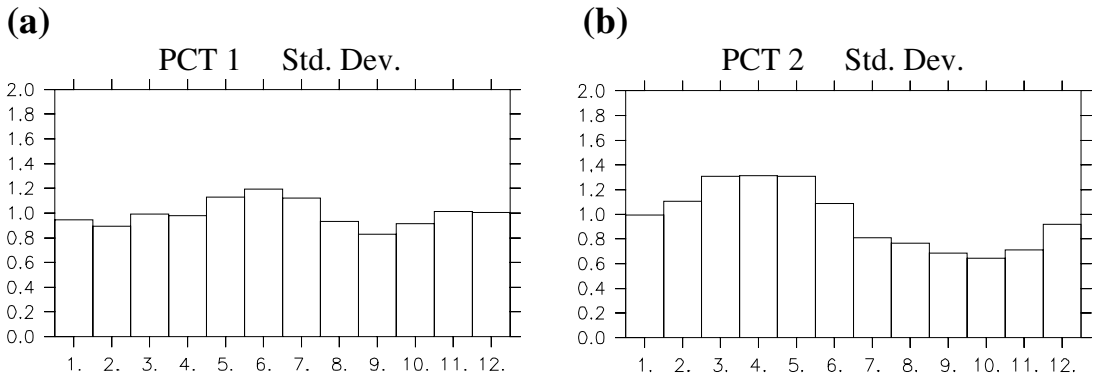

Figure 3.3. Standard deviation of the PC time series associated with the observed (a) zonal mode and (b) meridional mode shown in Figure3.1. The horizontal axis is calendar month.

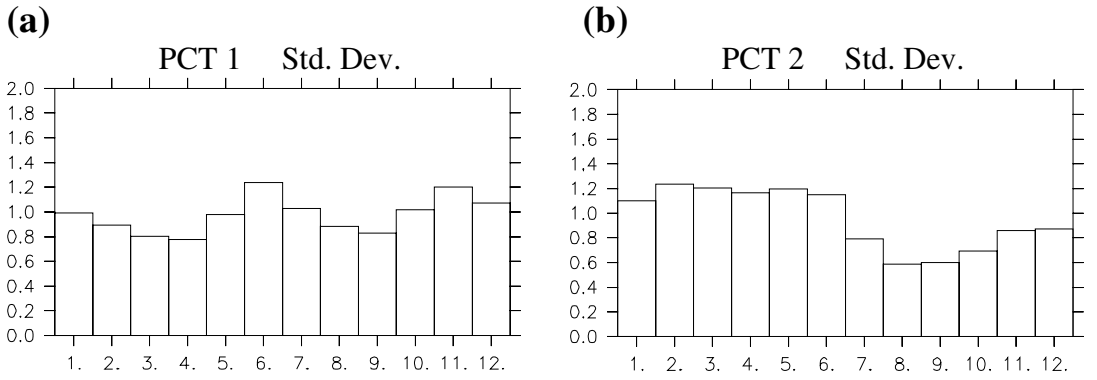

Figure 3.4. Standard deviation of the PC time series associated with the (a) zonal mode and (b) meridional mode simulated by the CTRL experiment. The horizontal axis is calendar month.

winter and spring and weak variability in boreal fall, agreeing with observations (Figure 3.3b), but the variability peak during MAM in the simulation is not as pronounced as in the observations. Overall, the seasonality of the meridional mode is consistent with the observation.

1.2 Composite Analysis

a. Winds

Wind is an important element of climate variability in the tropical Atlantic region. It can either change the surface heat fluxes through its effect on evaporation or change the ocean circulation, both of which can affect SST. Previous studies have identified at least two prominent features of the wind's response to the remote influence of El Nino. One is the weakening of the northeasterly trades in the NTA during boreal winter (Curtis and Hastenrath, 1995; Enfield and Mayer, 1997; Giannini et al., 2000), and the other one is the anomalous cross equatorial flow during boreal spring, towards the northern hemisphere in which the SST is anomalously warm (Curtis and Hastenrath, 1995; Enfield and Mayer, 1997).

Figure 3.5 shows the composites of anomalous wind fields constructed using 11 warm ENSO events in 1951, 57, 63, 65, 69, 72, 76, 82, 87, 91, 97, which lasted at least for 9 months during the period of 1950-2000 (Trenberth, 1997). The data we used is the NCEP/NCAR reanalysis data, and the composites show the anomalous wind fields in the years following an El Nino from January to August. Similar composites were constructed based on 48 warm events simulated by the model (12 runs, each run has 4 warm events during the period of 1980-1999), and shown in Figure 3.6. The observations clearly show a strong southwesterly wind anomaly in the NTA (Figures 3.5a-3.5c). This wind anomaly starts to develop in January, prevails in February-March, and then fades away in April and onward. In the equatorial region, an anomalous cross-equatorial flow starts to develop in April, strengthens in May and June, and then decays

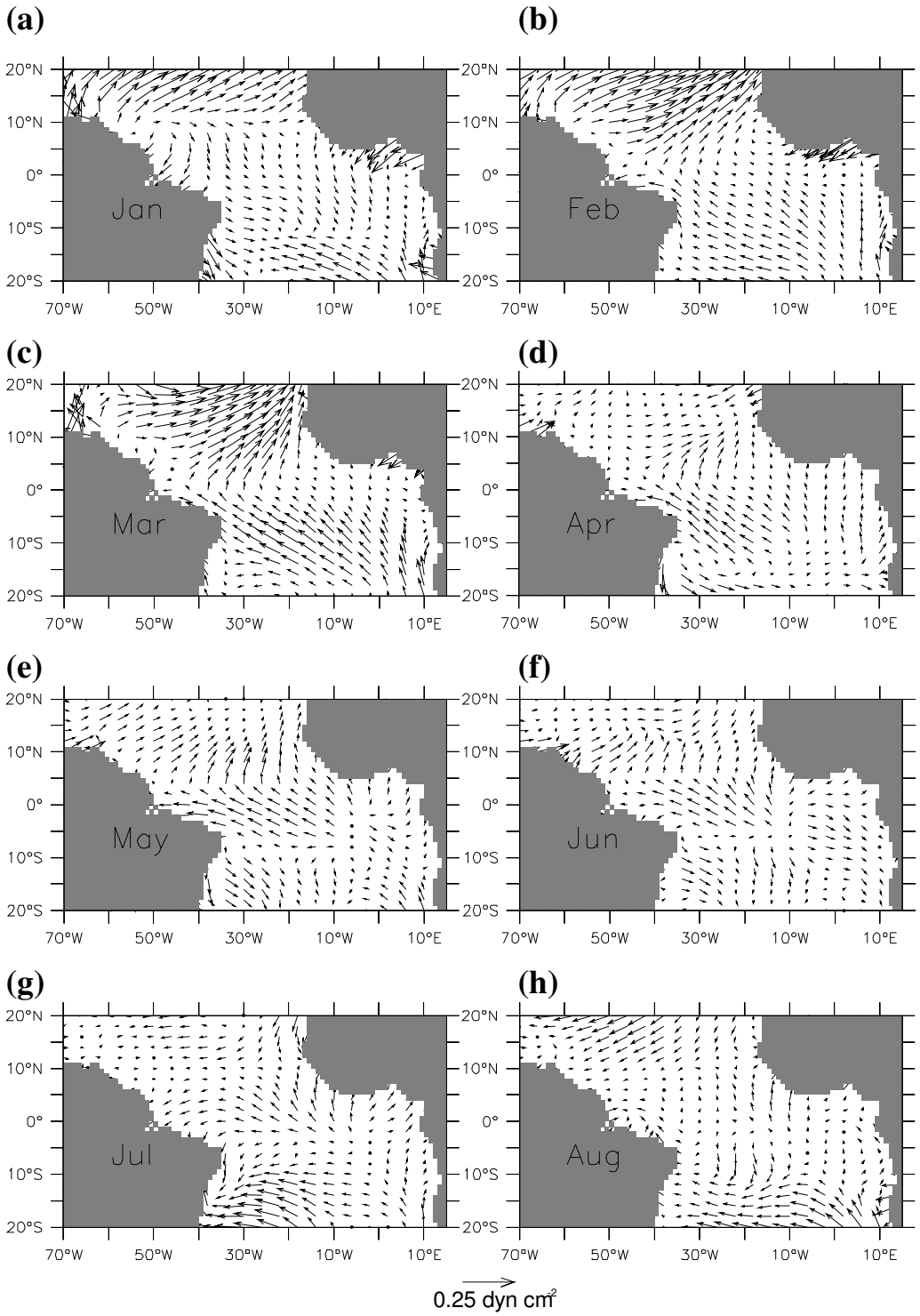

Figure 3.5. Evolution of wind stress anomalies from January to August constructed from NCEP/NCAR reanalysis. 11 warm ENSO events in 1951, 57, 63, 65, 69, 72, 76, 82, 87, 91, 97 during the period of 1950 to 2000 are used.

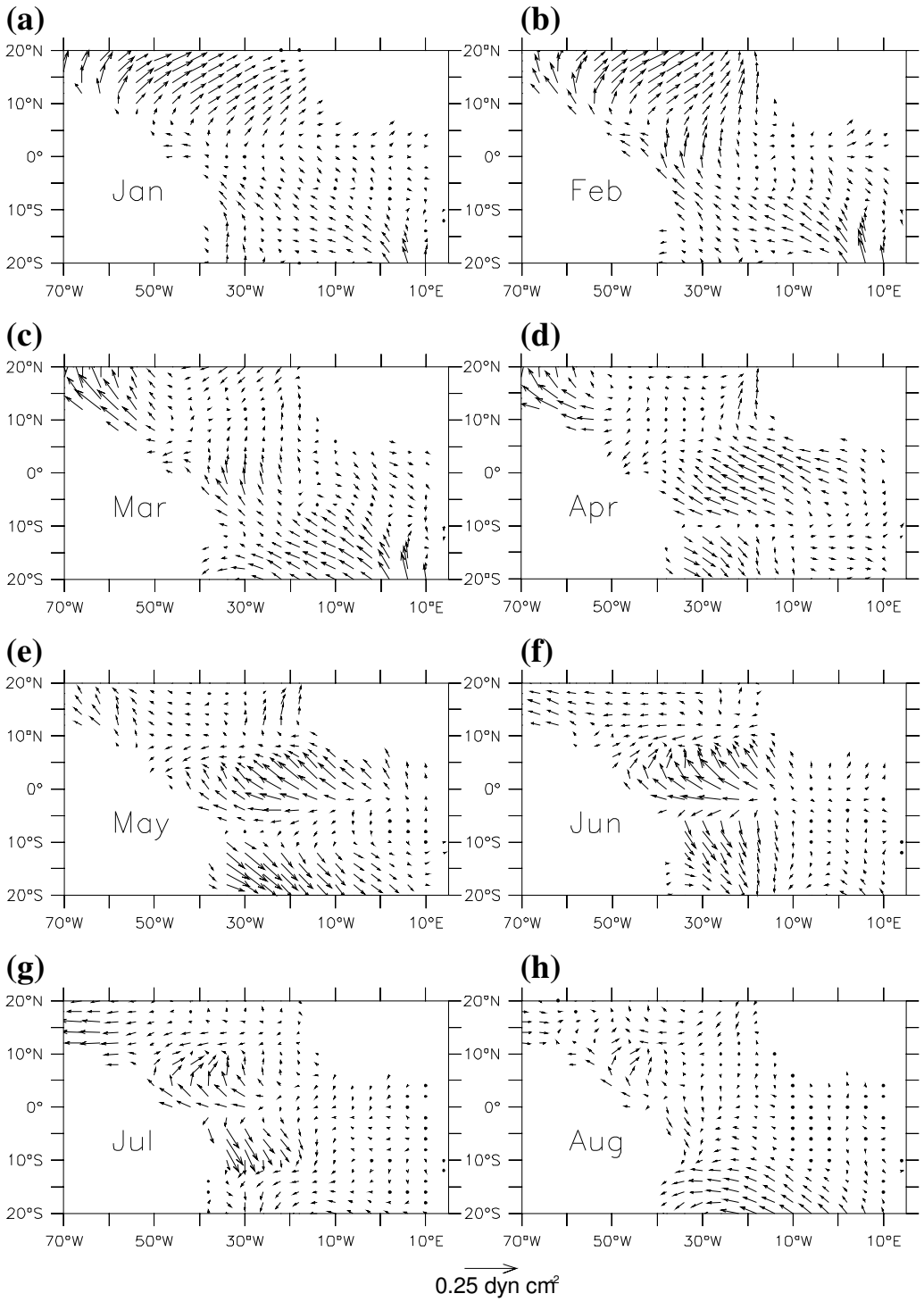

Figure 3.6. Evolution of wind stress anomalies from January to August constructed from the CTRL experiment. 48 warm ENSO events in 1982, 87, 91, 97 during the period of 1980 to 2000 from 12 runs are used.

in July (Figures 3.5d-3.5g). Comparing Figure 3.6 with Figure 3.5, it can be seen that these two predominant features are captured by the model very well. However, there are some differences. In the simulation, the southwesterly wind anomaly in the NTA starts to develop in previous year's December (figure not shown), this leads the observations by about one month. This "leading" gradually disappears as the seasons progress into boreal summer, but is still noticeable in spring. Another noticeable difference is that the simulated wind anomaly in the equatorial region during late spring to summer (Figures 3.6e-3.6g) is stronger than the observed anomaly (Figures 3.5e-3.5g), although its distribution agrees very well with the observations. These discrepancies are also reflected in the composites of SST evolution, which will be discussed in the next subsection. Despite the minor discrepancies between the observation and simulation, the model is generally capable of capturing key features of the wind anomalies induced by ENSO influence.

Another feature of the anomalous wind fields is worth mentioning here. As shown in Figures 3.5, the wind anomaly in the STA seems to be much noisier than the wind anomaly in the NTA and equatorial region. But the southeasterly wind anomaly in the STA, although weaker than the anomalous southwesterly wind anomaly in the NTA, does persist from late winter into early spring (Figures 3.5a-3.5c). This feature is also captured by the model (Figures 3.6a-3.6c). In the trade wind belt of the tropical Atlantic, the wind anomaly can have great impact on heat flux by changing the rate of evaporation, thus the persisting southeasterly wind anomaly in the STA, although not strong, could be an important factor in SST variability in this region.

b. SST

Figure 3.7 shows the composites of observed SST anomalies constructed using the same 11 warm ENSO events that were used in the wind composites shown in Figure 3.5. It shows the evolution of SST following El Nino from January to August. Similar composites based on 48 warm events are also constructed and presented in Figure 3.8 for

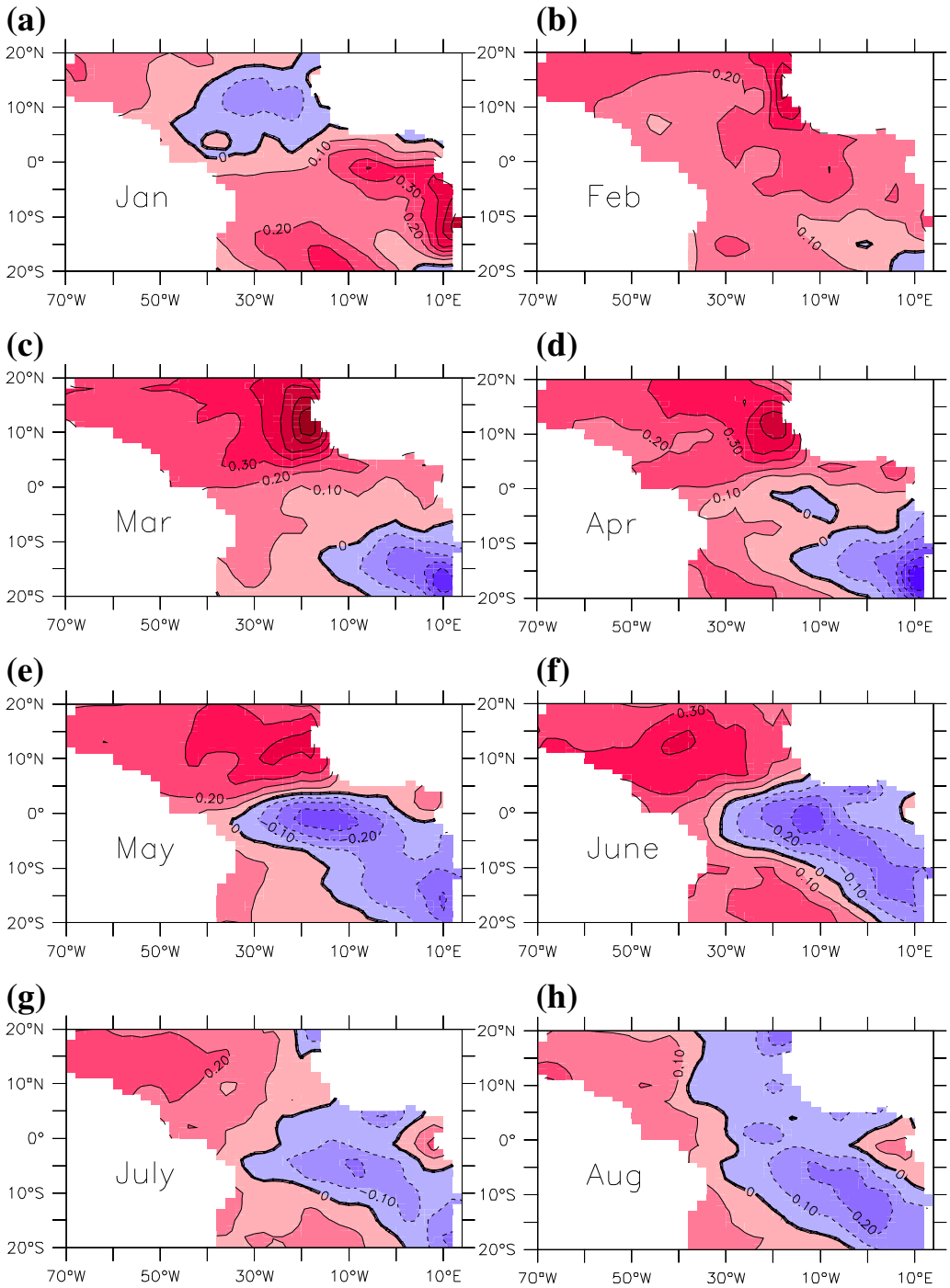

Figure 3.7. Evolution of SST anomalies from January to August constructed from Reynold's SST (Smith et al., 1996). 11 warm ENSO events in 1951, 57, 63, 65, 69, 72, 76, 82, 87, 91, 97 during the period of 1950 to 2000 are used. Contour interval is 0.1°C.

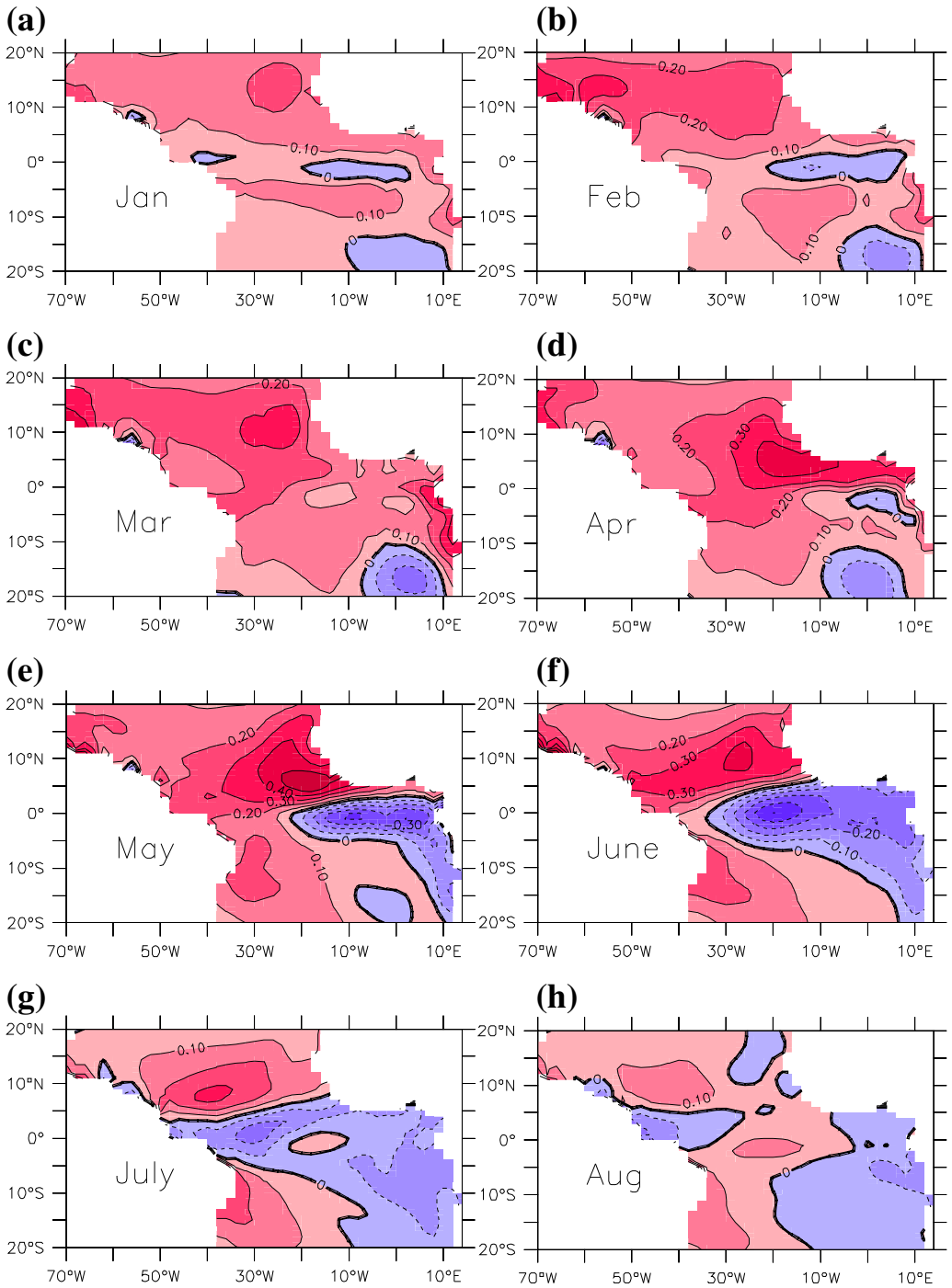

Figure 3.8. Evolution of SST anomalies from January to August constructed from the CTRL experiment. 48 warm ENSO events in 1982, 87, 91, 97 during the period of 1980 to 2000 from 12 runs are used. Contour interval is 0.1°C.

comparison. A prominent feature in this figure is a basin-wide strong positive SST anomaly in the NTA during boreal spring. In February (Figure 3.7b), the SST anomaly in the NTA is generally warmer than the SST anomaly in the STA. As the season progresses, the SST anomaly in the NTA starts to develop and peaks during boreal spring (Figures 3.7c and 3.7d) then weakens from May onward (Figures 3.7e-3.7g). This feature has been demonstrated by many previous studies (e.g., Curtis and Hastenrath, 1995; Enfiled and Mayer, 1997), and is well captured by the model (Figure 3.8), although the amplitude of simulated SST anomalies are smaller than observations. Further comparison shows that the onset of the warm SST anomaly in the model is about one month earlier than in observations. This is probably because the onset of the southwesterly wind anomaly simulated by the model is earlier than the observations, as noted earlier.

In addition to the warm SST anomaly in the NTA, a cold SST anomaly appears in boreal winter in the simulation (Figures 3.8a), which strengthens in early spring (Figure 3.8c), and then fades away. In boreal spring, another cold SST anomaly starts to develop in the equatorial region (Figures 3.8d and 3.8e), prevails in summer, and then decays (Figures 3.8f-3.8h). The occurrence of the cold SST anomaly bears a close resemblance to observations (Figure 3.7). The composites constructed by Curtis and Hastenrath (1995) and Nobre and Shukla (1996) also show a cold SST anomaly in the ESA. A comparison of the amplitude of the simulation and the observations suggests that the model tends to underestimate the cold SST anomaly in boreal spring and overestimate it in the equatorial region in boreal summer.

2. Extracting ENSO-forced Response Using an Ensemble of Coupled Integration

Having demonstrated that the model is capable of capturing observed TAV in response to ENSO forcing, we next focus on a more detailed analysis of the coupled simulations. The large ensemble size allows us to better separate the variability forced by ENSO from that generated by processes internal to the Atlantic. As described in

Chapter II, the ensemble of 12 CTRL runs uses the same SST forcing outside the tropical Atlantic. Therefore, a simple ensemble average will give a reasonable estimate of ENSO-forced TAV. We will consider the ensemble average as an approximation for the "signal", and departure from the ensemble average as the "noise".

To avoid "noise" contamination due to insufficient ensemble size, a signal-to-noise maximizing EOF analysis (Hasselmann, 1979; Allen and Smith, 1997), which has been successfully employed by many studies (e.g., Venzke et al., 1999; Chang et al., 2000), will also be used to get a more accurate estimate of the "signal". Unless noted otherwise, all the analyses presented in this section are based on the "signal" part of the model response estimated by a signal-to-noise EOF analysis.

2.1 Dominant SST "Signal"

Figure 3.9 shows the first two leading EOFs of the SST "signal" of the CTRL experiment. The first leading pattern, which explains about 30% of total variance of the signal, shows a basin-wide SST anomaly with higher amplitude in the NTA and smaller amplitude in the ESA (Figure 3.9a). While the second leading pattern (Figure 3.9b), which explains about 24% of total variance, shows an SST anomaly similar to the zonal mode (Figure 3.2a). The PC time series (Figure 3.9c) of the EOFs show that the first EOF is phase-locked to boreal spring (Figure 3.10a), while the second EOF is phase-locked to boreal summer (Figure 3.10b). The different seasonal dependence of these two leading patterns raises an interesting question: are the SST responses during the two seasons connected or independent? To investigate this issue, EOF analysis is applied to the seasonally averaged SST signal of boreal spring and summer, respectively. The leading EOFs for each of the two seasons are presented in Figures 3.11.

The first leading EOF of boreal spring (Figure 3.11a), which explains 61% of the total variance in that season, is well separated from the second leading pattern (not shown), which explains only about 16% of variance. The first leading EOF of boreal summer (Figure 3.11b), which explains even a larger amount (68%) of the total seasonal

(a)

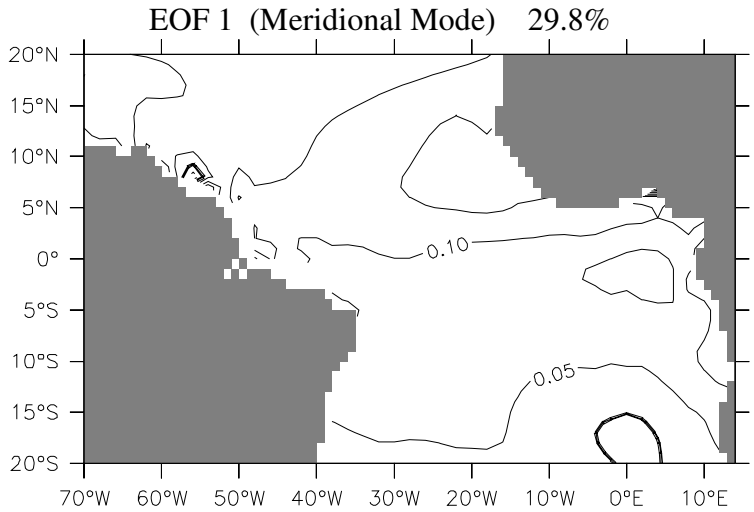

(b)

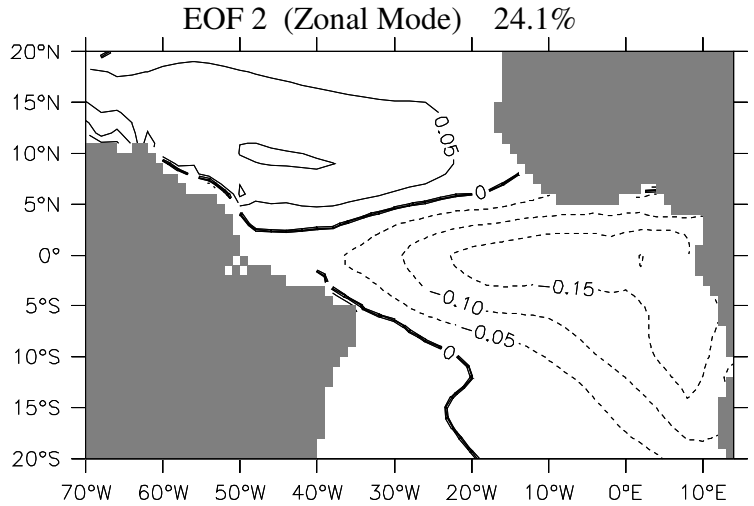

Figure 3.9. (a) First leading EOFs, (b) second leading EOFs, and (c) their associated PC time series derived from the CTRL experiment. Black line and red line are the PC time series associated with the first and second leading EOFs, respectively. Contour interval is 0.05°C.

(c)

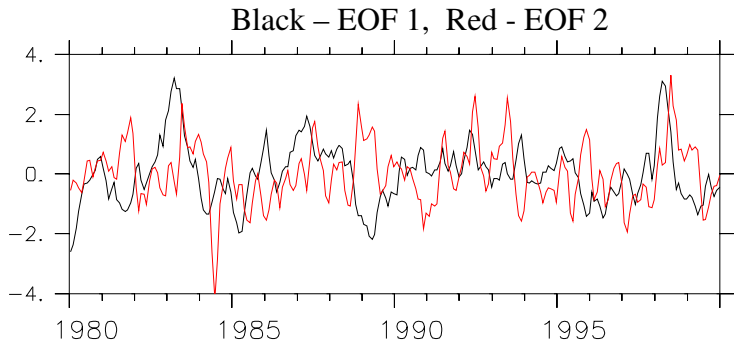

Figure 3.9. (Continued)

(a)

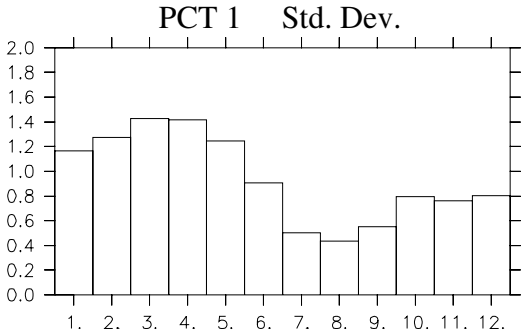

(b)

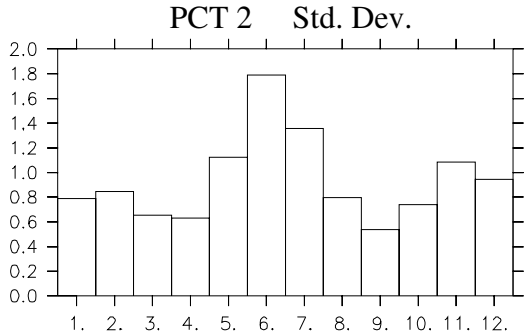

Figure 3.10. Standard deviation of the PC time series associated with the (a) first leading EOFs and (b) second leading EOFs derived from the CTRL experiment. The horizontal axis is calendar month.

a)

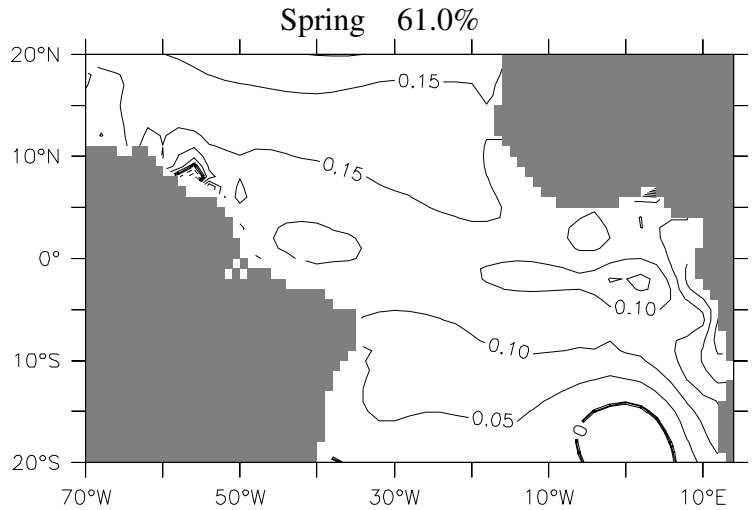

(b)

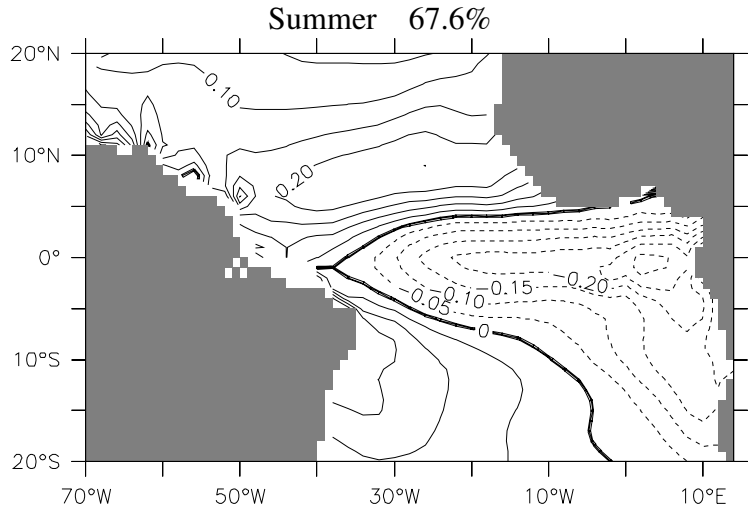

Figure 3.11. First leading EOFs of (a) boreal spring and (b) boreal summer, and (c) associated PC time series derived from the CTRL experiment. Black line is for spring; red line for summer. Contour interval is 0.05°C.

(c)

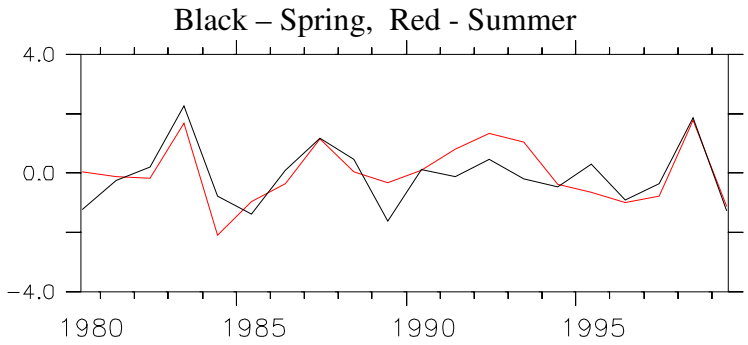

Figure 3.11. (Continued)

variance, is also well separated from the second leading pattern (not shown) from that season, which explains 11% of the variance. It can be seen that the seasonal EOFs (Figure 3.11) resemble the first two leading EOFs shown in Figure 3.9. This suggests that the SST response to ENSO forcing in the tropical Atlantic consists of two distinctive patterns, one of which dominates in boreal spring and the other which dominates the response during boreal summer. Furthermore, the PC time series (Figure 3.11c) associated with the seasonal EOFs are highly correlated with the November-December-January (NDJ) Nino-3 Index (defined as averaged SST anomaly in 5°S-5°N, 150°-90°W) at 0.89 and 0.74, respectively. The two seasonal EOFs are also highly correlated at 0.74, as anticipated.

Considering that the TT mechanism, which affects SST mainly through surface heat flux, is most effective during boreal winter and spring, we hypothesize that ocean dynamics play a key role in connecting the evolution of SST from boreal spring to summer, particularly in equatorial region where the sign of SST anomaly is reversed (Figure 3.11b).

2.2 Heat Flux Anomaly

To test our hypothesis, we first take a closer look at the relationship between heat flux and SST in different parts of the tropical Atlantic Ocean. We chose the following three regions, NTAI (8°-20^oN, 60°-20^oW), EAI (3^oS-3^oN, 35^oW-5^oE) and STAI (8°-20^oS, 30^oW-10^oE), to define indices to represent the spatially averaged state of climate variations in the NTA, equatorial Atlantic, and STA regions, respectively (Figure 3.12).

We computed the lag correlations between the surface heat flux and the SST indices in these regions. The results are shown in Figure 3.13. The lag correlations of the NTAI and the STAI have a similar appearance, and in both regions the heat flux and SST are positively correlated when heat flux leads. This result is consistent with the hypothesis that surface heat flux is driving SST variability in the off-equatorial regions. Another feature common to the correlations in the NTAI and the STAI regions are that the correlation drops sharply to zero when SST leads heat flux, suggesting that the SST

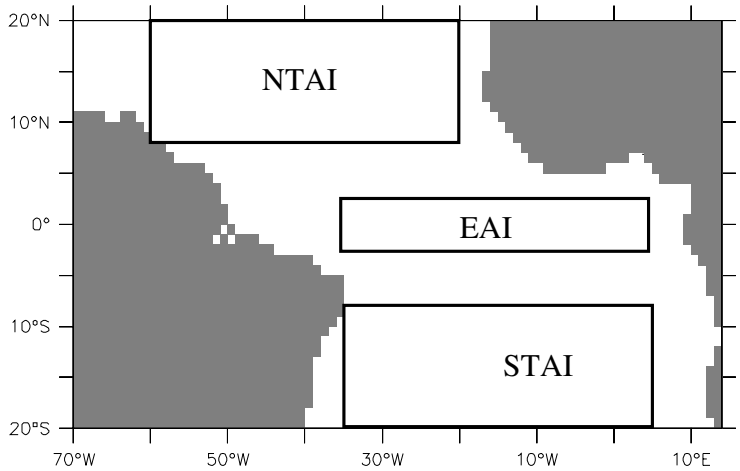

Figure 3.12. Boxed areas, from north to south, are regions where the indices are defined to represent the climate variability in the NTA, equatorial Atlantic, and STA, respectively.

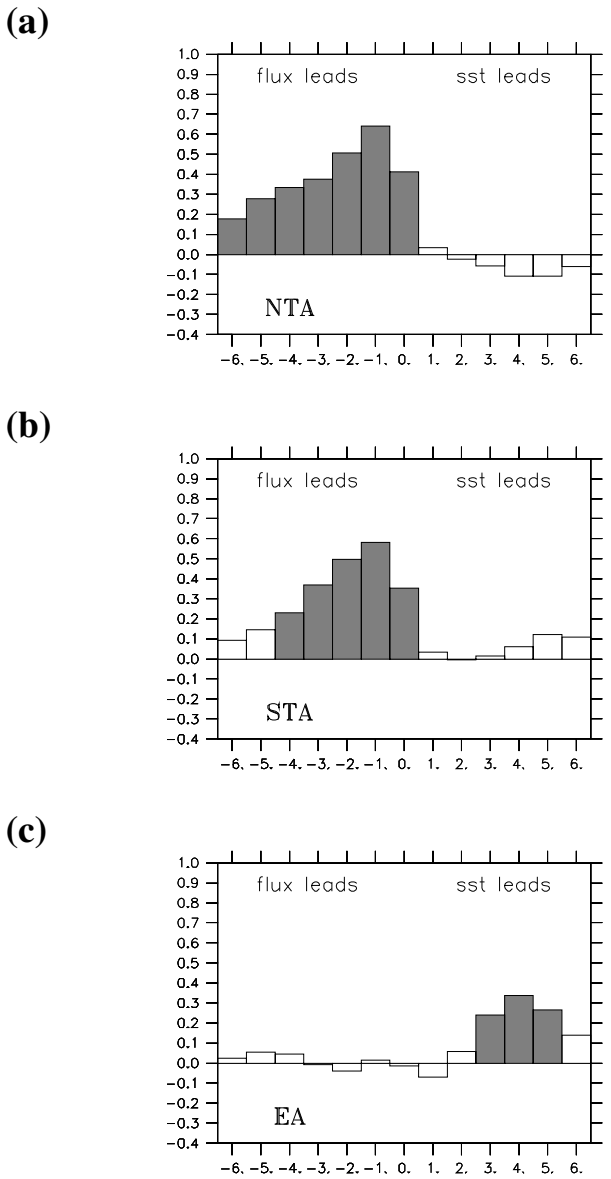

Figure 3.13. Lag correlations between the downward surface heat flux and the SST in the (a) NTAI, (b) STAI, and (c) EAI regions computed from the CTRL experiment. Horizontal axis is the lead time (in months); negative number implies the surface heat flux lead, and positive number, the SST leads. Shaded bars passed 99% significant level.

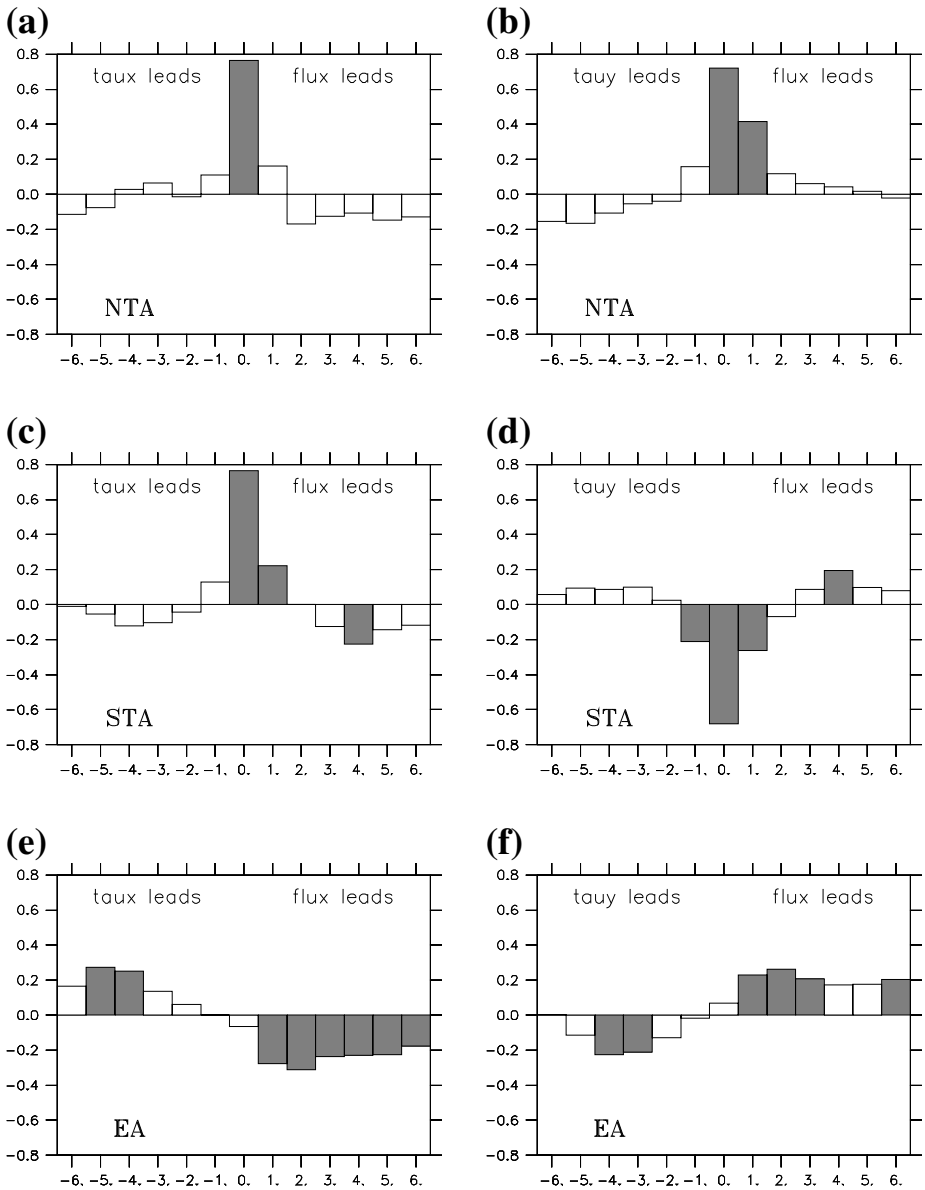

Figure 3.14. Lag correlations between the wind stress and downward surface heat fluxes in the NTAI (upper panel), STAI (middle panel), and EAI (lower panel) regions computed from the CTRL experiment. Horizontal axis is the lead time (in months); negative number implies the winds lead, and positive number, the surface heat fluxes lead. Shaded bars passed 99% significant level.

has little influence on heat flux. This again points to the fact that the SST is just a response to heat flux forcing (Frankignoul et al., 1998) in off-equatorial region. In contrast, the correlation in the EAI region is entirely different. In this region, there is essentially no correlation when heat flux leads, suggesting that the heat flux is not a driving force for SST variability in the equatorial region.

In the tropics, the prevailing trade winds play an important role in determining surface heat flux primarily through its effect on evaporation, and thus the latent heat flux. If the wind is a dominant factor in changes in surface heat flux, we would expect no obvious time delay between the wind and the response in the surface heat flux because the wind can change the rate of evaporation almost instantly. Figure 3.14 presents the lag correlations between wind and net surface heat flux over the NTAI, STAI, and the EAI. It shows that the heat flux is indeed highly correlated with the zonal component of the wind at zero lag and the correlations approach zero rapidly as the lead/lag time increases (Figures 3.14a-3.14d), consistent with the idea that in off-equatorial regions the changes in surface heat flux are mainly induced by wind anomalies. In the equatorial region, no significant correlations can be found between heat flux and wind (Figures 3.14e and 3.14f), suggesting that wind-induced latent heat flux is not a major component of surface heat flux in the equatorial region.

2.3 Thermocline Variation

Another important factor that can affect SST is the variation of the thermocline in response to changes in the winds. This effect is very important, particularly in the eastern equatorial regions where the thermocline is shallow, so that the thermocline fluctuations can effectively influence SST variability.

Figure 3.15a shows the simultaneous correlation between variations of thermocline depth and SST. Two large areas of high positive correlation are identified. One is located in the eastern equatorial region, and one is located at around 15°S, 10°E. The maximum correlation between SST and thermocline exceed 0.6 in these regions.

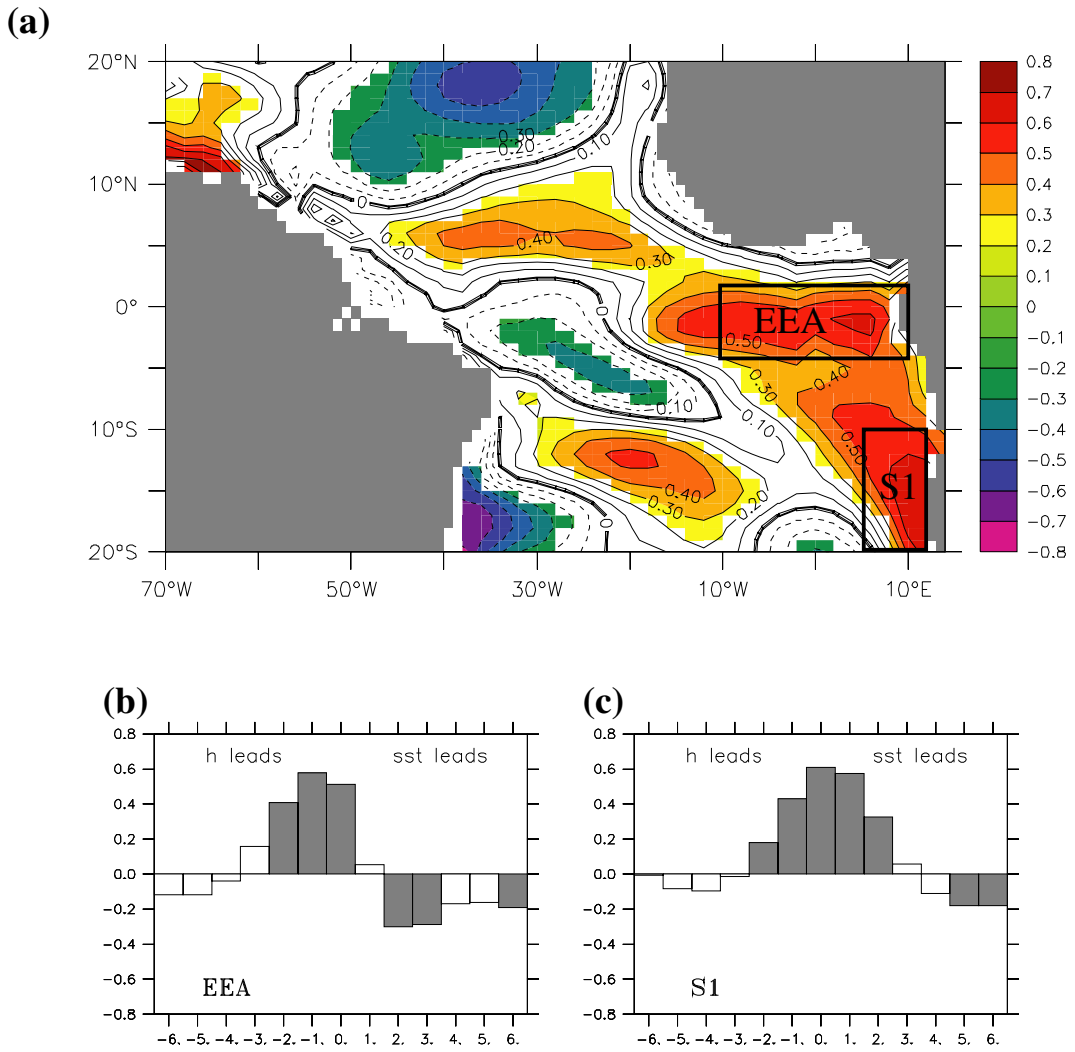

Figure 3.15. (a) Correlation between the thermocline and SST at zero lag computed from the CTRL experiment; and the lag correlations between the thermocline and SST in (b) eastern equatorial Atlantic (EEA) and (c) Angola-Namibia (S1) regions. Shaded bars passed 99% significant level.

One would expect this since subsurface ocean variability has a large impact on SST because of strong upwelling. The other interesting feature is the dipole-like structure in the off-equatorial regions. This structure is probably caused by NECC changes in response to the wind changes. The high correlation results from the fact that the wind drives both SST and thermocline. Lag-correlations (Figures 3.15b) indicate that in the equatorial zone, the thermocline leads the SST by one month, suggesting that subsurface ocean may be driving the SST in this region. Such a lead-lag relationship is absent off the coast of Africa where maximum correlation occurs at zero lag (Figure 3.15c), suggesting a possible local feedback.

2.4 Ekman Feedback

In addition to the thermocline variation, the Ekman divergence is also an important factor that can contribute to the SST variation via changing the vertical velocity at the bottom of mixed layer, thus the entrainment. In the equatorial Pacific, most of the ENSO-related SST variability can be explained by the variations of the thermocline, but in Atlantic Ocean, variations of thermocline can only explain part of the SST variability. Considering that the heat flux basically plays a role of damping in the equatorial region, Ekman feedback (Chang & Philander, 1994) could play an important role in SST variability in equatorial Atlantic.

Figure 3.16a shows the correlation between the variations of entrainment velocity induced by Ekman pumping and SST at zero lag. It can be seen that the regions that have high correlations (<-0.33, circled by red dashed lines in the Figure 3.16a) are mainly confined to the western equatorial region, with maximum correlations located at around 30°W. This implies that Ekman divergence may be very important in the western equatorial Atlantic. Figure 3.16b shows the lag correlations between the variations of Ekman divergence and SST in the western equatorial Atlantic (WEA) region (3°S-3°N, 35-10°W; Figure 3.16a). An important feature of the diagram is that, the Ekman divergence and SST are maximally correlated at zero lag and significant correlations

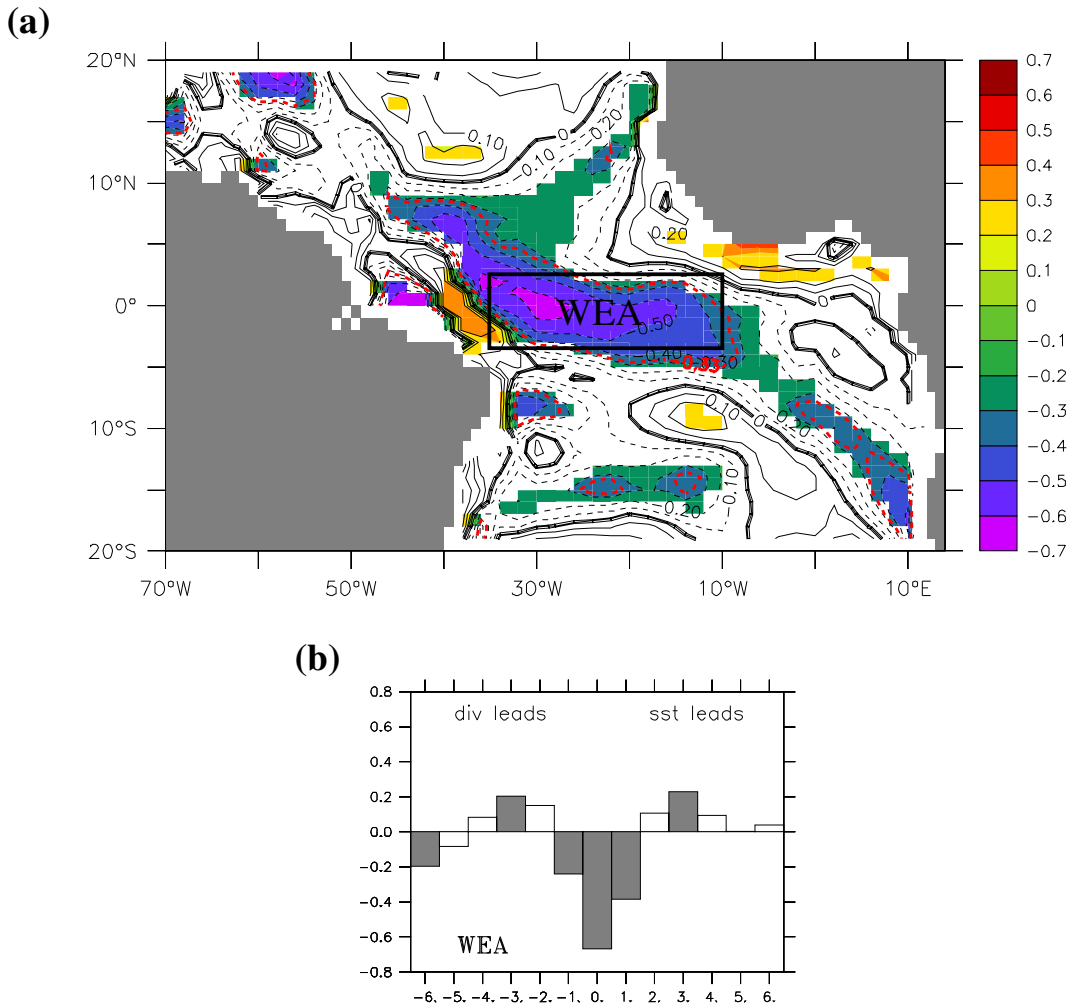

Figure 3.16. (a) Correlation between the entrainment velocity induced by Ekman pumping and SST at zero lag computed from the CTRL experiment; and (b) lag correlations between the entrainment velocity and SST in western equatorial Atlantic (WEA) region. Shaded bars passed 99% significant level.

also exist at +1 or -1 month. This symmetric feature is consistent with a positive feedback between the two fields, supporting the idea that Ekman feedback may be operating.

3. Discussion

3.1 North Tropical Atlantic

The anomalous warming and the weakened northeasterly trades in the NTA following a warm ENSO event are two well-defined characteristics of remote influence of ENSO that have been documented by many previous studies (e.g., Curtis and Hastenrath, 1995; Enfiled and Mayer, 1997). These features are well captured by the coupled model (Figure 3.8).

Recent modeling studies indicate that much of the SST variability in this region can be captured by AGCMs coupled to a slab ocean or a mixed layer ocean (e.g., Alexander et al., 2002; Chang et al., 2003), suggesting a secondary role of ocean dynamics. The NADV and NENT experiments, which will be discussed in detail in Chapter IV, also support this finding. Therefore, it is concluded that the mechanism for the NTA SST is primarily a heat flux driven mechanism. Our analysis further supports the idea that wind-induced latent heat flux plays an important role in driving the SST in this region, as shown by the close relationship between the winds and surface heat flux (Figures 3.14a and 3.14b).

An alternative mechanism is the TT mechanism of Chiang and Sobel (2002) where air-sea temperature and humidity difference is a driver for ENSO-related SST variability in the tropical Atlantic. The TT mechanism predicts a uniform warming in the tropical Atlantic following a warm ENSO event (Figure 1.3). Although we have not carefully examined the role of the TT mechanism in our model simulation, the first leading EOFs of the SST “signal” (Figure 3.9a) do show a basin-wide warming pattern, consistent with the TT mechanism. Furthermore, it is interesting to note that both the

wind-induced warming and the TT-induced warming are working in concert in the NTA region. This may explain the question of why the remote influence of ENSO is most pronounced in NTA region.

3.2 South Tropical Atlantic

Compared with the NTA, the mechanisms responsible for climate variations in the STA are less clear. This is probably because the climate variations in the STA are much weaker than in the NTA. But the overall condition of the STA during late spring and early summer following a warm ENSO is warmer than normal. This does point to the possibility that the TT mechanism may drive the SST variability in the STA. Our model result is consistent with this assertion, based on the finding that a positive surface heat flux is observed at all latitudes from boreal winter to spring (Figure 3.17).

Chiang and Sobel (2002) computed the correlation between the SST simulated by their single-column model with the NCEP/NCAR reanalysis surface temperature, and found that the correlation is not high in the southeast tropical Atlantic. This may indicate that the SST in this region is not significantly associated with ENSO. They speculated that the lack of SST response in that region may be because of the convective response to TT forcing, which links the surface and boundary layer to the free troposphere, is counteracted by the stratus cloud response to TT.

As we have demonstrated in Section 2.2, the wind-induced surface heat flux change is an important forcing for SST in the STA. This is particularly evident in the southeast tropical Atlantic, where a cold SST anomaly is associated with a southeasterly wind anomaly during boreal winter to early spring (Figures 3.6 and 3.8), although both anomalies are relatively weak. Thus the wind-induced latent heat flux may also play a role in canceling the warming induced by the TT mechanism in the STA. Note that in the model, the SST in the western STA region is warmer than that in eastern region. This may be due to the fact that the wind-induced cooling is not stronger in the west than in the east. It is also worth mentioning that the divergence of the southeasterly wind

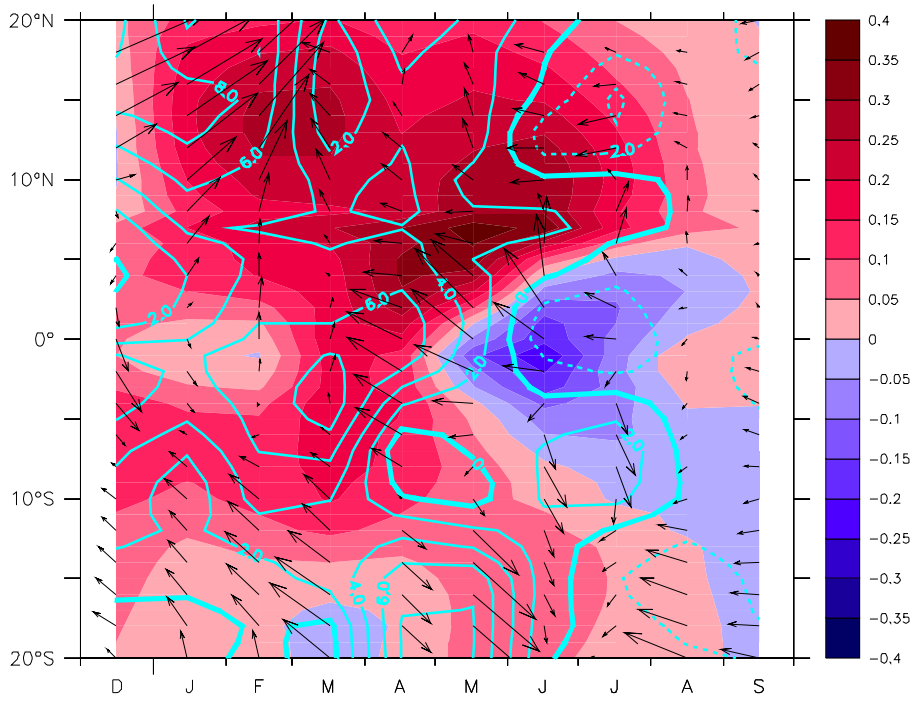

Figure 3.17. Composite map of zonally averaged SST, wind stress, and downward surface heat fluxes constructed for the CTRL experiment. 48 warm ENSO events in 1982, 87, 91, 97 from 12 runs of the experiment are used. Shaded areas are SST; arrows are wind stress; contours are surface heat fluxes. Contour interval is 4.0 W/s.

anomaly can also play a role in cooling the SST in the STA, although its role appears to be secondary.

In contrast to the NTA where the wind-induced and TT-induced fluxes work in concert, those two mechanisms work against each other in the STA. Therefore, one would expect a less significant SST response to ENSO in the STA than in the NTA. Whether this argument is valid remains to be tested.

We have emphasized the importance of the role of the TT mechanism and the role of wind-induced heat flux in SST variability in the STA, but these two mechanisms

can not explain the SST variations in the region close to the Angola-Namibia coast, where extreme warming in SST has been observed and has given the name, “Benguela Nino”. Florenchie et al. (2003, 2004) found that these coastal warming events can be traced back to the anomalous wind events in the equatorial Atlantic that excite a subsurface temperature anomaly and propagate to the coast as a Kelvin wave, eventually producing a warming at the surface.

Our model simulation also shows a high correlation between the SST and thermocline variations in that region (Figure 3.15a), but found no evidence that the thermocline leads the SST (Figure 3.15c). Correlation between the meridional wind component and the thermocline (Figure 3.18a) seems to rule out the possibility that changes in thermocline are generated by the local winds. To test the argument put forward by Florenchie et al., the correlation between thermocline variations in the EEA region and the S1 region (Figure 3.15a) is also calculated, and shown in Figure 3.18b. It shows that the thermocline variation in the EEA region is highly correlated with the thermocline variation in the S1 region at 0.85 when the former leads the latter by about one month. This supports the argument by Florenchie et al. But the significant correlation between the zonal winds and SST in the S1 region (Figure 3.18c) suggests that the surface coupling may also be important.

3.3 Equatorial Atlantic

Turning to the equatorial Atlantic, a distinct feature of the spring anomalous condition following a warm ENSO event in this region is a northwestward cross-equatorial flow (Figure 3.6d). This wind anomaly results from the hydrostatic adjustment of atmospheric boundary layer in response to the interhemispheric SST gradient. This circulation anomaly is very important to the climate perturbations in the tropical Atlantic because it can shift the meridional position of maximum surface wind convergence and thus the ITCZ.

Given the similarity between the Atlantic zonal mode (Figure 3.1a) and the

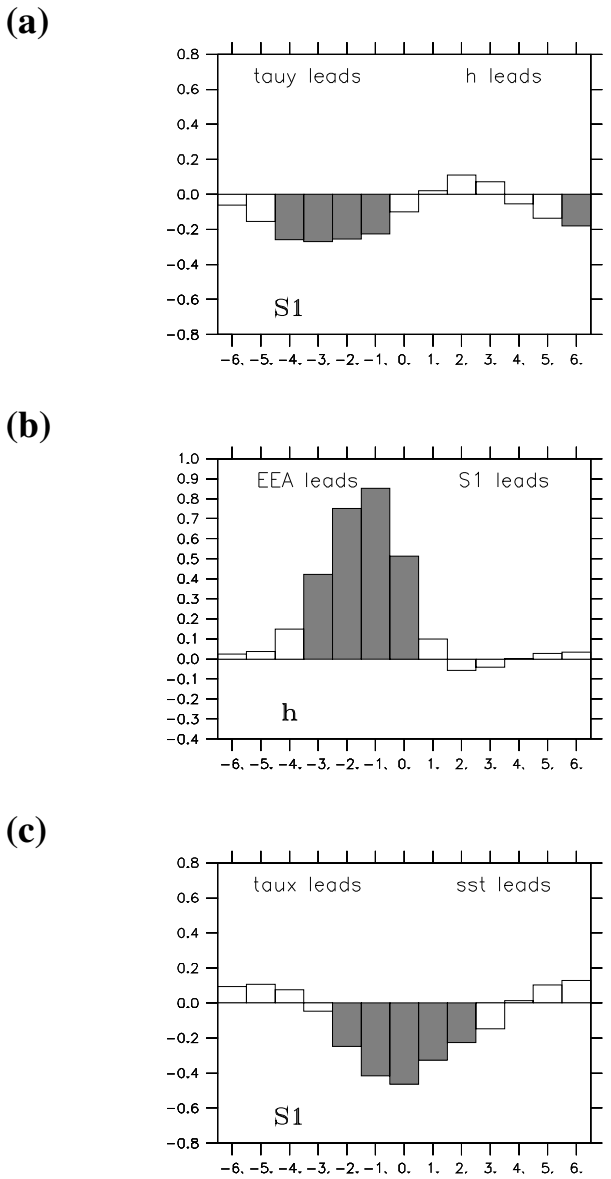

Figure 3.18. Lag correlations between (a) the meridional component of wind stress and thermocline in the S1 region; (b) the thermocline in the EEA region and the S1 region; and (c) the zonal component of wind stress and SST in the S1 region. Shaded bars passed 99% significant level.

Pacific ENSO mode (not shown), Bjerknes feedback (1969), which has been shown to be the key underlying mechanism for ENSO, is expected to operate for the Atlantic zonal mode. Figure 3.8 shows a cold SST anomaly in the eastern equatorial region, which appears in April and persists through June. This cold anomaly may be attributed to the Bjerknes-type dynamics because there is a strengthening of the southeasterly trade winds near the equator. However, the correlation between the thermocline and SST variations (Figure 3.15a) shows that the region, where Bjerknes feedback is expected to operate, is mainly confined to the eastern equatorial region. Moreover, the correlation in this region is only marginally significant with a value of 0.5~0.6, suggesting that Bjerknes feedback may not be the only mechanism at work.

Chang and Philander (1994) suggest that Ekman feedback can operate in equatorial regions where upwelling prevails. Model simulation suggests that this is the case in the equatorial Atlantic. Figure 3.16a identified a band of high negative correlations between the Ekman divergence and SST, expanding from the western to the central equatorial Atlantic. From Figure 3.6d, it can be further seen that the cross-equatorial wind anomaly produces a divergence in the western and central equatorial regions. This divergence strengthens the entrainment at the bottom of the mixed layer, producing a cooling within the mixed layer. The cold SST can strengthen the divergence of wind by enhancing the cross-equatorial flow. This positive feedback appears to be particularly strong in May and June (Figures 3.8e and 3.8f for SST; Figures 3.6e and 3.6f for wind). Therefore, the leading pattern of boreal summer (Figure 3.11b) reflects the SST variability induced by ocean dynamics. This supports our hypothesis (Section 2.1) that ocean dynamics play a key role in connecting the evolution of SST from boreal spring to summer.

CHAPTER IV

OCEAN DYNAMICS IN REMOTE INFLUENCE OF ENSO

Horizontal advection and entrainment are the two dynamical oceanic processes that can contribute to significant changes to SST. In this chapter, we will compare the results from the NADV, NENT, and SLAB experiments, in which one or both of the two processes are disabled, to those of the CTRL experiment in an attempt to shed light on the role of ocean dynamics in TAV response to the remote ENSO forcing. The questions that we would like to address are: How do the horizontal advection and entrainment affect the SST evolution following a warm ENSO event? In what region and during which time are these ocean processes most effective in affecting SST? How does the relative importance of the oceanic process vary in location and time?

1. NADV Experiment

Figure 4.1 shows composites of SST from the NADV experiment, in which the horizontal advection of heat is disabled. It can be seen that the general characteristics of the SST evolution shown in Figure 4.1 resembles the one shown in Figure 3.8. In both cases, the warm SST anomaly in the NTA during boreal winter to spring and the cold SST anomaly in the STA during boreal spring to summer - the two key features in the SST evolution following a warm ENSO event - are captured. This similarity between the two experiments is more evident by comparing Figure 4.2 with Figure 3.17. This suggests that the horizontal advection of heat is of secondary importance in determining the overall pattern of the SST evolution in response to the remote ENSO influence.

A careful comparison between the Figures 4.1 and 3.8 shows that in the NTA, the SST anomaly tends to be stronger in the NADV experiment from January to March, while it tends to be weaker during May and June (Figure 4.3). To understand this

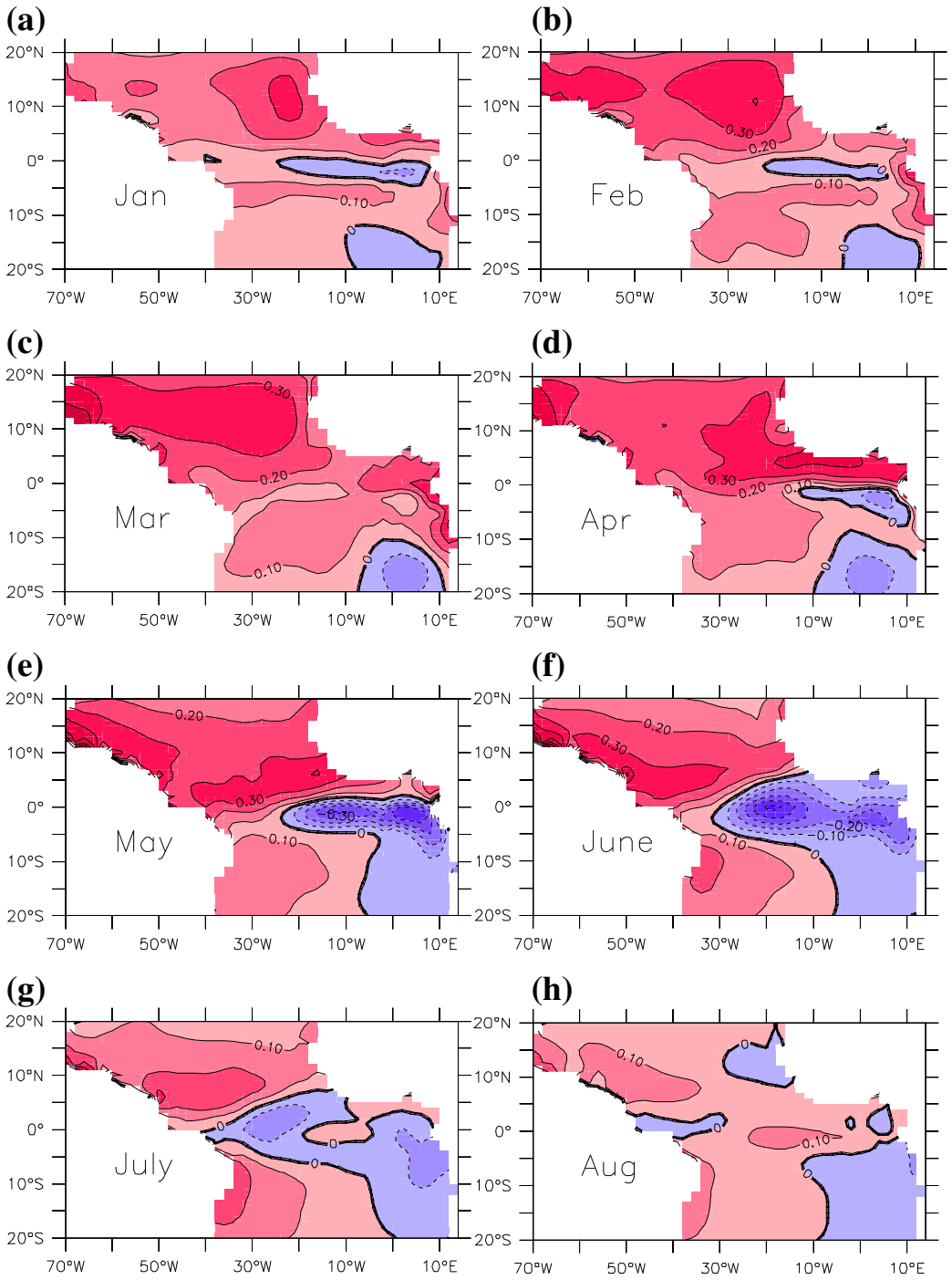

Figure 4.1. As in Figure 3.8, but for the NADV experiment.

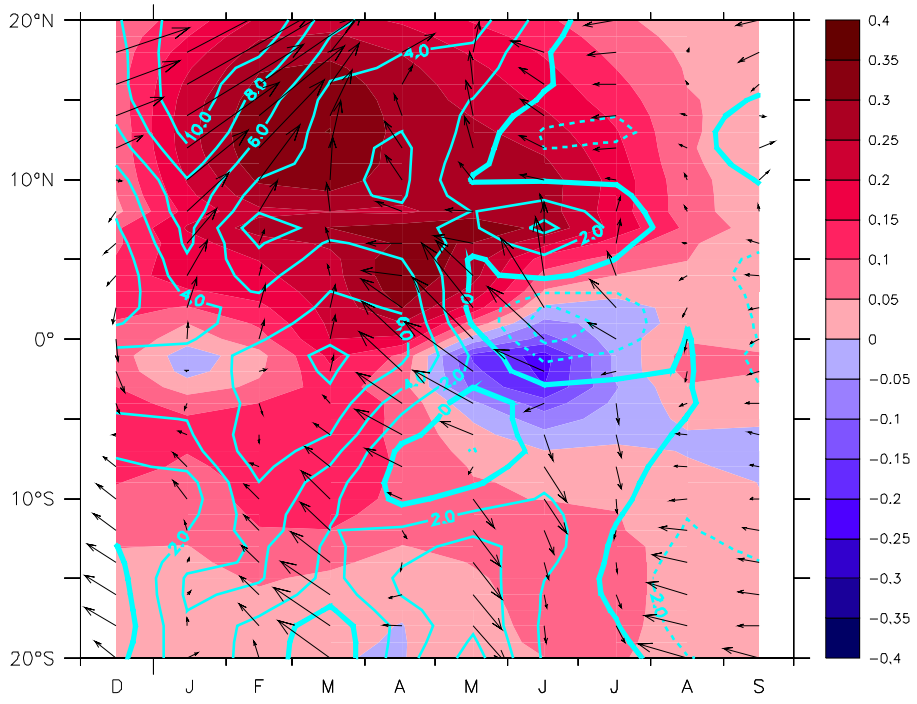

Figure 4.2. As in Figure 3.17, but for the NADV experiment.

difference between the two experiments, wind composites are constructed for the NADV experiment (Figure 4.4). Comparing Figure 4.4 with Figure 3.6, one can see that the northeasterly wind anomaly of the NADV experiment during the boreal winter is stronger than that of the CTRL experiment during the same season. This difference is clearly shown in Figure 4.5. Therefore, given that the surface heat flux in the NTA is mainly dominated by winds (see Chapter III), it is not difficult to understand why the warm SST anomaly of the NADV experiment is stronger. This is indeed the case when comparing the total downward surface heat flux of these two experiments during this period, which shows a stronger downward surface heat flux in the NADV experiment (figures not shown). However, the weaker SST anomaly during late spring to early

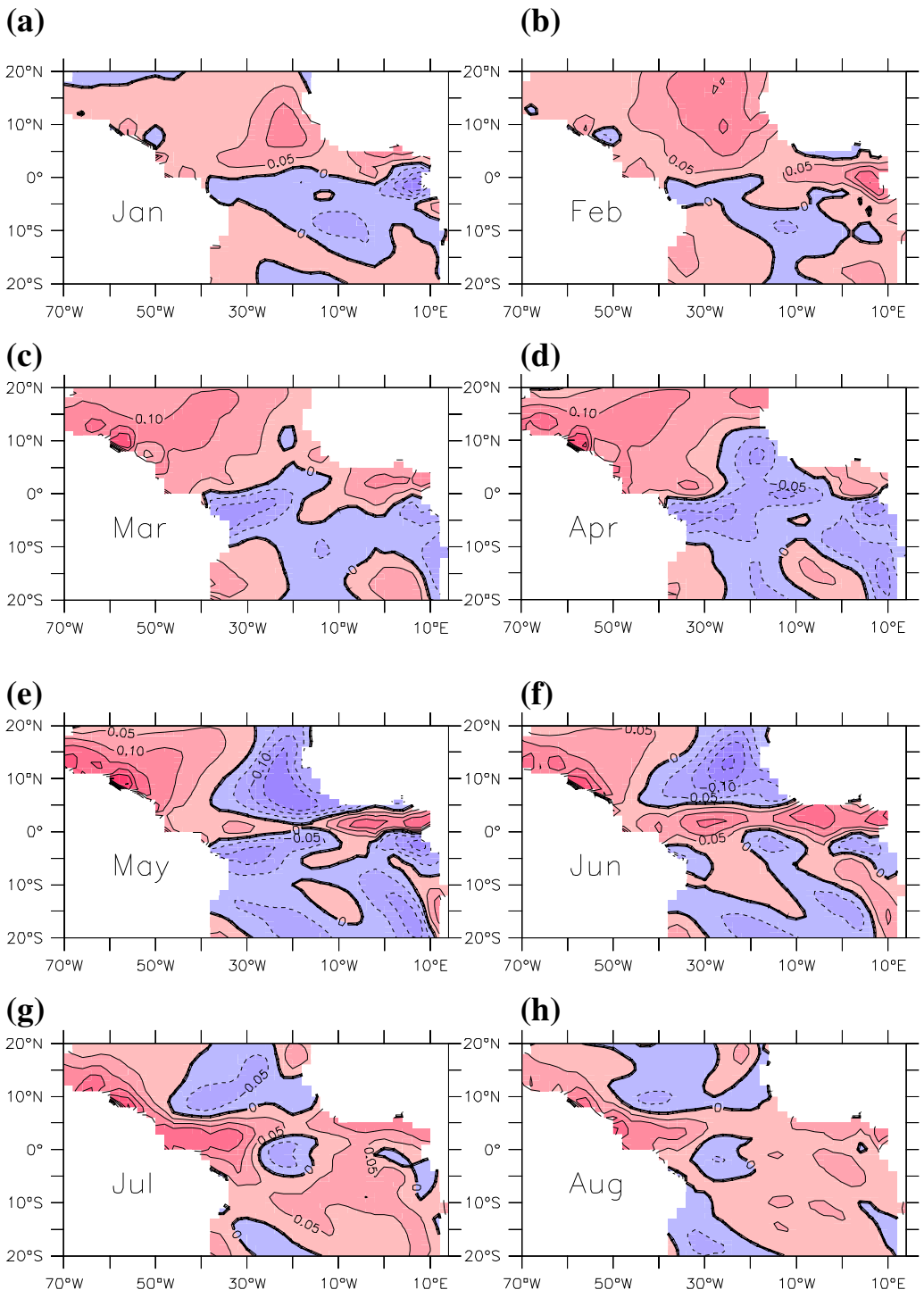

Figure 4.3. Differences in SST anomalies between the NADV and CTRL experiments (NADV minus CTRL). Contour interval is 0.05°C.

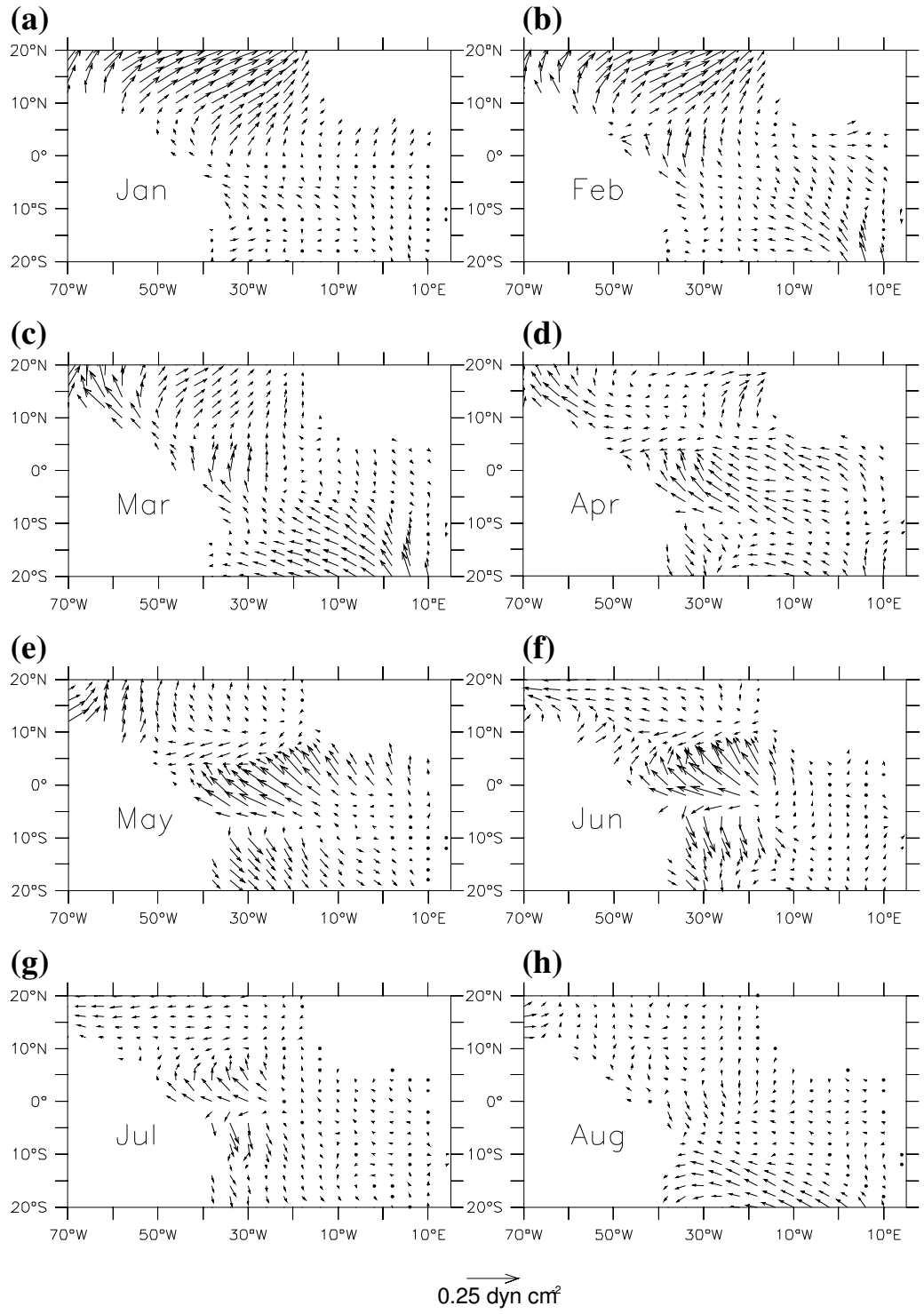

Figure 4.4. As in Figure 3.6, but for the NADV experiment.

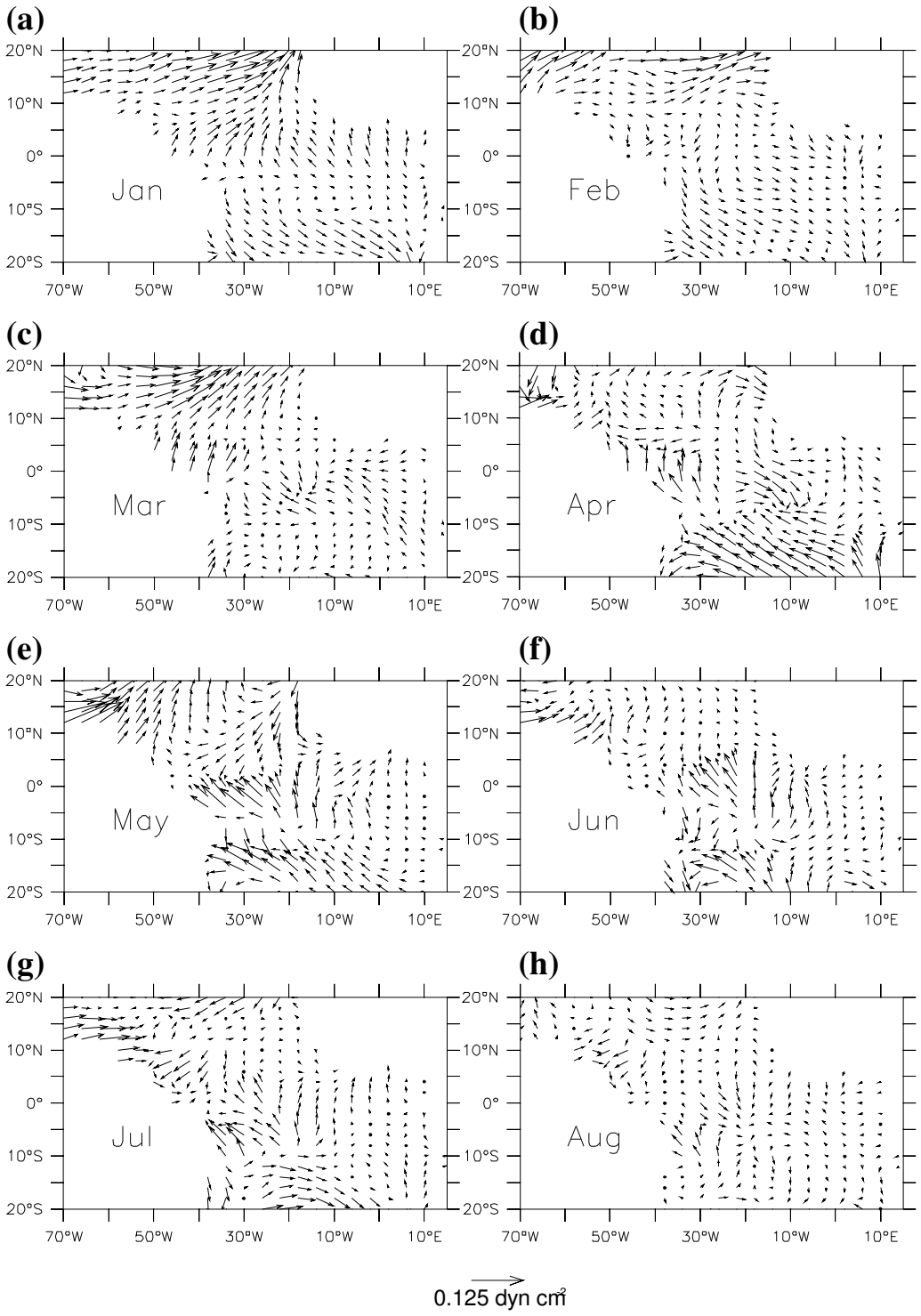

Figure 4.5. Differences in wind stress anomalies between the NADV and CTRL experiments (NADV minus CTRL).

summer in the NADV experiment can only be explained by the missing horizontal advection of heat. This is because there is little difference in the surface heat flux between these two experiments during this period (figures not shown). Since the cross-equatorial wind anomaly, which happens during boreal spring (Figures 3.6c-3.6e), can effectively strengthen the NECC, the advection of mean SST by the anomalous eastward current tends to warm the SST in the eastern NTA. Figures 4.6 shows the composites of the anomalous surface currents in May and June constructed from the CTRL experiment. One can see that there is a strong anomalous eastward current which appears in the 5°-15°N band. During this period, the gradient of the mean SST field is also very strong along this band, particularly in the eastern NTA (Figure 4.7). This gives rise to a positive advection of heat in this region, thus an anomalous warming. Therefore, the absence of this positive advection of heat causes the warm SST anomaly in the NTA from the NADV experiment weaker than in the CTRL experiment.

In the STA, the SST anomaly of the NADV experiment during boreal spring is generally colder than that of the CTRL experiment (Figures 4.3c-4.3e). These

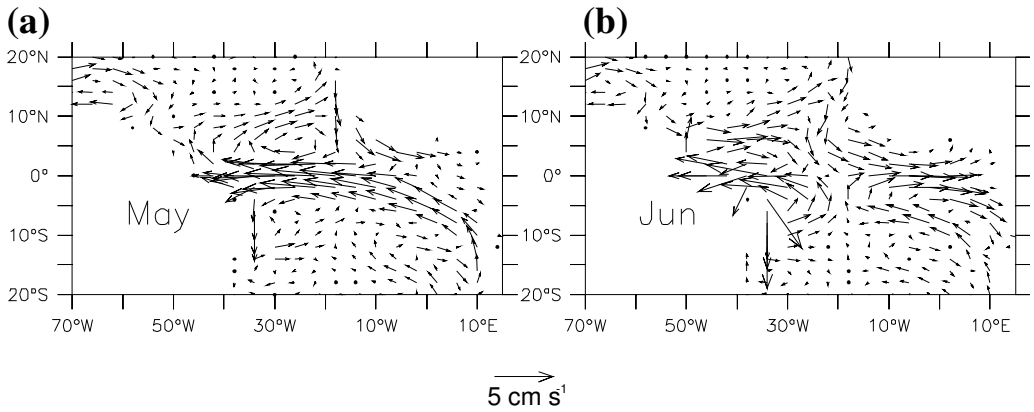

Figure 4.6. Composites of anomalous surface currents in May and June constructed from the CTRL experiment. 48 warm ENSO events in 1982, 87, 91, 97 during the period of 1980 to 2000 from 12 runs are used.

(a)

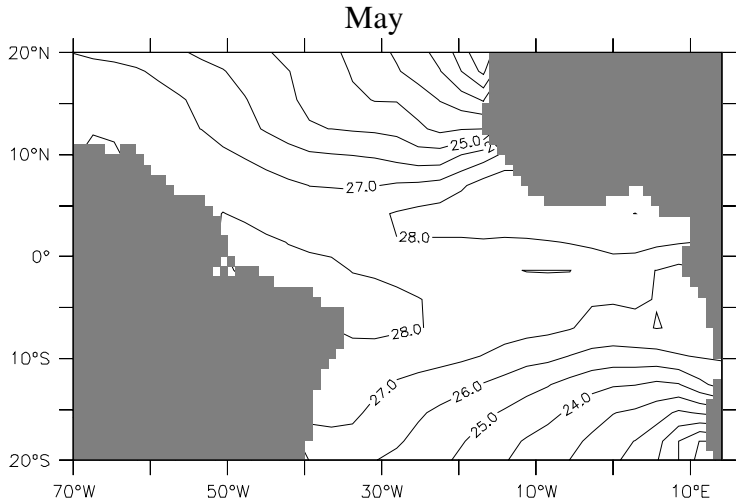

(b)

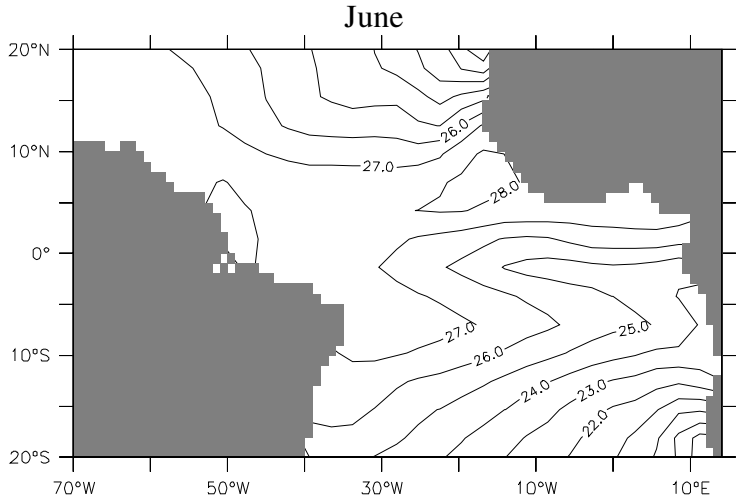

Figure 4.7. SST Climatology of (a) May and (b) June derived from Reynold's SST (Smith et al., 1996) during the period of 1950 to 2000. Contour interval is 1°C.

differences in SST anomaly coincide with those in the wind anomaly between the two experiments, suggesting that the differences are mainly caused by the winds. Therefore, the role of horizontal advection is negligible in the STA.

In the equatorial Atlantic, the surface current is expected to show more variability than the currents in off-equatorial regions because of the strong variability of the winds in this region (Figure 3.6). Therefore, the differences in SST in this region between the NADV and CTRL experiments are anticipated. The differences are particularly obvious during May-June-July (Figure 4.3). But the absence of the horizontal advection from the NADV experiment does not appear to have any major impact on the formation of the cold SST anomaly during this season (Figure 4.1). This is because the entrainment induced by Ekman and Bjerknes feedbacks is so dominant in the SST variability in this region that the SST variability resulting from horizontal advection is negligible compared with the SST variability induced by Ekman and Bjerknes feedbacks.

2. NENT Experiment

To examine the importance of entrainment in determining the Atlantic SST response to remote influence of ENSO, composites of SST evolution are constructed from the NENT experiment, and shown in Figure 4.8. It shows that during boreal winter to early spring, the SST anomaly in the northern hemisphere is generally warmer than that in the southern hemisphere except in the coastal regions of the eastern STA. This SST pattern resembles the one simulated by the CTRL experiment (Figure 3.8), suggesting that the entrainment process is less important during this season.

However, as the season progresses into boreal spring, the entire equatorial region and the eastern STA region, in the NENT experiment, are dominated by a strong warm SST anomaly (Figures 4.8c-4.8e). During the boreal summer, a weak cold SST anomaly is seen in the eastern NTA. This pattern of the SST anomalies in the tropical Atlantic is in sharp contrast with the pattern of SST shown in Figure 3.8. The difference between

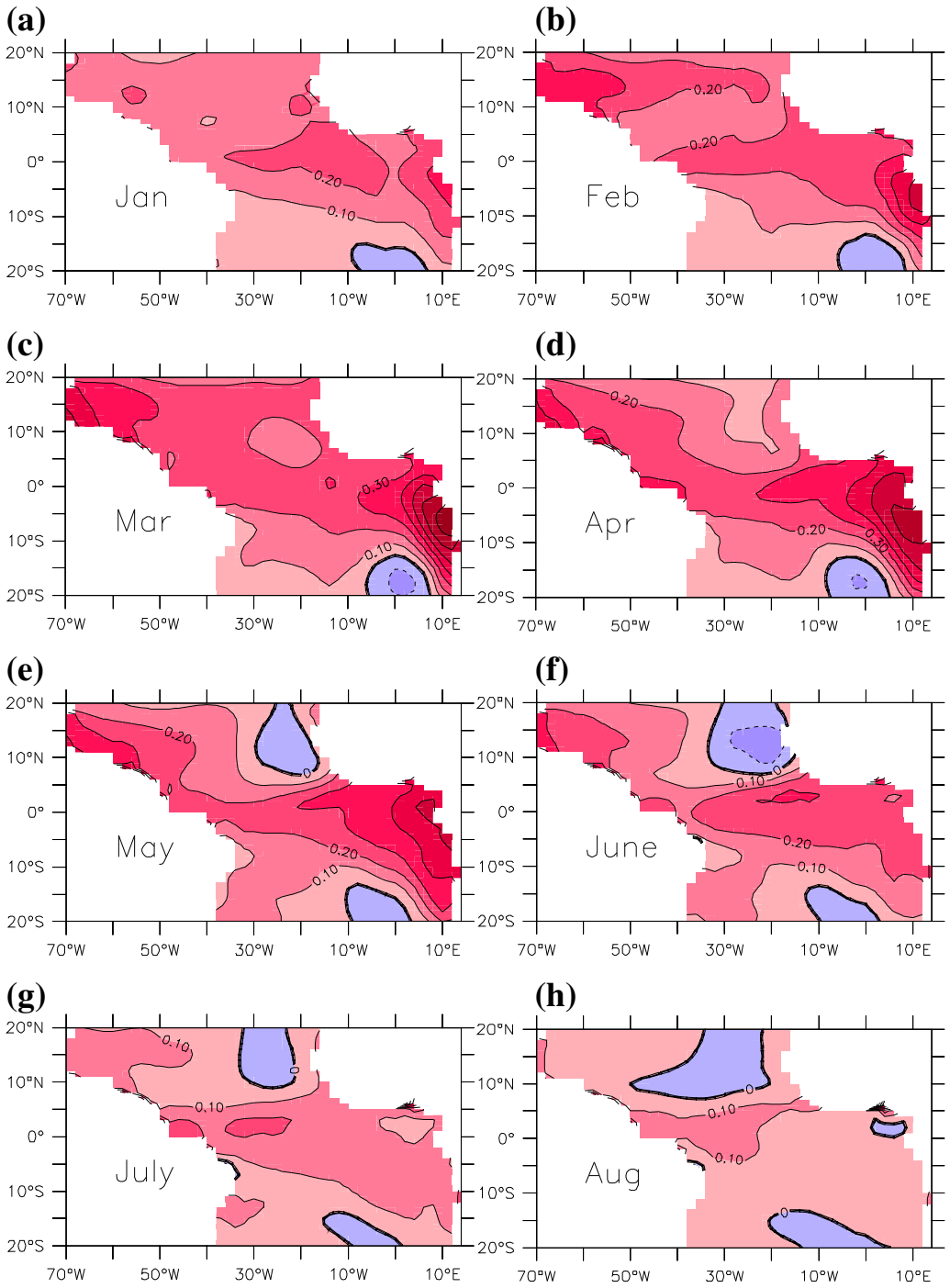

Figure 4.8. As in Figure 3.8, but for the NENT experiment.

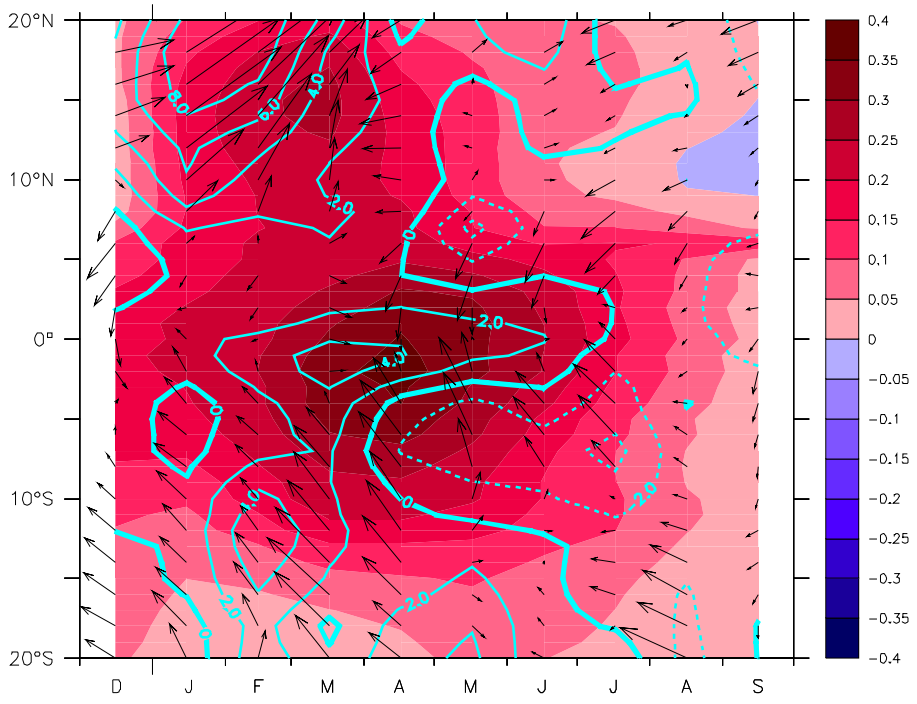

Figure 4.9. As in Figure 3.17, but for the NENT experiment.

the two experiments is more obvious if we compare the zonally averaged SST shown in Figure 4.9 and Figure 3.17. The cold SST anomaly, which appears during May-August in the CTRL experiment (Figure 3.17), is entirely absent from the NENT experiment (Figure 4.9). Therefore, the entrainment is critically important to the SST evolution in the tropical Atlantic during boreal spring to summer. Without the entrainment process, the model cannot capture the key features of the SST evolution during the late boreal spring to summer following an ENSO event.

In the NENT experiment, the warm SST anomaly in the equatorial region and eastern STA region, which is most prominent during boreal spring, is actually induced by the strong downward surface heat flux during the earlier season (Figure 4.9). In fact,

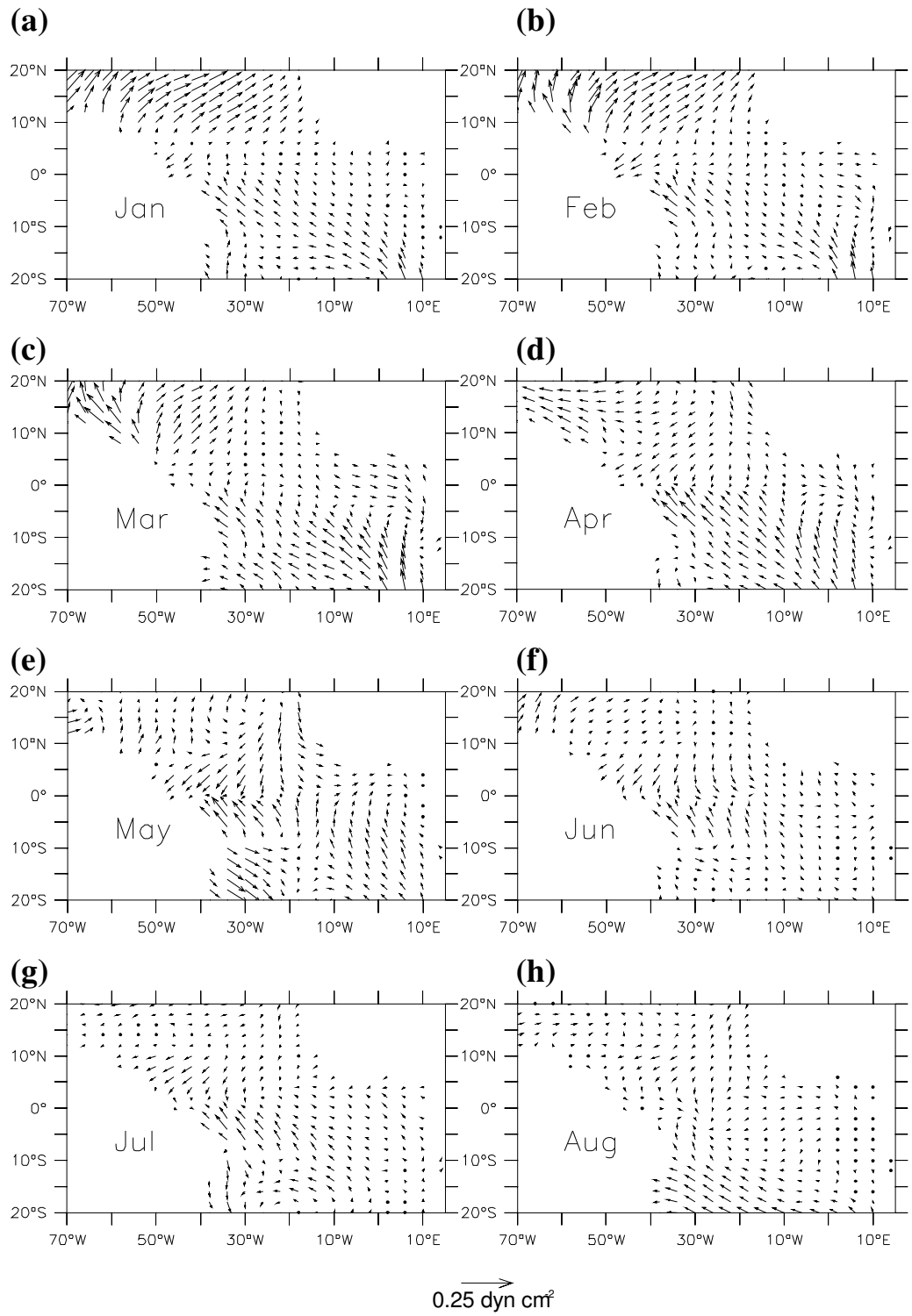

Figure 4.10. As in Figure 3.6, but for the NENT experiment.

similar downward heat flux anomalies can also be found in the CTRL and NADV experiments (Figures 3.17 and 4.2), but in these two cases a cold SST anomaly is formed during the late spring to early summer. This is because in both cases, the entrainment process is not disabled, thus the cold water entrained from the subsurface can effectively cancel the warming induced by the surface heat flux, thus forming a cold anomaly at the surface.

In the off-equatorial regions, the wind variations (Figure 4.10) are consistent with the SST variations (Figure 4.8, also see Figure 4.9). This further confirms the dominant role of wind-induced heat flux in the SST variability in these regions.

3. SLAB Experiment

Figures 4.11-4.13 show the composites similar to those constructed from the other experiments. Since the advection of heat is of secondary importance in the tropical Atlantic as noted in Section 1, it is not surprising that the results of the SLAB experiment resemble those of the NENT experiment. But there are some noticeable differences in the SST composites between the SLAB and NENT experiments. It can be seen that in the eastern STA, the SST anomaly simulated by the NENT experiment (Figure 4.8) is relatively stronger than the one simulated by the SLAB experiment. This difference is probably caused by the horizontal advection of anomalous SSTs by the mean current because the westward SEC (Figure 2.1) can effectively transport anomalously warm SSTs in the eastern STA to the west in the NENT experiment.

Although the SLAB experiment captures the warming in SST during boreal winter to early spring (Figure 4.11) like the NENT experiment, it also missed the cooling in SST during late spring to summer, which has been found in the CTRL experiment and the observations. This experiment confirms the crucial role of the Ekman and Bjerknes feedback in the SST response to the remote influence of ENSO in the equatorial and eastern STA regions.

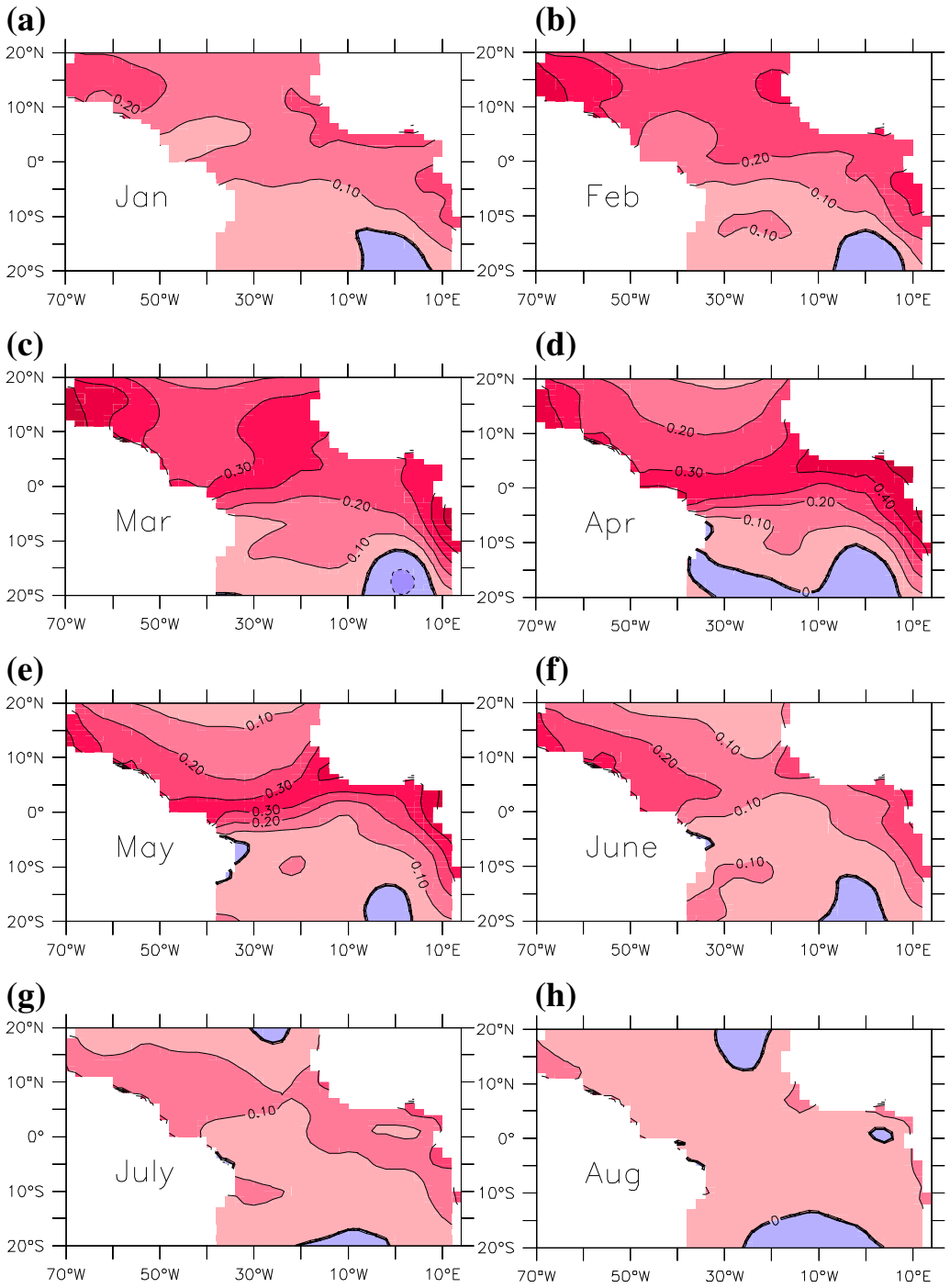

Figure 4.11. As in Figure 3.8, but for the SLAB experiment.

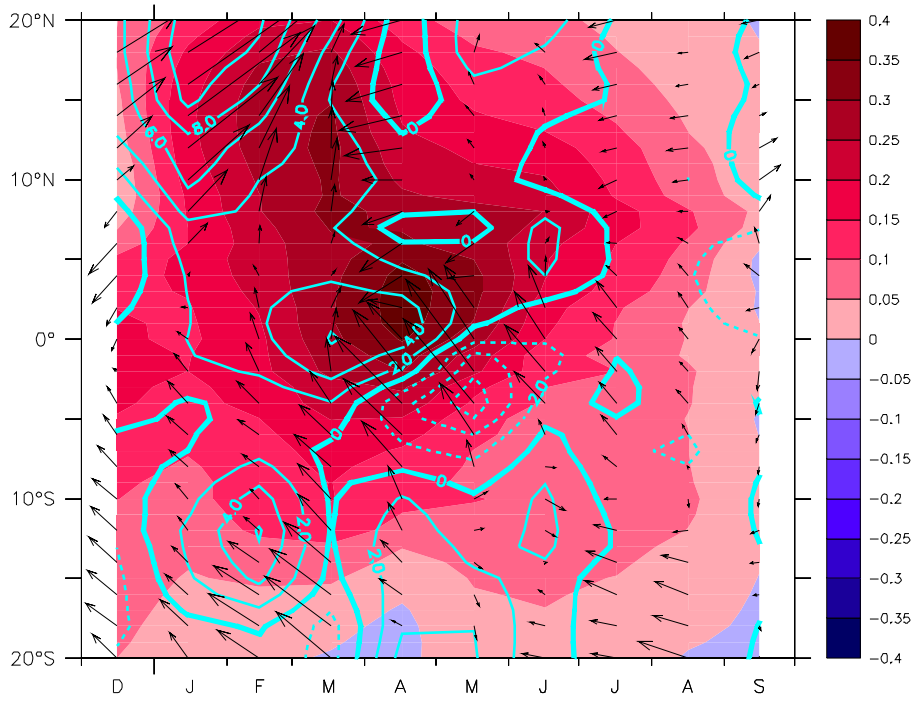

Figure 4.12. As in Figure 3.17, but for the SLAB experiment.

4. Discussion

The results of the three experiments (NADV, NENT, SLAB experiments), which are designed to assess the relative importance of ocean dynamics in the tropical Atlantic SST response to the remote influence of ENSO, have been investigated.

By comparing the composite maps of SST evolution, we found that the distributions of the SST anomaly during boreal winter to early spring simulated by the three experiments consistently show a pattern similar to the one simulated by the CTRL experiment when ocean dynamics are included. This suggests that in this season ocean dynamics are rather passive and do not seem to have any major impact on SST, and the

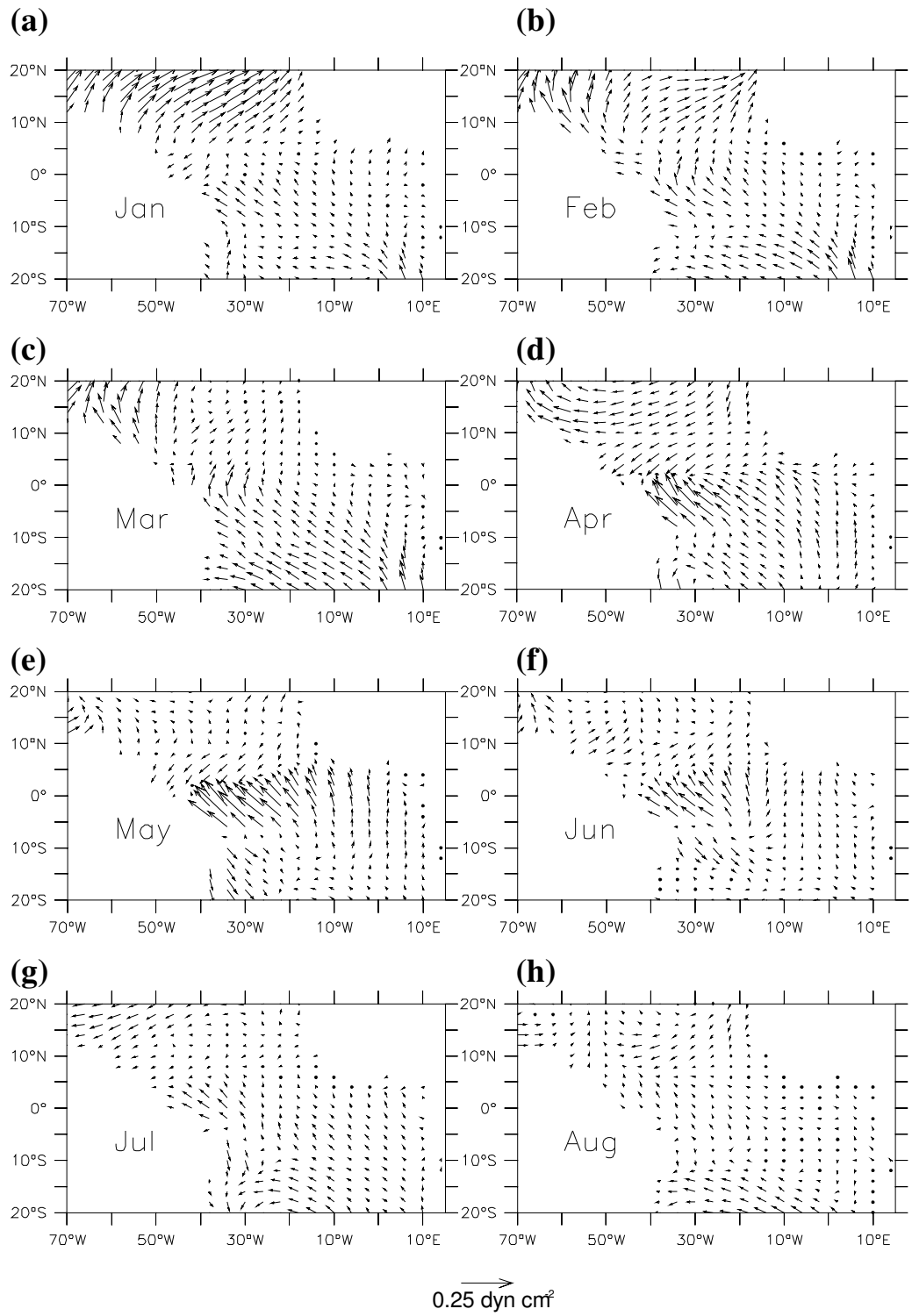

Figure 4.13. As in Figure 3.6, but for the SLAB experiment

(a) NADV

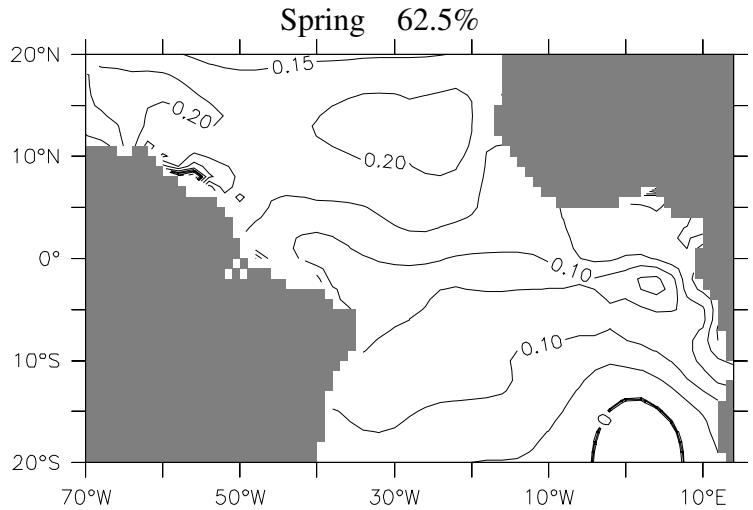

(b) NENT

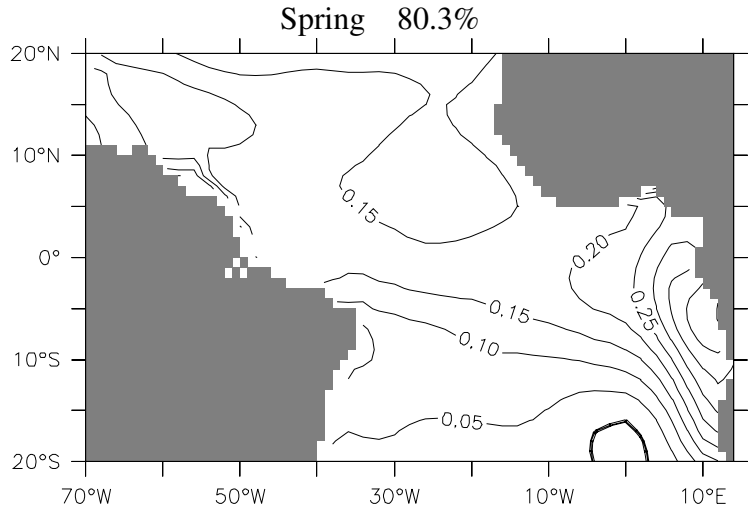

Figure 4.14. First leading EOFs during boreal spring derived from the (a) NADV, (b) NENT, and (c) SLAB experiments. Contour interval is 0.05°C.

(c) SLAB

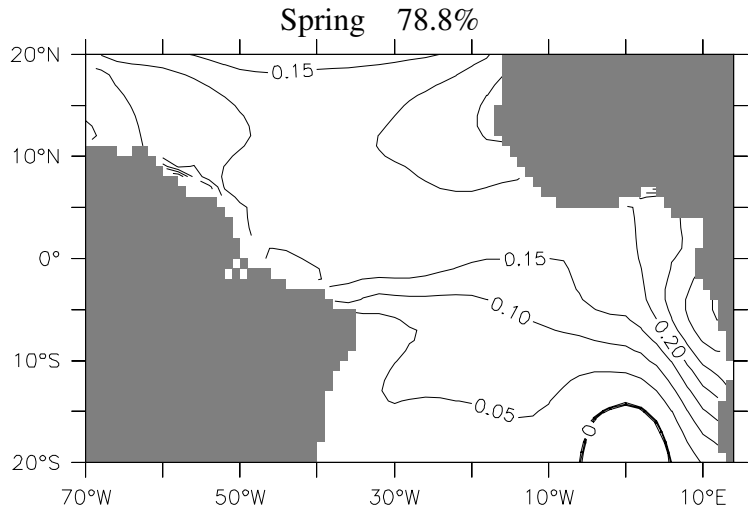

Figure 4.14. (Continued)

SST response to the remote influence of ENSO during this period is mainly controlled by surface heat fluxes. Thus, the air-sea feedback in this season is basically a thermodynamic feedback. This explains why an AGCM coupled to a simple mixed layer ocean, where ocean dynamics are absent, is able to capture the ENSO's influence during this season (Alexander and Scott, 2002; Chang et al., 2003).

The similar response of SST to the remote ENSO forcing in this season are clearly shown by the leading "signal" EOFs derived from the three experiments (Figure 4.14) and the CTRL experiment (Figure 3.11a). These patterns show a similar basin-wide warming with larger amplitudes in the northern hemisphere than in southern hemisphere. This uniform pattern reflects the direct influence of ENSO on SST in the tropical Atlantic in this season, and is consistent with the prediction of TT mechanism. The asymmetry of warming in SST in tropical Atlantic is mainly due to the asymmetry

(a) NADV

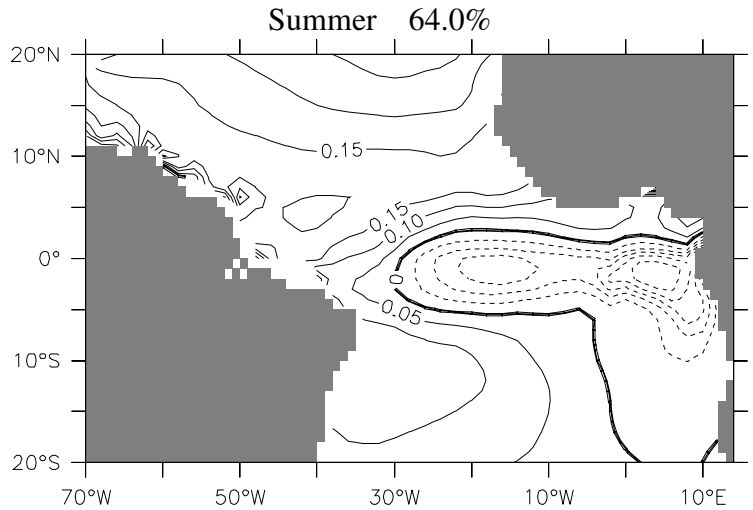

(b) NENT

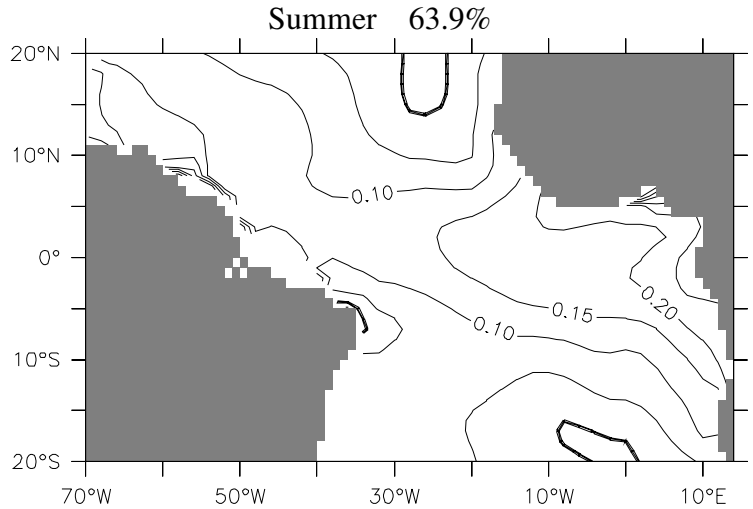

Figure 4.15. First leading EOFs during boreal summer derived from the (a) NADV, (b) NENT, and (c) SLAB experiments. Contour interval is 0.05^{o}C.

(c) SLAB

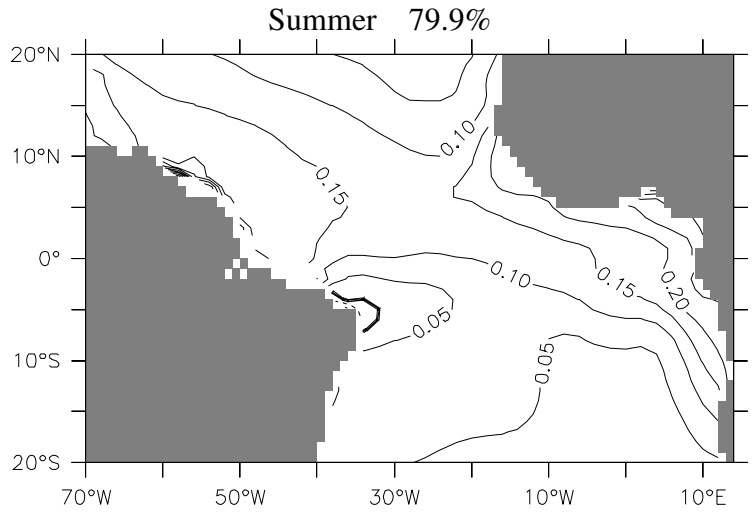

Figure 4.15. (Continued)

of wind anomalies in the two hemispheres. This asymmetry has little connection with the ocean dynamics except in the deep tropics where the surface currents are strong or the gradient of the mean SST field is strong.

Because of the similar distribution of SST anomalies during the boreal winter to spring in these experiments, a similar cross-equatorial wind anomaly during the boreal spring is expected. However, how the SST responds to this wind anomaly depends on what ocean dynamics are included in the ocean model. As we have seen, the SST response in the NENT and SLAB experiments is entirely different from the response in the CTRL and NADV experiments. This difference is clearly shown by the seasonal leading EOFs of the experiments (Figures 4.15 and 3.11b).

In the NENT and SLAB experiments, the summer leading patterns (Figures 4.15b and 4.15c) resembles their spring leading patterns (Figures 4.14b and 4.14c),

reflecting the fact that the spring SST persists through the summer season. While in the CTRL and NADV experiments, the entrainment tends to “destroy” their spring SST patterns, pointing to the active role of entrainment in the seasonal changes of dominant patterns from boreal spring to summer. Thus, if an ocean model is designed to capture the SST response to the remote influence of ENSO during the late boreal spring to summer, it should at least include the entrainment process.

CHAPTER V

SUMMARY AND DISCUSSION

1. Summary

A RP-CGCM model, in which an intermediate complexity ocean model is coupled to a state of the art atmospheric GCM, is developed to investigate the tropical Atlantic response to remote ENSO forcing. A suite of ensemble integrations are carried out to assess the relative importance of various oceanic processes contributing to Atlantic SST variability. The results show that the RP-CGCM is capable of capturing the major features of TAV and its response to ENSO forcing.

The results further show that the SST response to the remote influence of ENSO may be divided into two stages. In stage one, the effect of ENSO is felt in the tropical Atlantic basically through an atmospheric bridge effect which alters the surface heat flux. Of particular relevance is the TT mechanism, which predicts a uniform warming in the tropical Atlantic following the mature phase of El Nino. In the NTA, the anomalous southwesterly winds induced by the Walker mechanism and the PNA mechanism, also contribute to the warming due to the wind-induced latent heat flux. These mechanisms work in concert with the TT mechanism in the NTA region, giving rise to a robust SST response during the boreal spring. In the STA, the southeasterly wind anomaly, albeit relatively weak, causes cooling in SST by enhancing the latent heat flux. Moreover, the increased stratus clouds in response to TT in the STA imply a reduction of net downward short wave surface flux - also a cooling effect. Both these mechanisms work against the TT-induced warming in the STA, resulting in a much weaker SST response in this region. Therefore, although the SST response to the ENSO forcing shows a basin-wide spatial pattern, the amplitude is larger and robust in the NTA than in the STA. The response in the Atlantic lags ENSO by about a season and peaks in boreal spring. At this

stage, the response can largely be explained by the ocean mixed layer response to changes in surface heat fluxes induced by ENSO, although we did note that ocean advection plays a role in altering its strength.

In stage two, ocean dynamics play a more active role in determining the evolution of SST. A key factor that triggers the significant response in ocean dynamics during this stage is the cross-equatorial wind anomaly, which is driven by the interhemispheric SST gradient formed in stage one. This wind anomaly is most prominent in the western to central equatorial Atlantic, and can change the SST in the eastern equatorial Atlantic through Bjerknes feedback and the SST in the central equatorial Atlantic through Ekman feedback. The Benguela Nino in the Angola-Namibia coastal region is also found to be related to the thermocline changes in the equatorial region. For a warm ENSO event, the above feedbacks result in a cooling of SST in the ESA region. This cooling is so overwhelming that it cancels the warming effect induced by the TT mechanism and reverses the sign of the warm SST anomaly that is formed during stage one in this region. Therefore, the SST response to the ENSO forcing has characteristics of the zonal mode, and peaks in boreal summer. The SST response in this season is largely determined by the thermocline's response to changes in zonal wind and the upwelling response to changes in wind divergence. Therefore, the response is strongly affected by the wind-driven ocean dynamics and less so by atmospheric heat flux.

Experiments show that in general the horizontal advection of heat plays a secondary role in the SST response to the remote influence of ENSO. Only in the region north of the equator where the NECC dominates and the equatorial region where the SST variability is strong during the late boreal spring to summer does the horizontal advection play a role in determining the amplitude of SST response. Experiments also show that entrainment is particularly important in maintaining the correct SST structure during boreal summer. Without the entrainment process the simulated equatorial SST anomaly tends to have the opposite sign of the observed SST. The entrainment plays a critically important role in the equatorial region and certain coastal regions of Africa

where the upwelling and Ekman divergence are strong. Therefore, in practice, the mixed layer model is expected to be able to capture the SST response to the remote ENSO influence during the boreal winter to spring. But in order to capture the correct SST structure during late boreal spring to summer, ocean dynamics, or at least the entrainment process, are required in the coupled model.

2. Discussion and Future Work

2.1 Model Biases

As noted before, the RP-CGCM tends to underestimate the variability of the meridional mode and overestimate the variability of the zonal mode, and the variability simulated by the model tends to lead the observations during boreal winter to spring. These systematic biases may be caused by approximations in the model.

Since much of the SST variability in the tropical Atlantic is driven by surface heat flux (Carton et al., 1996; Chang et al., 1997), the mixed layer depth, which determines the heat capacity of the surface layer, is very important for the model to accurately capture the thermodynamic feedback. The importance of the mixed layer has been demonstrated in studies by Saravanan and Chang (1999) and Chiang and Sobel (2002). They suggest that the mixed layer depth can influence the patterns, amplitudes, and adjustment time of the SST in response to the surface heat flux forcing. But the mixed layer in RP-CGCM, albeit a spatially varying field, does not vary with time.

The surface currents estimated by Equations 2.4 and 2.5 may also contain significant errors, particularly in regions close to the equator (Bonjean and Lagerloef, 2002). The errors in the surface currents will further cause biases in the entrainment velocity. Another approximation that can produce error in the entrainment cooling is the simple parameterization of subsurface temperature. Although the multivariate linear relationship that is used to calculate the subsurface temperature can give a qualitative estimate of the entrained water temperature, this method only explains a relatively small

part of the subsurface temperature variability. Therefore, optimizing the estimation of the currents and the parameterization of the subsurface temperature is a key step to further improve the model's skill. This is particularly important in the equatorial region where the SST variability is known to be dominated by ocean dynamics.

A weak point of the regional ocean model are the closed boundaries. The errors in the horizontal advection caused by the northern and southern boundaries are not a severe problem when studying seasonal and interannual variability because the horizontal advection of heat plays a secondary role in the off-equatorial regions. However, it would be a severe handicap if this regional model were used to study variability at longer time scales because there is no communication between the tropics and extratropics. Hickey and Weaver (2004) found that the thermocline variation in the STA, particularly in the Angola-Namibia coastal region, is connected with the high seasonal and interannual variability – in both temperature and salinity – in the Southern Ocean. Therefore, the underestimation of the SST variability in the southeastern tropical Atlantic is attributed to the artificial southern boundary of the ocean model.

2.2 Intrinsic TAV

The practical value of understanding the mechanisms of TAV in response to the remote ENSO forcing is to improve the skill of predicting disastrous climate events. As we mentioned before, the climate variability in the tropical Atlantic sector, in addition to the component that is forced by ENSO, has also a component that is driven by processes intrinsic to the Atlantic. Therefore, knowing only the mechanisms of the ENSO-induced TAV is not sufficient to make an accurate prediction of TAV.

In fact, the intrinsic TAV accounts for a larger amount of the total variance of the SST anomalies in the tropical Atlantic than that induced by ENSO. This can be estimated by this "noise" component of the CTRL experiment. The result shows that the "noise" explains about 77% of total variance in the tropical Atlantic from 20°S-20°N. Therefore, it is important that we have a good understanding of the mechanisms

responsible for the intrinsic TAV.

Figure 5.1 shows the first two leading EOFs derived from the “noise” of the CTRL experiment. The similarity between Figures 5.1 and 3.2 is anticipated because the intrinsic TAV explains most of the variability in the tropical Atlantic. The similarity is also reflected in the seasonal phase-locking of this mode (Figures 5.2 and 3.4). If one compares Figures 5.1 and 5.2 with Figures 3.9 and 3.10, one can see that the meridional mode and zonal mode derived from the “noise” resemble the two modes derived from the “signal”, respectively. In Chapter III, we argued that the meridional mode and zonal mode are connected, and the key phenomenon for the connection is the cross-equatorial flow, which is coupled with the interhemispheric SST gradient. In fact, this interhemispheric SST gradient can also be found in the meridional mode of the “noise” part (Figure 5.1b). This leads to the hypothesis that the meridional mode and zonal mode of the intrinsic TAV may also be interrelated.

Upon a careful examination of the “noise”, we did find evidence that in many cases a warm meridional mode evolves into a cold zonal mode, similar to the characteristics observed in the SST evolution in response to the remote influence of ENSO. But we also found cases where a warm meridional mode did not evolve into a cold zonal mode, and also cases where a cold zonal mode was not preceded by a warm meridional mode. These results raise the following questions: Can the zonal mode be excited by the meridional mode? If so, what is the excitation mechanism? Furthermore, what implication does the connection between the two modes have for TAV predictability? These questions will be addressed by future work.

(a)

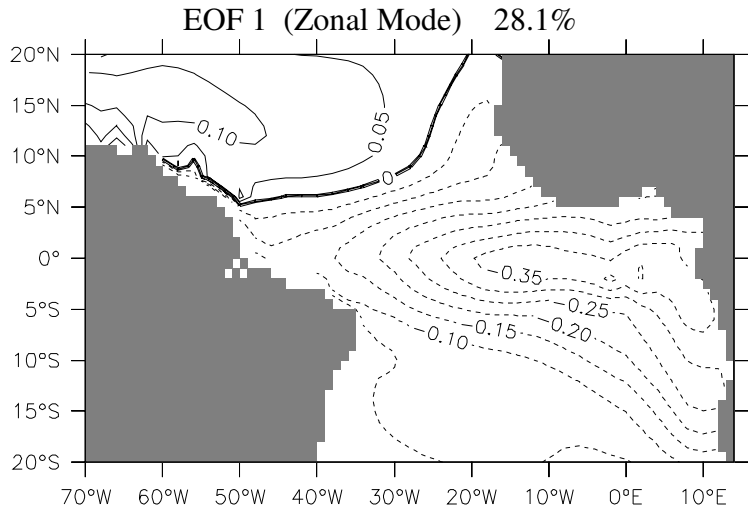

(b)

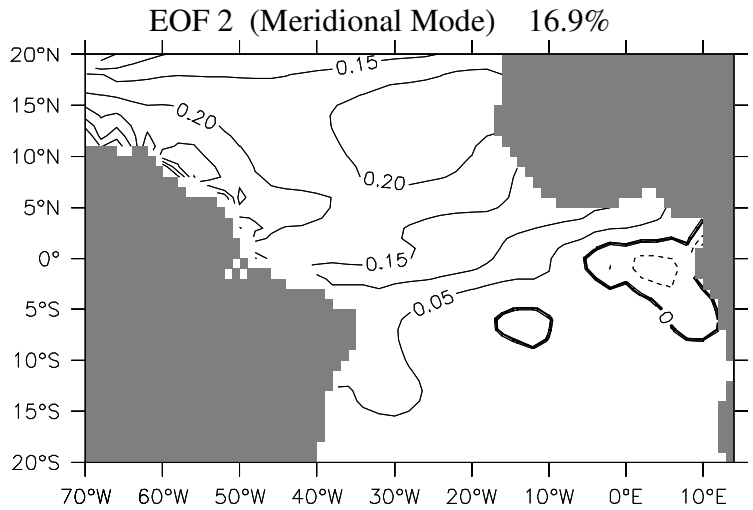

Figure 5.1. (a) First and (b) second leading EOFs derived from the SST "noise" of the CTRL experiment (The associated PC time series have been normalized by their standard deviations). Contour interval is 0.05^{o}C.

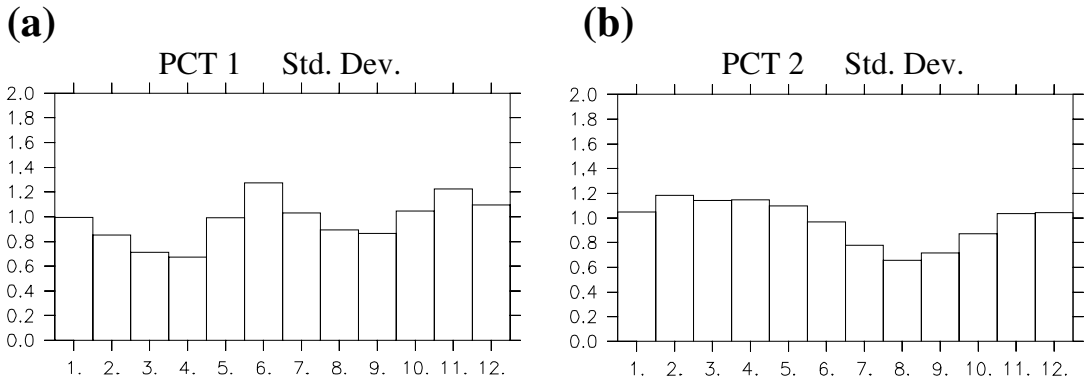

Figure 5.2. Standard deviation of the PC time series associated with the (a) first leading EOFs and (b) second leading EOFs derived from the "noise" of the CTRL experiment. The horizontal axis is calendar month.

REFERENCES

Allen, M. R., and L. A. Smith, 1997: Optimal filtering in singular spectrum analysis. *Phys. Lett.*, **234**, 419-428.

Alexander, M., and J. Scott, 2002: The influence of ENSO on air-sea interaction in the Atlantic. *Geophys. Res. Lett.*, **29**, doi: 10.1029/2001GL014347.

Alexander, M., I. Blade, M. Newman, J. R. Lanzante, N.-C. Lau, and J. D. Scott, 2002: The atmospheric bridge: The influence of ENSO teleconnections on air-sea interaction over the global oceans. *J. Climate*, **15**, 2205-2231.

Battisti, D. S., and A. C. Hirst, 1989: Interannual variability in the tropical atmosphere-ocean system: Influence of the basic state and ocean geometry. *J. Atmos. Sci.*, **45**, 1687-1712.

Bonjean, F., and G. S. E. Lagerloef, 2002: Diagnostic model and analysis of the surface currents in the tropical Pacific Ocean. *J. Phys. Oceanogr.*, **32**, 2938-2953.

Bjerknes, J., 1969: Atmospheric teleconnections from the equatorial Pacific. *Mon. Wea. Rev.*, **97**, 163-172.

Bonan, G. B., 1998: The land surface climatology of the NCAR Land Surface Model coupled to the NCAR Community Climate Model. *J. Climate*, **11**, 1307–1326.

Cane, M. A., 1979: The response of an equatorial ocean to simple wind-stress patterns, I, model formulation and analytical results. *J. Mar. Res.*, **37**, 233-252.

Carton, J.A., and B. Huang, 1994: Warm events in the Tropical Atlantic. *J. Phys. Oceanogr.*, **24**, 888-903.

Carton, J. A., X. Cao, B. S. Giese, and A. M. Da Silva, 1996: Decadal and interannual SST variability in the tropical Atlantic. *J. Phys. Oceanogr.*, **26**, 1165-1175.

Chang, P., and G. Philander, 1994: A coupled ocean-atmosphere instability of relevance to the seasonal cycle. *J. Atmos. Sci.*, **51**, 3627-3648.

Chang, P., 1994: A study of the seasonal cycle of sea surface temperature in the tropical Pacific Ocean using reduced gravity models. *J. Geophys. Res.*, **99**, 7725-7741.

Chang, P., L. Ji, and H. Li, 1997: A decadal climate variation in the tropical Atlantic Ocean from thermodynamic air-sea interactions. *Nature*, **385**, 516-518.

Chang, P., R. Saravanan, L. Ji, and G. C. Hegerl, 2000: The effect of the local sea surface temperature on atmospheric circulation over the tropical Atlantic sector. *J. Climate*, **13**, 2195-2216.

Chang, P., L. Ji, and R. Saravanan, 2001: A hybrid coupled model study of tropical Atlantic varriability. *J. Climate*, **14**, 361-390.

Chang, P., R. Saravanan, and L. Ji, 2003: Tropical Atlantic seasonal predictability: The Roles of El Niño remote influence and thermodynamic air-sea feedback. *Geophys. Res. Lett.*, **30**, 1501-1504.

Chang, P., T. Yamagata, P. Schopf, S. K. Behera, J. Carton, W. S. Kessler, G. Meyers, T. Qu, F. Schott, S. Shetye, T. Stockdale, and S.-P. Xie, 2004: Climate fluctuations of tropical coupled system – the role of ocean dynamics. *Submitted to J. Climate*.

Chiang, J. C. H., and A. H. Sobel, 2002: Tropical tropospheric temperature variations caused by ENSO and their influence on the remote tropical climate. *J. Climate*, **15**, 2616-2631.

Covey, D. L., and S. Hastenrath, 1978: Pacific El Nino phenomenon and Atlantic circulation. *Mon. Wea. Rev.*, **106**, 1280-1287.

Curtis, S., and S. Hastenrath, 1995: Forcing of anomalous sea surface temperature evolution in the tropical Atlantic during Pacific warm events. *J. Geophys. Res.*, **100**, 15835-15847.

Czaja, A., P. Van Der Varrt, and J. Marshall, 2002: A diagnostic study of the role of remote forcing in tropical Atlantic variability. *J. Climate*, **15**, 3280-3290.

Czaja, A., 2004: Why is north Atlantic SST variability stronger in boreal spring? *J. Climate*, **17**, 3017-3025.

Davey, M., M. Huddleston, and K. R. Sperber, 2000: STOIC: A study of coupled model climatology and variability in tropical ocean regions. *CLIVAR Exhanges*, Vol. 5, No. 3, International CLIVAR Project Office, Southhampton, United Kingdom, 21-23.

Delecluse, P., J. Servain, C. Levy, K. Arpe, and L. Bengtsson, 1994: On the connection between the 1984 Atlantic warm event and the 1982-1983 ENSO, *Tellus*, **46**, 448-464.

Enfield, D. B., 1996: Relationships of inter-American rainfall to tropical Atlantic and Pacific SST variability. *Geophys. Res. Lett.*, **23**, 3305-3308.

Enfield, D. B., D. A. Mayer, 1997: Tropical Atlantic sea surface temperature variability and its relation to El Nino Southern Oscillation. *J. Geophys. Res.*, **102**, 929-945.

Enfield, D. B., and E. J. Elfaro, 1999: The dependence of Caribbean rainfall on the interaction of the tropical Atlantic and Pacific Oceans. *J. Climate*, **12**, 2093-2103.

Florenchie P., J. R. E. Lutjeharms, C. J. C. Reason, S. Masson, and M. Rouault, 2003a: The source of Benguela Niños in the South Atlantic Ocean, *Geophy. Res. Lett*., **30**, 1505, doi: 10.1029/2003GL017172.

Florenchie, P., C.J.C., Reason, J. R. E. Lutjeharms, M. Rouault,C. Roy, and S. Masson, 2003b: Evolution of interannual warm and cold events in the South-East Atlantic Ocean, *J. Climate*, **17**, 2318-2334.

Folland, C. K., T. N. Palmer, and D. E. Parker, 1986: Sahel rainfall and wordwide sea temperatures, 1901-85. *Nature*, **320**, 602-607.

Folland, C. K., J. A. Owen, N. M. Ward, and A. W. Coleman, 1991: Prediction of seasonal rainfall in the Sahel region using empirical and dynamical methods, *J. Forecasting*, **10**, 21-56.

Frankignoul, C., A. Czaja, and B. L'Heveder, 1998: Air-sea feedback in the North Atlantic and surface boundary conditions for ocean models. *J. Climate*, **11**, 2310-2324.

Fratantoni, D. M., W. E. Johns, T. L. Townsend, and H. E. Hurlburt, 2000: Low-latitude circulation and mass transport pathways in a model of the tropical Atlantic Ocean. *J. Phys. Oceanogr*., **30**, 1944-1966.

Giannini, A., Y. Kushnir, amd M. A. Cane, 2000: Interannual variability of Caribbean rainfall, ENSO, and Atlantic Ocean. *J. Climate*, **13**, 1131-1145.

Giannini, A., R. Saravanan, and P. Chang, 2004: The preconditioning role of Tropical Atlantic Variability in the development of the ENSO teleconnection: Implications for the prediction of Nordeste rainfall. *Climate Dyn*., **22**, 839-855.

Gray, W. M., 1990: Strong association between West Africa rainfall and US landfall of intense hurricanes. *Science*, **249**, 1251-1256.

Hasselmann, K., 1979: On the signal-to-noise problem in atmospheric response studies. *Meteorology over the Tropic Oceans*, D. B. Shaw, Ed., Roy. Meteor. Soc., 251-259.

Hastenrath, S., 1976: Variations in low latitude circulation and extreme climatic events in the tropical Americas. *J. Atmos. Sci*., **33**, 202-215.

Hasternrath, S., and L. Heller, 1977: Dynamics of climatic hazards in northeast Brazil. *Quart. J. Roy. Meteor. Soc*. **103**, 77-92.

Hastenrath, S., 1984: Interannual variability and annual cycle: Mechanisms of circulation and climate in the tropical Atlantic sector. *Mon. Wea. Rev*., **112**, 1097-1107.

Hastenrath, S., M-C. Wu, and P-S. Chu, 1984: Towards the monitoring and prediction of north-east Brazil droughts. *Quart. J. Roy. Meteor. Soc*., **110**, 411-425

Hastenrath, S., L. C. Castro, and P. Acietuno, 1987: The Southern Oscillation in the tropical Atlantic Sector. *Contributions to Atmospheric Physics*, **60**, 447-463.

Hickey, H., and A. J. Weaver, 2004: The Southern Ocean as a source for tropical Atlantic variability. *J. Climate*, **17**, 3960-3972.

Horel, J. D., and M. J. Wallace, 1981: Planetary scale phenomenon associated with the southern oscillation. *Mon. Wea. Rev*., **109**, 813-829.

Huang, B., P. S. Schopf, and J. Shukla, 2004: Intrinsic ocean-atmosphere variability of the tropical Atlantic Ocean. *J. Climate*, **17**, 2058-2077.

Kidson, J. W., 1975: Tropical eigenvector analysis and the southern oscillation. *Mon. Wea. Rev*., **103**, 187-196.

Kiehl, J. T., J. J. Hack, G. B. Bonan, B. A. Boville, D. L. Williamson, and P. J. Rasch, 1998: The National Center for Atmospheric Research Coomunity Climate Model: CCM3. *J. Climate*, **11**, 1131-1149.

Kirtman, B. P., and J. Shukla, 2002: Interactive coupled ensemble: A new coupling strategy for CGCMs. *Geophys. Res. Lett*., **29**, doi: 10.1029 /2002GL014834.

Klein, S. A., B. J. Soden, and N. C. Lau, 1999: Remote sea surface temperature variations during ENSO: Evidence for a tropical atmospheric bridge, *J. Climate*, **12**, 917–932.

Kushnir, Y., 1994: Interdecadal variations in North-Atlantic sea surface temperature and associated atmospheric conditions. *J. Climate*, **7**, 141-157.

Kushnir, Y., W. A. Robinson, P. Chang, and A. W. Robertson, 2004: The physical basis for predicting Atlantic sector seasonal-to-interannual climate variability. *CLIVAR Workshop on Atlantic Predictability*, University of Reading, Berkshire, UK, 30 pp.

Lamb, P. J., 1978: Case studies of tropical Atlantic surface circulation patterns during recent sub-Saharan weather anomalies: 1967 and 1968. *Mon. Wea. Rev*., **106**, 282-291.

Latif, M., and T.P. Barnett, 1995: Interactions of the tropical oceans. *J. Climate*, **8**, 952-964.

Levitus, S., 1982: *Climatological Atlas of the World Oceans*, NOAA Prof. Paper 13, 173 pp. US Government Printing Office, Washington DC.

Lough, J. M., 1986: Tropical Atlantic sea surface temperature and rainfall variations in Subsharan Africa. *Mon. Wea. Rev*., **114**, 561-570.

Moura, A. D., and J. Shukla, 1981: On the dynamics of droughts in northeast Brazil: Observation, theory, and numerical experiments with a general circulation model. *J. Atmos. Sci*., **38**, 2653-2675.

Nobre, P., J. Shukla, 1996: Variations of sea surface temperature, wind stress, and rainfall over the tropical Atlantic and south America. *J. Climate*, **9**, 2464-2479.

Rao, V. B., M. C. De Lima, and S. H. Franchito, 1993: Seasonal and interannual variations of rainfall over eastern northeast Brazil. *J. Climate*, **6**, 1754-1763.

Saravanan, R., and P. Chang, 1999: Oceanic mixed layer ffedbacks and tropical Atlantic variability. *Geophys. Res. Lett*., **26**, 3629-3632.

Saravanan, R., and P. Chang, 2000: Interaction between tropical Atlantic variability and El Nino-Southern Osciallation. *J. Climate*, **13**, 2177-2194.

Servain, J., and D. M. Legler, 1986: Empirical orthogonal function analysis of tropical Atlantic sea surface temperature and wind stress: 1964-1979. *J. Geophys. Res*., **91**, 14181-14191.

Seager, R., S. E. Zebiak, and M. A. Cane, 1988: A model of the tropical Pacific sea surface temperature climatology. *J. Geophys. Res*., **93**, 1265-1280.

Smith, T. M., R. W. Renolds, R. E. Livezey, and D. C. Stokes, 1996: Reconstruction of historical sea surface temperatures using emperical orthogonal functions. *J. Climate*, **9**, 1403-1420.

Sutton, R. T., S. P. Jewson, and D. P. Rowell, 2000: The elements of climate variability in the tropical Atlantic region. *J. Climate*, **13**, 3261-3284.

Trenberth, K. E., 1997: The definition of El Nino. *Bull. Amer. Meteor. Soc*., **78**, 2771-2777.

Venzke, S., M. R. Allen, R. T. Sutton, and D. P. Rowell, 1999: The atmospheric response over the North Atlantic to decadal changes in sea surface temperature. *J. Climate*, **12**, 2562-2584.

Wallace, J.M., and D. S. Gutzler, 1981: Teleconnections in the geopotential height field

during the Northern Hemisphere winter. *Mon. Wea. Rev*., **109**, 784-812.

Wallace, J. M, C. Smith, and C. S. Bretherton, 1992: Singular value decomposition of winter-time sea surface temperature and 500-mb height anomalies. *J. Climate*, **5**, 561-576.

Wang, B., and T. Li, 1995: An intermediate model of the tropical Pacific ocean. *J. Phys. Oceanogr*., **25**, 1599-1616.

Wang, B., 1995: Interdecadal changes in El Nino onset in the last four decades. *J. Climate*, **8**, 267-285.

Ward, M. N., and C. K. Folland, 1991: Prediction of seasonal rainfall in the north Nordeste of Brazil using eigenvectors of sea surface temperature. *Int. J. Climatol*., **11**, 711-743.

Xie, S.-P. and Y. Tanimoto, 1998: A pan-Atlantic decadal climate oscillation. *Geophys. Res. Lett*., **25**, 2185-2188.

Zebiak, S. E., and M. A. Cane, 1987: A model ENSO. *Mon. Wea. Rev*., **115**, 2262-2278.

Zebiak, S. E., 1993: Air-sea interaction in the equatorial Atlantic region. *J. Climate*, **6**, 1567-1586.

Zhang, Y., J. M. Wallace, and D. S. Battisi, 1997: ENSO-like interdecadal variability: 1900-93. *J. Climate*, **10**, 1004-1020.

APPENDIX

ABBREVIATIONS USED IN THIS DISSERTATION

AGCM	atmospheric GCM
CCM3	Community Climate Model version 3
CGCM	coupled GCM
CTRL	Control experiment
EAI	equatorial Atlantic index
EEA	eastern equatorial Atlantic
ENSO	El Nino-Southern Oscillation
EOF	empirical orthogonal function
ESA	equatorial south Atlantic
EUC	Equatorial Undercurrent
GCM	global circulation model
GFDL	Geophysical Fluid Dynamics Laboratory
GOGA	global ocean global atmosphere
ICM	intermediate coupled model
ITCZ	Intertropical Convergence Zone
MAM	March-April-May
NADV	No-advection experiment
NAO	North Atlantic Oscillation
NBC	North Brazil Current
NCAR	National Center for Atmospheric Research
NCEP	National Centers for Environmental Prediction
NDJ	November-December-January
NEC	North Equatorial Current
NENT	No-entrainment experiment
NECC	North Equatorial Countercurrent

NTA	north tropical Atlantic
NTAI	NTA index
ODA	ocean data assimilation
PNA	Pacific - North America
RP-CGCM	reduced physics - coupled GCM
SEC	South Equatorial Current
SLAB	Slab ocean experiment
SLP	sea level pressure
STA	south tropical Atlantic
STAI	STA index
SST	sea surface temperature
SVD	singular value decomposition
TAV	tropical Atlantic variability
TT	troposphere temperature
WEA	western equatorial Atlantic

VITA

Yue Fang was born in Qingdao, China. He received his B.S. degree in oceanography from Ocean University of China in 1992. After two years of research at the Marine Forecasting Center, State Oceanic Administration (SOA), he was admitted to the M.S. program in oceanography at First Institute of Oceanography, SOA, and received his M.S. degree in 1997. During the following two years, he worked at the Institute of Oceanology, Chinese Academy of Sciences. In 1999, he went to Texas A&M University to pursue his Ph.D. degree in oceanography. He received his Ph.D. degree in May 2005.

His permanent address is: 21 Haier Road Apartment #11-402, Qingdao, Shandong 266100, China.